UCLA
UCLA Electronic Theses and Dissertations

Title

Analysis of the Neural and Glial Lineages Establishing the Cytoarchitecure of the Drosophila melanogaster Central Brain

Permalink

https://escholarship.org/uc/item/88c9q8fp

Author

Omoto, Jaison Jiro

Publication Date

2017

Peer reviewed|Thesis/dissertation

eScholarship.org Powered by the California Digital Library
University of California

UNIVERSITY OF CALIFORNIA

Los Angeles

Analysis of the Neural and Glial Lineages Establishing the Cytoarchitecure of the *Drosophila melanogaster* Central Brain

A dissertation submitted in partial satisfaction of the

requirements for the degree Doctor of Philosophy

in Molecular, Cell, and Developmental Biology

by

Jaison Jiro Omoto

2017

© Copyright by

Jaison Jiro Omoto

2017

ABSTRACT OF THE DISSERTATION

Analysis of the Neural and Glial Lineages Establishing the Cytoarchitecure of the *Drosophila melanogaster* Central Brain

by

Jaison Jiro Omoto

Doctor of Philosophy in Molecular, Cell, and Developmental Biology

University of California, Los Angeles, 2017

Professor Volker Hartenstein, Chair

Proper central nervous system (CNS) function in vertebrates and invertebrates alike requires the sufficient production of, and suitable interaction between, different classes of neurons and glial cells. Although a large heterogeneity exists between individual cells of the CNS, one can begin dissecting its construction, and ultimately function, based on developmental principles. One such principle is the lineage concept; accumulating evidence suggests that in the CNS of the fruit fly *Drosophila melanogaster*, classes of cells can be defined based on their progenitor origin, or lineage. Neurons and/or glial cells which derive from an individual progenitor, of which there are approximately 100 per brain hemisphere, exhibit common structural properties. In this dissertation we describe the lineage relationship, and resultant characteristics, of *Drosophila* brain cells in two contexts: glial cells populating the

neuropil-cortex interface (neuropil glia) and ensembles of neurons transmitting visual information to a higher-order brain region called the central complex (Anterior Visual Pathway). In the first context, we find that astrocyte-like glial cells (ALGs), a neuropil glia subtype reminiscent of vertebrate astrocytes, are generated in two distinct waves. The first wave results from the proliferation of embryonic progenitors in the basal brain, and produces the mature ALGs of the larval brain. ALGs of the adult brain, produced during the second wave, are generated from a completely separate population of progenitors in the larva. We also characterize the cytology of these glial populations. In the second context, we find that all ring neurons of the ellipsoid body, a subcompartment of the central complex, are generated from a single lineage called DALv2. Ring neurons are a peculiar neuronal class which has been previously shown to respond to visual stimuli and are required for higher-order visually-guided behaviors. We identify two further lineages, DALcl1 and 2, which generate parallel ensembles of neurons providing visual input to ring neurons. Importantly, neurons of DALcl1 and 2 are not only developmentally-distinct, but also exhibit structural and functional differences, highlighting the rarely demonstrated principle that functional neuronal circuitry can be mapped to developmental cell lineage. Taken together, this thesis validates the utility of employing the lineage principle to formulate hypotheses of circuit function and nervous system assembly in general.

The dissertation of Jaison Jiro Omoto is approved.

Alvaro Sagasti

Frank A. Laski

David E. Krantz

Volker Hartenstein, Committee Chair

University of California, Los Angeles

2017

DEDICATION

For Family, Friends, the Humble Fly, and Jasna

TABLE OF CONTENTS

Abstract of the Dissertation ii
Committee iv
Dedication v
Table of Contents vi
List of Figures and Tables vii
Acknowledgements viii
VITA xi

Introduction Part 1 Nervous system structure and function from the perspective of cell lineage: an overview 1
References 11
Introduction Part 2 Origins of glial cell populations in the insect nervous system. 17
Figures 28
References 37

Chapter One Origin and development of neuropil glia of the *Drosophila* larval and adult brain: Two distinct glial populations derived from separate progenitors. 44
Introduction 45
Materials and Methods 50
Results 54
Discussion 67
Figures 77
References 101

Chapter Two Visual input to the *Drosophila* central complex by developmentally and functionally distinct neuronal populations 110
Introduction 112
Materials and Methods 116
Results 119
Discussion 129
Figures 135
References 152

Chapter Three Development of the anterior visual pathway to the *Drosophila* central complex 158
Introduction 159
Materials and Methods 163
Results 166
Discussion 177
Figures 187
References 203

LIST OF FIGURES AND TABLES

INTRODUCTION

Figure Intro-1 28
Figure Intro-2 30
Figure Intro-3 32
Figure Intro-4 35

CHAPTER ONE

Table 1-1 77
Figure 1-1 78
Figure 1-2 81
Figure 1-3 84
Figure 1-4 86
Figure 1-5 88
Figure 1-6 90
Figure 1-7 92
Figure 1-8 94
Figure 1-9 96
Figure 1-10 98
Figure 1-11 100

CHAPTER TWO

Figure 2-1 135
Figure 2-2 138
Figure 2-3 141
Figure 2-4 144
Figure 2-5 146
Figure 2-6 149

CHAPTER THREE

Figure 3-1 187
Figure 3-2 188
Figure 3-3 191
Figure 3-4 193
Figure 3-5 195
Figure 3-6 197
Figure 3-7 199
Figure 3-8 201

ACKNOWLEDGEMENTS

Thank you to Mr. Drew Lord, for showing me the door of science. Thank you to Dr. Sepehr Eskandari, for providing me a path beyond that door. Thank you to Dr. Volker Hartenstein, for swarming me with flies while on that path.

Introduction Part 1

Introduction Part 1 is an overview of nervous system structure and function from the perspective of cell lineage.

This work was supported by grants from the National Institutes of Health (grant number R01 NS29357-15) and the University of California, Los Angeles (Dissertation Year Fellowship).

Contribution: Jaison J. Omoto wrote the manuscript.

Introduction Part 2

Introduction Part 1 is adapted from Omoto ***et al.*** *"*Origins of glial cell populations in the insect nervous system." (2016). *Curr. Opin. Insect Sci.* **18**:96-104. doi: 10.1016/j.cois.2016.09.003.

This work was supported by grants from the National Institutes of Health (grant number R01 NS29357-15) and the University of California, Los Angeles (Dissertation Year Fellowship).

Contribution: Jaison J. Omoto wrote the manuscript. Jennifer K. Lovick reviewed and edited the manuscript. Volker Hartenstein wrote the manuscript and advised the project.

Chapter One

Chapter one is adapted from Omoto *et al.* “Origin and development of neuropil glia of the Drosophila larval and adult brain: Two distinct glial populations derived from separate progenitors.” (2015) *Dev. Biol.* **404**(2):2-20. doi: 10.1016/j.ydbio.2015.03.004.

We thank the members of the Hartenstein laboratory and Philipp Kuert for critical discussions during the preparation of this manuscript. We are grateful to the Bloomington Stock Center and the Developmental Studies Hybridoma Bank for fly strains and antibodies. We thank Dr. Heinrich Reichert for anti-Labial antibody. We thank Diana Rigueur and Karen Lyons for assistance with the TUNEL assay. We also thank Dr. Marc Freeman for critical fly strains (alrm-Gal4) and antibodies (rabbit anti-GAT). This work was supported by NIH grant (R01 NS29357-15). J.J.O. is supported by the Ruth L. Kirschstein National Research Service Award (No. GM007185).

Contribution: Jaison J. Omoto designed, performed, and analyzed experiments and wrote the manuscript. Puja Yogi performed experiments. Volker Hartenstein wrote the manuscript and advised the project.

Chapter Two

Chapter two is adapted from Omoto *et al.* “Visual input to the Drosophila central complex by developmentally and functionally distinct neuronal populations” (manuscript submitted).

We kindly thank Orkun Akin for sharing the image alignment algorithm. We also thank Hiroshi Shiozaki and Hokto Kazama for discussing unpublished results. This work was supported by the National Institutes of Health (R01 NS096290 to V.H., and RO1 EY026031 to M.A.F.), the Ruth L. Kirschstein National Research Service Award (J.J.O,

No. GM007185), the UCLA Edith Hyde Fellowship (M.F.K), and the University of California, Los Angeles Dissertation Year Fellowship (J.J.O and M.F.K).

Contribution: Jaison J. Omoto and Mehmet F. Keleş designed, performed, and analyzed experiments and wrote the manuscript. Bao-Chau M. Nguyen, Cheyenne Bolanos, and Jennifer K. Lovick performed experiments. Mark A. Frye and Volker Hartenstein wrote the manuscript and advised the project.

Chapter Three

Chapter three is adapted from Lovick et al., “Development of neural lineages that establish the architecture of the *Drosophila* central complex and its visual input pathway” (manuscript in preparation).

Contribution: Jennifer K. Lovick, Jaison J. Omoto, and Kathy Ngo performed experiments. Volker Hartenstein analyzed experiments, wrote the manuscript, and advised the project.

VITA

Education

2004-2008	B.S., Biology California Polytechnic University, Pomona Pomona, CA
2008-2010	M.S., Biology California Polytechnic University, Pomona Pomona, CA

Experience

Graduate Student Researcher (September 2011 – Present)
Laboratory of Volker Hartenstein, Ph.D., University of California, Los Angeles – Los Angeles, CA
• Optimized immunohistochemical and imaging methods to visualize anatomy and development of the *Drosophila* nervous system.
• Initiated collaboration with the laboratory of Dr. Mark Frye (UCLA); obtained skillset to conduct two-photon functional imaging of neuronal subpopulations.
• Mentored ~10 undergraduate or highschool students from a wide spectrum of ethnocultural/socioeconomic backgrounds on a multitude of projects, several of which have or will become authors on publications.

Graduate Student Researcher and Laboratory Technician (September 2008 – June 2010)
Laboratory of Sepehr Eskandari, Ph.D., California Polytechnic University, Pomona – Pomona, CA
• Conducted an electrophysiological and biochemical analysis of the γ-aminobutyric acid transporter using the *Xenopus laevis* oocyte expression system.
• Provided technical assistance; tended to the *Xenopus laevis* colony, performed *Xenopus laevis* surgery (partial ovarectomy).

Publications

Omoto, J.J. *, Keleş, M.F. *, Nguyen, B.C., Bolanos, C., Lovick, J.K., Frye, M.A., Hartenstein, V. Visual input to the Drosophila central complex by developmentally and functionally distinct neuronal populations. *Curr. Biol. (in press).* *equal contribution

Omoto, J.J., Lovick, J.K., Hartenstein, V. Origins of glial cell populations in the insect nervous system. (2016). *Curr. Opin. Insect Sci.* **18**:96-104. doi: 10.1016/j.cois.2016.09.003.

Lovick, J.K. *, **Omoto, J.J.** *, Hartenstein, V. Flies to the locomotion. (2015) Flies do the locomotion. *Elife* doi: 10.7554/eLife.10317. *equal contribution

Lovick, J.K., Kong, A., **Omoto, J.J.**, Ngo, K.T., Younossi-Hartenstein, A., Hartenstein, V., (2015) Patterns of growth and tract formation during the early development of

secondary lineages in the Drosophila larval brain. *Dev Neurobiol.* doi: 10.1002/dneu.22325.

Hartenstein, V., Younossi-Hartenstein, A., Lovick, J.K., Kong, A., **Omoto, J.J.**, Ngo, K.T., Viktorin, G., (2015) Lineage-associated tracts defining the anatomy of the Drosophila first instar larval brain. *Dev Biol.* 406(1), 14-39.

Omoto, J.J., Yogi, P., Hartenstein, V., (2014) Origin and development of neuropil glia of the Drosophila larval and adult brain: two distinct glial populations derived from separate progenitors. *Dev Biol.* 404(2), 2-20.

Lovick, J.K., Ngo K.T., **Omoto, J.J.**, Wong, D.C., Nguyen, J.D., Hartenstein, V., (2013) Postembryonic lineages of the Drosophila brain: I. Development of the lineage-associated fiber tracts. *Dev Biol.* 384(2), 228-257.

Wong, D.C., Lovick, J.K., Ngo, K.T., Borisuthirattana, W., **Omoto, J.J.**, Hartenstein, V., (2013) Postembryonic lineages of the Drosophila brain: II. Identification of lineage projection patterns based on MARCM clones. *Dev Biol.* 384(2), 258-289.

Omoto, J.J., Maestas, M.J., Rahnama-Vaghef, A., Choi, Y.E., Salto, Jr. G., Sanchez, R.V., Anderson, C.M., Eskandari, S. (2012) Functional Consequences of Sulfhydryl Modification of the γ-Aminobutyric Acid Transporter 1 (GAT1) at a Single Solvent-Exposed Cysteine Residue. *J. Membr Biol.* 245(12), 841-857.

Presentations

Omoto, J.J., Nguyen, B-C., Lovick, J.K., Ngo, K.T., Hartenstein, V. Developmentally-related parallel circuit elements form a putative relay to the central complex in the anterior visual pathway. Meeting on Central Complex IV: A new hope to understand a multifaceted brain region. Janelia Research Campus, Ashburn, Virginia. (2016).

Omoto, J.J., Lovick, J., Nguyen, B.C., Hartenstein, V. The Drosophila brain DALcl lineages as putative parallel circuit relays to the central complex in the anterior visual pathway. Meeting on Neurobiology of Drosophila, Cold Spring Harbor Laboratory, Cold Spring Harbor, New York. (2015).

Omoto, J.J., Hartenstein, V. Characterization of Astrocyte-like (Reticular) glia in the Drosophila brain. Meeting on Glia in Health and Disease, Cold Spring Harbor Laboratory, Cold Spring Harbor, New York. (2012).

Omoto, J.J., Maestas, M.J., Rahnama-Vaghef, A., Anderson, C.M., Eskandari, S. Functional consequences of sulfhydryl modification of the γ-aminobutyric acid transporter 1 (GAT1) at a single solvent-exposed cysteine residue. Society for Neuroscience, San Diego, California. 2010.

Introduction Part 1 - Nervous system structure and function from the perspective of cell lineage: an overview

Complex nervous systems of both vertebrates and invertebrates consist of two principal cell types: neurons and glial cells. An enormous structural and functional heterogeneity exists within these two basic types; a continual effort in the neuroscience community lies in further discerning individual neuronal and glial classes, defining them based on a number of molecular, structural, and/or physiological criteria (Darmanis et al. 2015; Tasic et al., 2016; Zhang et al., 2014). Appropriate nervous system function depends on multiple parameters, such as the generation of suitable numbers of these individual cell classes, proper interactions between classes on diverse spatial and temporal scales, and maintenance of these cells during the animal's lifetime. Although ample resources are dedicated to defining the differences between individual cells of the nervous system, and deservedly so, an alternative approach lies in finding commonalities between them. For example, from a developmental perspective, central nervous systems are typically derived from a relatively stereotyped, species-specific number of neural progenitors. In principle, the enormous cell number and diversity that one observes in the mature central nervous system (CNS), can be traced back in development to a numerically smaller set of progenitors, each of which gives rise to a unique family tree, or lineage, of cells (Kriegstein and Alvarez-Buylla, 2009; Spindler and Hartenstein, 2010). Therefore, for clarity, a lineage is defined herein as a clonally-related population, rather than a class of cells with shared characteristics, such as its usage in the mammalian hematopoietic system (i.e. lymphoid or myeloid lineage). Is there any significance of this so-called "lineage principle"? Does a developmental

commonality, such as a shared progenitor origin, influence the structural properties of resultant cells, and thus the cytoarchitecture of the mature brain? Would such a developmentally-dictated organization bear any influence on the function of neural circuits?

To address the role of lineage in mammalian circuits, a knowledge of the brain's basic organization, and how this organization is achieved during development, is required. The most conspicuous structure of the mammalian brain is the cerebral cortex, neural tissue forming the superficial layer of the cerebrum. It has long been known that the cerebral cortex is a structure important for higher brain functions such as memory, attention, thought, language, and processing of sensory modalities. The entire structure is organized into six cortical layers, defined as such by global histological characteristics that are dictated by the cytological properties of the neurons that comprise them. This layered structure can be subdivided in a puzzle piece-like fashion; each piece, or "Brodmann area", represents a domain defined by its distinct histological, or "cytoarchitectonic", characteristics. Brodmann areas also roughly correspond to functionally-distinct regions of the cortex (Brodmann area 17 being the primary visual cortex, for example). As early as the 1950's, Vernon Mountcastle suggested that the cortex also exhibits a columnar organization; these so-called "cortical columns" were proposed to behave as the elementary computational unit of the brain (Mountcastle et al., 1955). Evidence that cortical columns operated as functional units were supported by the studies of Hubel and Wiesel in the cat visual cortex. They, in addition to discovering the foundational principles of visual neuroscience, also observed that neurons located within a given column were similarly tuned, that is, responded to the

same or similar stimulus (Hubel and Wiesel, 1962; 1968). The “radial unit hypothesis” put forth by Pasko Rakic proposed that this 2-dimensional array of structurally and functionally-defined “ontogenic” columns were in turn constructed from an array of progenitors whose somata line the ventricles during embryonic development (Rakic, 1988). These cells, known as radial glia progenitors (RGPs), exhibit many properties which make this an attractive hypothesis. RGPs extend a short process to contact the ventricle, and their somata remain close to the ventricular surface (ventricular zone), exhibiting an apico-basal polarity. They extend a long, radial process that remains in contact with the pial surface, which progressively extends in conjunction with the thickening cortex. More recent, sophisticated single progenitor lineage tracing methods demonstrated that the radial unit hypothesis in fact the case. Using the pial-contacting process as a scaffold, individual neurons generated by the RPG migrate in a radial fashion, an elegant mechanism underlying the radial unit organization of the cortex (Noctor et al., 2001).

Even still, the significance of lineage in circuit formation and function in the vertebrate brain has been historically undefined, perhaps even controversial (Horton and Adams, 2005). It was not until single progenitor lineage tracing was combined with physiological characterization of clonally-related sister neurons, did the role of lineage, at least for excitatory cortical neurons, become apparent. Li et al., 2012 turned to the mammalian visual cortex; their method allowed them to identify GFP-labelled, clonally-related sister neuron pairs in the mouse. Injection of calcium indicator dye near the labeled pair allowed them to optically record the activity of this pair, along with unlabeled, presumably non-sister neighboring neurons, using two-photon excitation

microscopy. By presenting the mice with a wide-field grating visual stimulus with different orientations, they found that clonally-related sister neurons prefer similarly oriented visual stimuli, a correlation that was not observed between clonally-related and unrelated neurons (Li et al., 2012). Findings by Ohtsuki et al., 2012 largely corroborated these findings, albeit with much larger clones (600-800 neurons each) generated by induction at an earlier developmental time point, rather than individual neuron pairs. However, although orientation preference was more similar within this large clone in comparison to unrelated neurons, the tuning properties within this population was not homogenous, suggesting that “clonal identity is not the only determinant of response selectivity” (Ohtsuki et al., 2012). The similar tuning properties of sister cortical neurons makes sense considering that clonally-related neurons exhibit preferential chemical synaptic interactions (Yu et al., 2009), a property dependent upon transient electrical coupling via gap junctions during early development (Li et al., 2012; Yu et al., 2012). Lineage-specific electrical communication enhances the synchronous firing of these neurons, which is thought to underlie the preferential synaptic wiring observed later in development. Epigenetic transcriptional regulation of cell adhesion genes, or birthdate-dependent migration and “inside-out” patterning, may also contribute to connectivity between clonally-related neurons (He et al., 2015; Tarusawa et al., 2016). Thus, a framework for the role of lineage in sculpting vertebrate brain circuits has emerged; clonally-related sister neurons from a given progenitor talk to each other early and often, growing radially into a column to process information as a group.

Are all mammalian circuits constructed within this framework? The hippocampus, known primarily for its role in learning and memory is one of, if not, the most studied

structures of the mammalian brain. Considered part of the limbic system, the hippocampus, like any other brain region, must be constructed during development from progenitor cells. Investigators can apply similar approaches as to those used to study the cortex, to probe the lineage-structure-function relationships of the hippocampus. In contrast to the cortex, Xu et al. 2014 found that clonally-related sister neurons were distributed as neighboring clusters in a laminar-fashion, rather than in a columnar fashion. Interestingly, the long radial glia fiber which acts as a scaffold for radial neural migration in the cortex, bends in the hippocampus, leading to the horizontally-oriented depositing of sister neurons. Also in contrast to the cortex, electrophysiological recordings demonstrated that these clonally-related neurons were not preferentially connected by electrical or chemical synapses. So, what role might lineage play in this context? The investigators observed that, despite not being preferentially connected to each other, sister neurons exhibited synchronized spontaneous activity. Remarkably, this synchrony was due to the tendency of clonally-related pyramidal neurons to receive inhibitory synaptic input from a shared GABAergic interneuron (Xu et al., 2014). The functional significance of this developmentally-organized arrangement for information processing within the hippocampus remains to be seen, but one can conclude that lineage relationships differentially influence the construction of functional neural circuits depending on the context.

Does lineage play a role in sculpting every neural circuit? In the case of GABAergic interneurons of the cortex, the answer seems debatable. Most cortical interneurons derive from the medial ganglion eminence and preoptic area, which migrate tangentially to populate multiple laminae of the cortex (reviewed in Batista-Brito

and Fishell, 2009). Brown et al., 2011 and Ciceri et al., 2013 suggested that clonally-related interneurons tend to form non-random, spatially-discrete clusters, with both intralaminar and interlaminar distributions. Two recent studies challenged this assertion, suggesting that there does not seem to be a clear relationship between lineage and the spatial distribution of cortical interneurons (Harwell et al., 2015; Mayer et al., 2015). The discrepancy lies in the methodology; the former utilized selective and stable fluorescent labeling of individual progenitors and their progeny, whereas the latter utilized retrovirus-based barcoded libraries as a readout. Although follow up rebuttals from each group acknowledge certain shared conclusions and advantages and/or disadvantages of their respective approaches (Mayer et al., 2016; Sultain et al., 2016), the debate seemingly continues.

In the insect literature, particularly in the fruit fly *Drosophila melanogaster*, there is compelling evidence that the lineage principle also dictates the structure and function of progeny cells within the CNS. The relationship between neural progenitor and the structure of clonally-related progeny neurons is more straightforward due to the nature by which the CNS is organized. In the fly embryo, the neuroectoderm produces a stereotyped set of approximately 100 paired neural progenitors called neuroblasts that will form the central brain. Embryonic neuroblasts, at least initially, are organized into a 2-dimensional array, each one is defined by its unique gene expression pattern based on its spatial position within the array (Urbach and Technau, 2003). Each neuroblast forms a distinctive set of cellular progeny; clonally-related neuronal somata tend to cluster around the parent neuroblast with minimal migration, typically extending one or two fasciculated axon tract(s) into the neuropil with a highly stereotyped trajectory,

allowing for the unambiguous identification of individual or pairs of lineages (Spindler and Hartenstein, 2010). The distinctiveness of a lineage is a consequence of a given neuroblast's unique gene expression program. This is not to suggest that neurons of a given lineage are homogenous. Neuroblasts proliferate in a stem cell-like mode; they divide asymmetrically to produce a new neuroblast and an intermediate cell called a ganglion mother cell (GMC). On the surface, GMCs divide symmetrically to produce two post-mitotic neurons. However, the two neurons differ according to their level of Notch (N) activity; neurons of high N and low N produce A and B hemilineages, respectively (Truman et al., 2010). In addition, neuroblasts undergo a temporal cascade of transcription factor expression which modifies the phenotype of neurons born within discrete time windows (sublineages), further enhancing neural diversity. Finally, for holometabolous insects such as *Drosophila* in which the life cycle includes a distinct larval and adult period separated by a pupal metamorphosis, a given lineage includes two major proliferative phases. Each lineage contains a primary and secondary lineage; primary neurons are born during the embryonic phase of proliferation and give rise to functional neurons of the larval brain, whereas secondary neurons are born during the larva and produce much of the functional neurons of the adult brain (Spindler and Hartenstein, 2010). The arborizations of neurons from distinct lineages stereotypically overlap to form the neuropil compartments of the brain.

The structural properties of individual lineages and the neurons comprising them have been the focus of intense characterization by our lab and others (Ito et al., 2013; Kuert et al., 2014; Lovick et al., 2013; Pereanu and Hartenstein, 2006; Shepherd et al., 2016; Truman et al., 2004; Wong et al., 2013; Yu et al., 2013). Although lineages form

the structural “building blocks of macrocircuitry”, to what extent does the lineage principle influence the function of circuits in the fly? One particularly prominent case in point is in the fly olfactory pathway. The somata and dendrites of olfactory receptor neurons (ORNs) are located in sensilla that are subjected to chemical stimuli from the external world, and their outputs located in the antennal lobe, the primary olfactory processing compartment in the central brain. Each ORN expresses a single odorant receptor gene (out of approximately 50), and neurons which share a given receptor converge onto a single glomerulus in the antennal lobe (Wilson, 2013). Information is received from ORNs by an anatomically stereotyped population of olfactory projection neurons (PNs), which exhibit dendrites in the antennal lobe and axonal outputs in the mushroom body calyx and/or the lateral horn, two higher-order brain structures. Projection neurons are members of four paired lineages, generated from neuroblasts lNB/BAlc, adNB/BAmv3, vNB/BAla1, and lastly, BAlp4, which projects to the inferior protocerebrum rather than the calyx/lateral horn (Das et al., 2013; Lai et al., 2008). In other words, four identified neural progenitors out of 100 produce a highly anatomically (antennal lobe glomeruli to higher brain centers) and functionally (transmitting olfactory information) stereotyped set of neurons. Considering this, the utility of the lineage principle to formulate hypotheses of circuit function becomes evident; as such, the antennal projection has developed into a leading model to understand the development and function of circuitry.

The significance of clonal relationships in the construction of functional circuitry has also been assessed in other regions of the CNS. Another prominent example is that of the ventral nerve cord (VNC), the functional analog of the vertebrate spinal cord. Like

the brain, neurons of the VNC are similarly generated, albeit by a smaller set (approximately 30 per hemineuromere) of neuroblasts (Shepherd et al., 2016; Truman et al., 2004). As they form the majority of VNC interneurons, interacting with sensory afferents from the body and motorneuron efferents controling the muscles, Harris et al., hypothesized that lineally organized neuronal ensembles would also be functionally organized to somehow coordinate locomotor behaviors. Utilizing a novel suite of genetic tools, they were able to stably and specifically label individual hemilineages in the fly VNC and document their anatomical characteristics. In addition to simple labeling, they expressed a heat-sensitive ion channel in specific hemilineages and assessed the behavioral consequence of targeted activation of these neurons. Interestingly, hemilineage-specific activation led to a stereotyped behavioral response, the complexity of which correlated with the projection location and spatial distribution of hemilineage neurites (Harris et al., 2015).

Finally, the central complex (CX), a higher order brain center important for visually-guided behaviors, has become another heavily studied structure with the lineage concept in mind (Yang et al., 2013). Firstly, the CX itself is generated by a small set of well-defined lineages; primarily, but not exclusively, from so called type II lineages. In addition, defined in the second and third chapter of this dissertation, neuronal ensembles forming the input to the CX, are also developmentally organized. We find that two lineages, DALcl1 and DALcl2, form distinct ensembles that project from and to, distinct but neighboring subdomains in a parallel fashion. The input to DALcl1/2, located in the anterior optic tubercle, comes directly from projection neurons of the optic lobe medulla; the outputs of DALcl1/2 terminate in the bulb, a known domain of visual

input to the central complex. Neurons of DALcl1 and DALcl2 transmit fundamentally distinct visual information, revealed by two-photon calcium imaging from the two populations (Omoto et al., *Submitted*; Chapters 2). We document the development of these and other lineages of this pathway, from the larva to adult, in Chapter 3 (Lovick et al., *in prep*).

Thus far, we have discussed clear examples of neuronal circuits being structurally and functionally organized by the lineage principle; part 2 of this introduction is a review of the different glial cells populations in the insect nervous system, and what is known about how lineage shapes their properties (Omoto et al. 2016).

References

Batista-Brito, R., Fishell, G., 2009. The developmental integration of cortical interneurons into a functional network. Curr Top Dev Biol. 87:81-118.

Brown, KN, Chen, S, Han, Z, Lu, CH, Tan, X, Zhang, XJ, Ding, L, Lopez-Cruz, A, Saur, D, Anderson, SA, et al. 2011.Clonal production and organization of inhibitory interneurons in the neocortex. Science 334:480–486.

Ciceri, G1, Dehorter N, Sols I, Huang ZJ, Maravall M, Marín O. 2013. Lineage-specific laminar organization of cortical GABAergic interneurons. Nat Neurosci.16(9):1199-210.

Darmanis S, Sloan SA, Zhang Y, Enge M, Caneda C, Shuer LM, Hayden Gephart MG, Barres BA, Quake SR. 2015. A survey of human brain transcriptome diversity at the single cell level. Proc Natl Acad Sci U S A. 112(23):7285-90.

Das A, Gupta T, Davla S, Prieto-Godino LL, Diegelmann S, Reddy OV, Raghavan KV, Reichert H, Lovick J, Hartenstein V. 2013. Neuroblast lineage-specific origin of the neurons of the Drosophila larval olfactory system. Dev Biol. 373(2):322-37.

Gao P, Postiglione MP, Krieger TG, Hernandez L, Wang C, Han Z, Streicher C, Papusheva E, Insolera R, Chugh K, Kodish O, Huang K, Simons BD, Luo L, Hippenmeyer S, Shi SH. 2014. Deterministic progenitor behavior and unitary production of neurons in the neocortex. Cell. 159(4):775-88.

Harris RM, Pfeiffer BD, Rubin GM, Truman JW. 2015. Neuron hemilineages provide the functional ground plan for the Drosophila ventral nervous system. Elife. 4. doi: 10.7554/eLife.04493.

Harwell CC, Fuentealba LC, Gonzalez-Cerrillo A, Parker PR, Gertz CC, Mazzola E, Garcia MT, Alvarez-Buylla A, Cepko CL, Kriegstein AR. 2015. Wide Dispersion and Diversity of Clonally Related Inhibitory Interneurons. Neuron 87(5):999-1007.

He S, Li Z, Ge S, Yu YC, Shi SH. 2015. Inside-Out Radial Migration Facilitates Lineage-Dependent Neocortical Microcircuit Assembly. Neuron. 86(5):1159-66.

Horton JC, Adams DL. 2005. The cortical column: a structure without a function. Philos Trans R Soc Lond B Biol Sci. 360(1456):837-62.

Hubel D.H, Wiesel T.N. 1968. Receptive fields and functional architecture of monkey striate cortex. J. Physiol. (Lond.) 195:215–243.

Hubel D.H, Wiesel T.N. 1962. Receptive fields, binocular interaction and functional architecture in the cat's visual cortex. J. Physiol. (Lond.) 160:106–154.

Ito M, Masuda N, Shinomiya K, Endo K, Ito K. 2013. Systematic analysis of neural projections reveals clonal composition of the Drosophila brain. Curr Biol. 23(8):644-55.

Kriegstein A, Alvarez-Buylla A. 2009. The glial nature of embryonic and adult neural stem cells. Annu Rev Neurosci. 32:149-84.

Kuert PA, Hartenstein V, Bello BC, Lovick JK, Reichert H. 2014. Neuroblast lineage identification and lineage-specific Hox gene action during postembryonic development of the subesophageal ganglion in the Drosophila central brain. Dev Biol. 390(2):102-15.

Lai, S.-L., Awasaki, T., Ito, K., and Lee, T. 2008. Clonal analysis of Drosophila antennal lobe neurons: diverse neuronal architectures in the lateral neuroblast lineage. Development 135(17):2883-93.

Li Y, Lu H, Cheng PL, Ge S, Xu H, Shi SH, Dan Y. 2012. Clonally related visual cortical neurons show similar stimulus feature selectivity. Nature. 486(7401):118-21.

Lovick JK, Ngo KT, Omoto JJ, Wong DC, Nguyen JD, Hartenstein V. 2013. Postembryonic lineages of the Drosophila brain: I. Development of the lineage-associated fiber tracts. Dev Biol. 384(2):228-57.

Mayer C, Jaglin XH, Cobbs LV, Bandler RC, Streicher C, Cepko CL, Hippenmeyer S, Fishell G. 2015. Clonally Related Forebrain Interneurons Disperse Broadly across Both Functional Areas and Structural Boundaries. Neuron. 87(5):989-98.

Mountcastle V.B, Berman A.L, Davies P.W. Topographic organization and modality representation in first somatic area of cat's cerebral cortex by method of single unit analysis. Am. J. Physiol. 1955;183:464.

Noctor SC, Flint AC, Weissman TA, Dammerman RS, Kriegstein AR. Neurons derived from radial glial cells establish radial units in neocortex. Nature. 2001 Feb 8;409(6821):714-20.

Omoto JJ, Lovick JK, Hartenstein V. 2016. Origins of glial cell populations in the insect nervous system. Curr Opin Insect Sci. 18:96-104.

Pereanu W, Hartenstein V. 2006. Neural lineages of the Drosophila brain: a three-dimensional digital atlas of the pattern of lineage location and projection at the late larval stage. J Neurosci. 26(20):5534-53.

Rakic P. 1988. Specification of cerebral cortical areas. Science. 241(4862):170-6.

Shepherd D, Harris R, Williams DW, Truman JW. 2016 . Postembryonic lineages of the Drosophila ventral nervous system: Neuroglian expression reveals the adult

hemilineage associated fiber tracts in the adult thoracic neuromeres. J Comp Neurol. 524(13):2677-95.

Spindler SR, Hartenstein V. 2010. The Drosophila neural lineages: a model system to study brain development and circuitry. Dev Genes Evol. 220(1-2):1-10.

Sultan KT, Han Z, Zhang XJ, Xianyu A, Li Z, Huang K, Shi SH. 2016. Clonally Related GABAergic Interneurons Do Not Randomly Disperse but Frequently Form Local Clusters in the Forebrain. Neuron. 92(1):31-44.

Tarusawa E, Sanbo M, Okayama A, Miyashita T, Kitsukawa T, Hirayama T, Hirabayashi T, Hasegawa S, Kaneko R, Toyoda S, Kobayashi T, Kato-Itoh M, Nakauchi H, Hirabayashi M, Yagi T, Yoshimura Y. 2016. Establishment of high reciprocal connectivity between clonal cortical neurons is regulated by the Dnmt3b DNA methyltransferase and clustered protocadherins. BMC Biol. 14(1):103.

Tasic B, Menon V, Nguyen TN, Kim TK, Jarsky T, Yao Z, Levi B, Gray LT, Sorensen SA, Dolbeare T, Bertagnolli D, Goldy J, Shapovalova N, Parry S, Lee C, Smith K, Bernard A, Madisen L, Sunkin SM, Hawrylycz M, Koch C, Zeng H. 2016. Adult mouse cortical cell taxonomy revealed by single cell transcriptomics. Nat Neurosci. 19(2):335-46.

Truman JW, Moats W, Altman J, Marin EC, Williams DW. 2010. Role of Notch signaling in establishing the hemilineages of secondary neurons in Drosophila melanogaster. Development. 137(1):53-61.

Truman JW, Schuppe H, Shepherd D, Williams DW. 2004. Developmental architecture of adult-specific lineages in the ventral CNS of Drosophila. Development. 131(20):5167-84.

Urbach R, Technau GM. 2003. Molecular markers for identified neuroblasts in the developing brain of Drosophila. Development. 130(16):3621-37.

Wilson RI. 2013. Early olfactory processing in Drosophila: mechanisms and principles. Annu Rev Neurosci. 36:217-41.

Wong DC, Lovick JK, Ngo KT, Borisuthirattana W, Omoto JJ, Hartenstein V. 2013 Postembryonic lineages of the Drosophila brain: II. Identification of lineage projection patterns based on MARCM clones. Dev Biol. 384(2):258-89.

Xu HT, Han Z, Gao P, He S, Li Z, Shi W, Kodish O, Shao W, Brown KN, Huang K, Shi SH. 2014. Distinct lineage-dependent structural and functional organization of the hippocampus. Cell. 157(7):1552-64.

Yang, J.S., Awasaki, T., Yu, H.-H., He, Y., Ding, P., Kao, J.-C., and Lee, T. 2013. Diverse neuronal lineages make stereotyped contributions to the Drosophila locomotor control center, the central complex. J. Comp. Neurol. 521, 2645–2662.

Yu HH, Awasaki T, Schroeder MD, Long F, Yang JS, He Y, Ding P, Kao JC, Wu GY, Peng H, Myers G, Lee T. 2013. Clonal development and organization of the adult Drosophila central brain. Curr Biol. 23(8):633-43.

Yu YC, Bultje RS, Wang X, Shi SH. 2009. Specific synapses develop preferentially among sister excitatory neurons in the neocortex. Nature. 458(7237):501-4.

Yu YC, He S, Chen S, Fu Y, Brown KN, Yao XH, Ma J, Gao KP, Sosinsky GE, Huang K, Shi SH. 2012. Preferential electrical coupling regulates neocortical lineage-dependent microcircuit assembly. Nature. 486(7401):113-7.

Zhang Y, Chen K, Sloan SA, Bennett ML, Scholze AR, O'Keeffe S, Phatnani HP, Guarnieri P, Caneda C, Ruderisch N, Deng S, Liddelow SA, Zhang C, Daneman

R, Maniatis T, Barres BA, Wu JQ. 2014. An RNA-sequencing transcriptome and splicing database of glia, neurons, and vascular cells of the cerebral cortex. J Neurosci. 34(36):11929-47.

Introduction Part 2 - Origins of glial cell populations in the insect nervous system

Neurectodermal origin of glia

Cells of the nervous system fall into two main classes of cells: neurons and glia. In vertebrates, glial cells include three major types, astrocytes, oligodendrocytes, and microglia. Astrocytes and oligodendrocytes, together called macroglia, are generated by multipotent neural progenitors that constitute the neuroepithelium lining the neural tube (Bayraktar et al., 2014; Miller, 2002) (Fig.1A). During their first rounds of division these cells produce only neurons that segregate from the neuroepithelium (ventricular layer) and form a cellular mantle that matures into nerve tissue (Fig.1B). The neuroepithelial cells left in the ventricular layer become elongated cells, called radial glia. Continued proliferation of radial glia located at discrete domains within the neural tube produces oligodendroctye progenitors (OLPs) that spread throughout the central nervous system (CNS) and differentiate into oligodendrocytes (Fig.1C). The remainder of radial glia gives rise to astrocytes. Microglial cells are phagocytes combating degenerative processes and infections in the neural tissue. They are derived from blood-forming (hematopoietic) stem cells that migrate into the nervous system during the embryonic period (Lavin et al., 2015) (Fig.1A).

In *Drosophila*, and arthropods in general, glial cells include (1) surface glia (SG) that surrounds the CNS and peripheral nerves, forming the blood-brain barrier; (2) cell body glia (CBG; also called cortex glia), encapsulating neuronal cell bodies which form the outer cellular layer of the CNS; (3) neuropil glia (NPG), located at the interface between the cortex and the neuropil, forming sheaths around neuropil compartment boundaries, certain long axon bundles, and peripheral nerves (ensheathing glia (EG),

wrapping glia), as well as highly branched processes interacting with terminal nerve fibers and synapses [reticular or astrocyte-like glia (ALG)] (Awasaki et al., 2008; Cantera, 1993; Hoyle, 1986; Pereanu et al., 2005). Phagocytic microglial cells are absent; however, blood stem cell-derived macrophages occupy the outer surface of the CNS. Most *Drosophila* glial cells, along with neurons, are derived from a small number of uniquely identifiable progenitors, called neuroblasts, that delaminate from the neurectoderm of the early embryo (Fig.1G-I). Neuroblasts divide in an asymmetric, stem cell-like pattern, where each division produces a renewed neuroblast, and a ganglion mother cell that becomes postmitotic after one more round of mitosis. Most neuroblasts generate exclusively neurons (which, unlike in vertebrates, outnumber glia by a large margin). Some neuroblasts produce both neurons and glia ("neuro-glioblasts"); very few give rise to glia only ("glioblasts") (Altenhein, 2015; Beckervordersandforth et al., 2008). *Drosophila* exhibits a highly stereotyped nervous system along with a wealth of glial markers and genetic lineage tracing methods allowing for the specific and stable labeling of cells, frequently in a temporally-controlled manner. As a result, insights into the origin and development of the aforementioned progenitors and their glial progeny, often times at the single-cell level, has been assessed throughout multiple stages of the *Drosophila* life cycle.

Glia for the larval and adult nervous system: Primary and secondary gliogenesis

After delamination, embryonic neuroblasts enter an initial phase of proliferation to produce the functional neurons of the larval CNS (primary neurons). Many primary neurons, although remodeled during metamorphosis, are retained into adulthood, whereas many others undergo programmed cell death. Along with the neuroblasts,

embryonic glioblasts and neuro-glioblasts produce the functional glial cells that differentiate in the late embryo, forming processes around the surface, cell bodies, and neuropil of the larval CNS (“primary glia”; Fig.2A). Glioblasts only generate glia, and express the glial determinants *gcm* and *repo* right after they delaminate from the neurectoderm. Neuro-glioblasts show different modes of gliogenesis (Altenhein, 2015) (Fig.2B). In type 1 neuro-glioblasts, no early separation of neural vs glial fate takes place; instead, neurons and glial cells derive as siblings from the division of ganglion mother cells. Type 2 neuro-glioblasts switch from neurogenesis to gliogenesis at some point in proliferation. Type 3 neuro-glioblasts are defined by the fact that they comprise at least one pure glioblast progenitor. Finally, midline precursors (MPs) constitute a peculiar type of fundamentally-distinct glioblast (mesectodermally-derived) that divide just once to give rise to a subtype of primary neuropil glia, called midline glia (Bossing and Technau, 1994).

A second phase of neurogenesis and gliogenesis takes place during the larval period. Neuroblasts produce secondary neurons that integrate into the circuitry of retained primary neurons during metamorphosis. Thus, a typical neuroblast lineage consists of embryonically-born primary and postembryonically-born secondary neurons. Functional glial populations of the adult (“secondary glia”) appear to exhibit a more variable pattern of origin. (1) Secondary neuropil glial cells are generated by a select subpopulation of neuro-glioblasts that become active in the larva (Izergina et al., 2009; Omoto et al., 2015) (Fig.2A, C, F; see below). (2) By contrast, secondary perineurial and cell body glial cells of the adult brain are likely generated by the continued proliferation of their respective primary cell types (Awasaki et al., 2008; Avet-Rochex et

al., 2012; Colonques et al., 2007; Pereanu et al., 2005) (Fig.2A, C-E). (3) Primary subperineurial glia do not divide and probably persist into adulthood as a numerically-fixed population.

Neuropil Glia

The two types of glia in direct contact with nerve processes, astrocyte-like and ensheathing glia, may play different roles in the mature nervous system, but share a common origin. ALGs extend processes into the neuropil and express amino acid transporters, optimally situated to modulate synaptic and/or extrasynaptic processes and thus the circuit properties of neurons, via the uptake of neurotransmitters or other cell-cell signaling pathways (Liu et al., 2014; Macnamee et al., 2016; Stork et al., 2014). Ensheathing glia wraps around neuropil compartment boundaries, axon tracts, and fascicles, likely acting as structural insulators of mature neurons (Spindler et al., 2009). Dye injection experiments revealed that a single glioblast, the lateral glioblast (LGB), in each hemisegment gives rise to most of the primary neuropil glia of the embryonic ventral nerve cord, called longitudinal glia based on their association with the longitudinal connectives (Fig.3A-C). Longitudinal glial cells are differentially specified into six ALGs and three EGs, depending on their expression of *Notch*, *Pointed*, and *Prospero* (Peco et al., 2016) (Fig.3D-F). Other classes of embryonic primary neuropil glia include *repo*-negative midline glia (MG), produced from mesectodermally-derived midline precursors (Bossing and Technau, 1994), and nerve root glia (NRG), derived from the neuro-glioblast NB1-3 and NB7-4 (Beckervordersandforth et al., 2008) (Fig.3A-C). Primary neuropil glial cells of the brain are thought to be derived from the Td7 neuroblast [nomenclature according to (Urbach et al., 2003)], based on its expression of

glial specific genes, and its close proximity to the longitudinal glia equivalent of the brain, the basal procephalic longitudinal glia (BPLG) (Hartenstein et al., 1998; Omoto et al., 2015) (Fig.3G).

The number of differentiated primary neuropil glia remains constant throughout larval development. These cells increase in size presumably to account for the growing neuropil volume (Omoto et al., 2015). Temporally-controlled lineage tracing demonstrated that primary astrocyte-like glia, and likely ensheathing glia as well, undergoes programmed cell death during metamorphosis and is not retained into adulthood (Fig.3H-J). Although the number of differentiated primary neuropil glial cells does not change throughout the larval period, clone induction via MARCM (mosaic analysis with a repressible cell marker) during the secondary phase of neuroblast proliferation revealed that *repo*-positive neuropil glial precursors appear in large numbers as a result of the proliferation of a few secondary neuro-glioblasts (Izergina et al., 2009; Viktorin et al., 2011) (Fig.2C, F). Lineage tracing experiments revealed that these secondary neuropil glial precursors migrate from their site of origin in the brain cortex towards the neuropil, proliferate, spread out tangentially around the neuropil surface/between neuropil compartments, and differentiate into secondary neuropil glia (Omoto et al., 2015). The analogous process occurs in select, yet to be identified neuro-glioblasts of the ventral nerve cord. Although primary and secondary neuropil glia exhibit fundamental similarities, they differ in size and in gene expression profiles (Huang et al., 2015; Omoto et al., 2015). Primary midline glia of the ventral nerve cord show an unusual behavior: like other neuropil glia they degenerate during

metamorphosis, but they proliferate profusely prior to this event, possibly to assist in circuit formation (Awad ad Truman, 1997).

Surface Glia

Surface glia surrounding the larval and adult brain, as well as all peripheral nerves, can be subdivided into perineurial (PNG) and subperineurial glia (SPG). Subperineurial cells form conspicuous septate junctions (the invertebrate equivalent of tight junctions) and are thereby primarily important to generate a blood-brain barrier that prevents unregulated passage of molecules between the nervous system and hemolymph (Limmer et al, 2014). Perineurial glial cells are also involved in the blood-brain barrier, even though the mechanism by which it participates in this function is not clear, since perineurial glial cells do not form a complete sheath connected by septate junctions around the brain. Furthermore, in the early larva, PNGs are lacking at most locations; they only form a relatively dense cover after a phase of intense proliferation in later larval stages (Avet-Rochex et al., 2012, 2014; Pereanu et al., 2005) (Fig.2D). Recent evidence also suggests a role of surface glia in regulation of neuronal metabolism, as well as the coupling of systemic metabolism to brain development (Chell and Brand, 2010; Volkenhoff et al., 2015).

Primary surface glia of the ventral nerve cord derived from five neuro-glioblasts (Type 1: NB1-1, NB2-2, NB5-6; Type 2: NB1-3, NB7-4), located at the boundary between two adjacent segments (Altenhein, 2015; Beckervordersandforth, 2008) (Fig.3A). The contribution of primary surface glial cells to the insulating layers around the peripheral nerves have been revealed by Flybow, a stable, multicolor labeling technique [29,30], and their origins traced back to NB2-5 and NB5-6, or NB1-3,

respectively (Fig.3A, C). In addition, a subset of the surface glial cells of the peripheral nerve is produced by sensory organ progenitors which form outside the neurectoderm (Fig.3C). How surface glia is specified into the perineurial and subperineurial type is unknown. During the larval period, primary subperineurial cells increase in size, but not number, due to polyploidization, akin to what has been observed for primary neuropil glia (Unhavaithaya and Orr-Weaver, 2012). We posit that these cells are retained throughout metamorphosis and become the functional subperineurial glia of the adult brain. This hypothesis is supported by the developmental fate of subperineurial glia of the optic stalk (called carpet glia), which is also retained in the adult optic lobe (Edwards et al., 2012) (Fig.3K). Perineurial glia, in contrast to subperineurial glia, continually proliferates throughout the larval period, and likely forms the perineurial glia of the adult brain (Avet-Rochex et al., 2012; Awasaki et al., 2008). Proliferating perineurial cells may also contribute to other glial types, as observed for the perineurial glia of the optic stalk, which differentiates first into a cell type that envelops the retinal axons invading the optic lobe (wrapping glia) (Bauke et al., 2015), and ultimately gives rise to a type of cortex glia of the optic lobe (distal satellite glia) (Fig.3K) (Edwards, et al., 2012).

Cell body glia

Cell body glia ensheathes individual neuronal somata, and in doing so, structurally stabilizes them while simultaneously regulating whole nervous system excitability (Melom and Littleton, 2013). Primary cell body glial cells of the ventral nerve cord, numbering three per hemisegment, are generated by the neuro-glioblasts NB6-4 (Type 3) and 7-4 (Type 2; Fig.3A-C) (Altenhein, 2015). For the brain, the specific neuro-glioblasts which give rise to the primary cell body glia, as well as surface glia, have not

yet been identified. However, clusters of *repo*-positive cells that include precursors of both cell types were mapped to a domain at the border between protocerebrum and deuterocerebrum, and to the dorsal edge of the protocerebrum, respectively (Fig.3G) (Hartenstein et al., 1998). Primary cell body glia enters a phase of proliferation during the late larval period, likely forming the secondary population of the adult, similarly to perineurial glia. MARCM analysis revealed that proliferation for both glial types depends on several signaling pathways, among them Hippo (Reddy and Irvine, 2011), InR/TOR, and FGF (Avet-Rochex et al., 2012; 2014). The ligands activating these pathways appear to act locally; the FGF ligand Pyramus (Pyr) is secreted by neighboring glial cells (in case of perineurial glia) or neurons (in case of cell body glia). Likewise, the signal activating the InR/TOR pathway, *Drosophila* insulin-like peptide 6 (Dilp-6), is found in glial cells (Avet-Rochex et al., 2012).

Glia of the optic lobe

The optic lobe, which receives retinotopically ordered input from the compound eye, develops postembryonically from two neuroepithelial optic anlagen, called outer and inner optic anlagen, which, initially, grow by symmetric division, followed by their conversion into a large number of asymmetrically dividing neuroblasts (Fischbach and Hiesinger, 2008; Ngo et al., 2010). Glia of the optic lobe exhibits numerous morphologically distinct subclasses that are not evident in the central brain or ventral nerve cord. For example, cortex glia of the lamina include distal and proximal satellite glia; neuropil glia has epithelial glia and marginal glia, as well as outer chiasm glia (Edwards et al., 2012). Surface glia of the optic lobe is derived from the proliferating perineurial glia surrounding the larval brain and optic stalk (Fig.3K). Neuropil and cell

body glia of the lamina are formed by four distinct populations of glial progenitors that derive from the glial precursor zone (Chotard and Salecker, 2007; Edwards et al., 2012), a subdomain of the outer optic anlage (Fig.3K). Perineurial glia of the optic stalk, which first differentiates into wrapping glia (Bauke et al., 2015)**,** also contributes to the lamina cortex glia (distal satellite glia) (Edwards et al., 2012). Precursors of neuropil and cortex glia of the other optic ganglia (medulla, lobula, lobula plate) are born at a later stage during the asymmetric division of neuro-glioblasts of the outer and inner optic anlage (Fig.3K) (Edwards et al., 2012; Hartenstein, 2011).

Hemocytes and the nervous system

Blood cells populating the body cavity of the *Drosophila* larva (primary or "primitive" hemocytes) are formed in the head mesoderm of the early embryo (Tepass et al., 1994). *gcm*, the transcription factor specifying glial fate in the progeny of neuro-glioblasts, is also expressed and required for mesodermal cells to adopt a hemocyte fate (Bernardoni et al., 1997; Lebetsky et al., 2000). From their anterior location, hemocytes migrate along the surface of the nervous system and other inner organs, laying down components of the extracellular matrix (Fig.4A-D).

In addition, a major role of hemocytes (similar to vertebrate microglia) lies in phagocytosing apoptotic cell bodies resulting from programmed cell death. Loss or altered function of hemocytes results in severe defects in nervous system development (Olofsson and Page, 2005; Sears et al., 2003). The removal of cellular debris in the CNS, which in vertebrates is carried out by microglia, is a function shared between hemocytes and (macro-)glia in *Drosophila*. In the fly embryo, primary neuropil glia and surface glia, in addition to hemocytes, act as macrophages (Sonnenfeld and Jacobs,

1995). Postembryonically, neuropil glia exhibits functions reminiscent of vertebrate microglia, depending on the context; astrocyte-like cells clear neuronal debris as a consequence of neuronal remodeling during metamorphosis, whereas ensheathing glia clears neuronal debris during neurite injury in the adult brain (Doherty et al., 2008; Tasdemir-Yilmaz and Freeman, 2014). Interestingly, by triggering an immune response (activation of the Imd pathway) in glial cells resulted in the appearance of a non-neural/non-glial cell type within the brain neuropil that appeared to be migratory, and expressed markers for phagocytosis (Stratoulias and Heino, 2015). It is tempting to draw a close functional and ontogenetic connection between these cells, derived from immune-challenged glia or hemocytes (or both), and vertebrate microglia.

The conservation of many molecular pathways controlling their development and functions suggest that hemocytes in arthropods and blood cells in vertebrates, including microglia and other tissue-resident-macrophages, are homologous cell types. Certain types of macroglia, such as vertebrate astrocytes and *Drosophila* astrocyte-like cells, also share many functional properties, but it is currently uncertain whether this is based on homology on the cellular level. Thus, glial cells are absent from the nervous system of many basal metazoans (Hartline, 2011), and it is unclear that the common bilaterian ancestor possessed glial cells. Nevertheless, recent analyses provide an increasing body of evidence that molecular pathways controlling functions such as phagocytosis, transmitter re-uptake, or response to injury are shared between glial cells of vertebrates and *Drosophila* (Freeman, 2015), which would argue for a deep homology, where pre-existing, homologous gene networks controlling such functions were recruited into cells that then became glial cells. In all, due to its genetic amenability, progress to

understand the development and function of *Drosophila* glia has accelerated and will surely continue to yield valuable insight into glial biology in general.

Figures

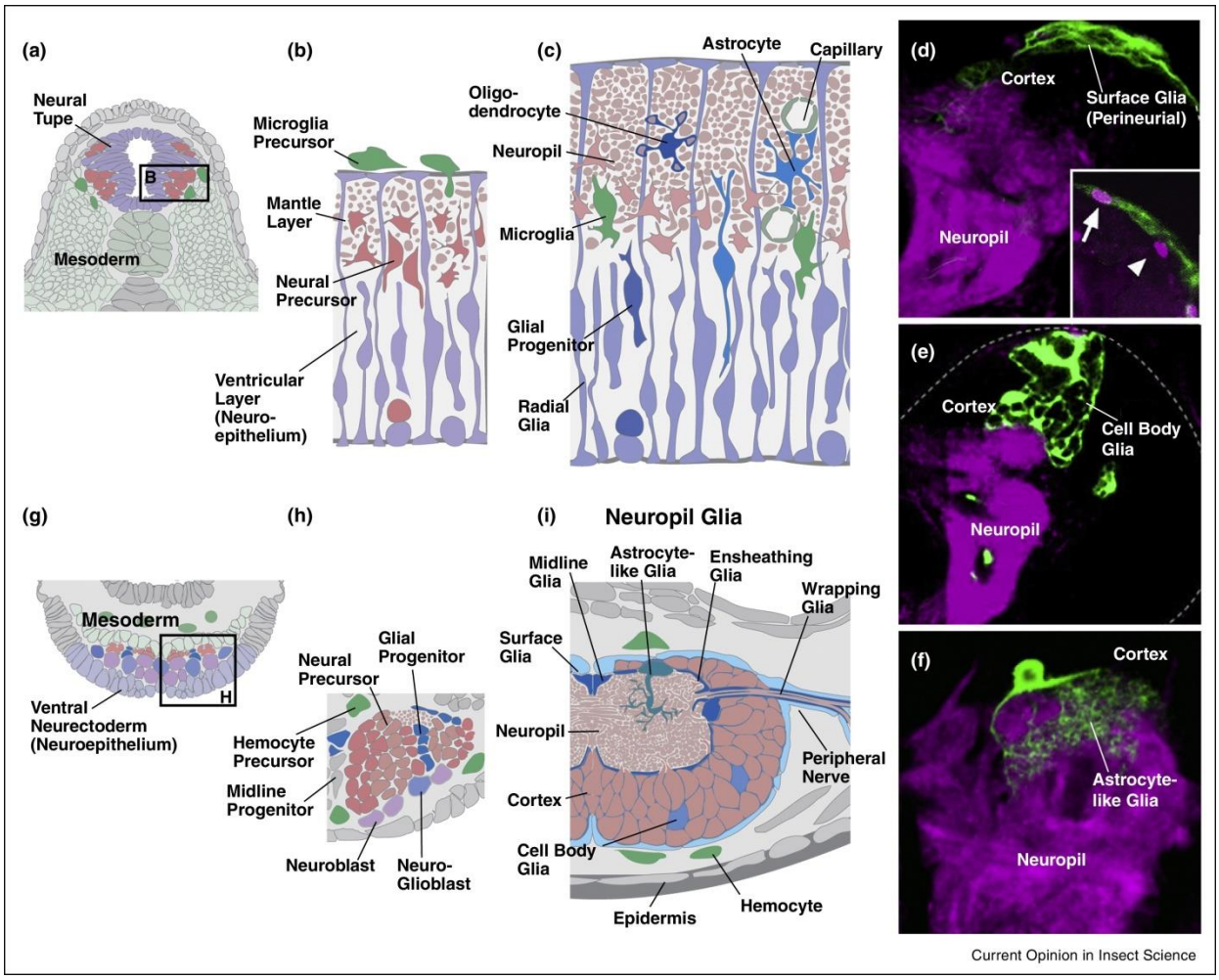

Figure Intro-1: (a–c) Schematic cross section of vertebrate neural tube at mid-embryo stage (a, b), and around birth (c). Neuroepithelial cells undergo symmetric and asymmetric divisions, thereby generating neural precursors and maintaining their own number. At later stages (c) neuroepithelial cells, now called radial glia, turn to the production of oligodendrocyte progenitors. Oligodendrocyte progenitors produce oligodendrocytes which have large, lamellar processes that assemble into the myelin sheath around long axons in the white matter of the CNS. Other radial glial cells become astrocytes (blue) which ensheath terminal nerve processes and synapses, as

well as the capillary network; they form the blood–brain barrier. Microglial cells derived from yolk sac-derived hematopoietic cells spread throughout the mesoderm of the early embryo (a) and infiltrate the neural tube at later stages (b, c). Design of panels (b, c) after [52]. (d–f) Types of neuroglia in Drosophila. Frontal confocal sections of late larval brain hemisphere, depicting GFP-labeled clones of perineurial surface glia (d; 4-cell clone), cell body glia (single cell clone; e), and astrocyte-like neuropil glia (single cell clone; f). Arrow in inset of (d) marks Repo-positive nucleus located within the GFP labeled perineurial clone; arrowhead points at Repo-positive, GFP-negative nuclei underneath which represent subperineurial glia. In all three panels, the neuropil is labeled with antibody against Drosophila N-cadherin (magenta) (modified from [13,16]). (g–i) Schematic cross sections of Drosophila ventral nerve cord at embryonic stages 11 (g), 13 (h), and 16 (i). Neuroblasts and Neuro-Glioblasts delaminate from the neuroepithelium (g) and give rise to fixed neural or neuro-glial lineages by asymmetric division (h). Glial cells then spread out throughout the growing ventral nerve cord and adopt the shape and function of neuropil glia, cell body glia, and surface glia (i). Mesodermally-derived hemocytes migrate along the outer surface of the central nervous system but do not penetrate inside.

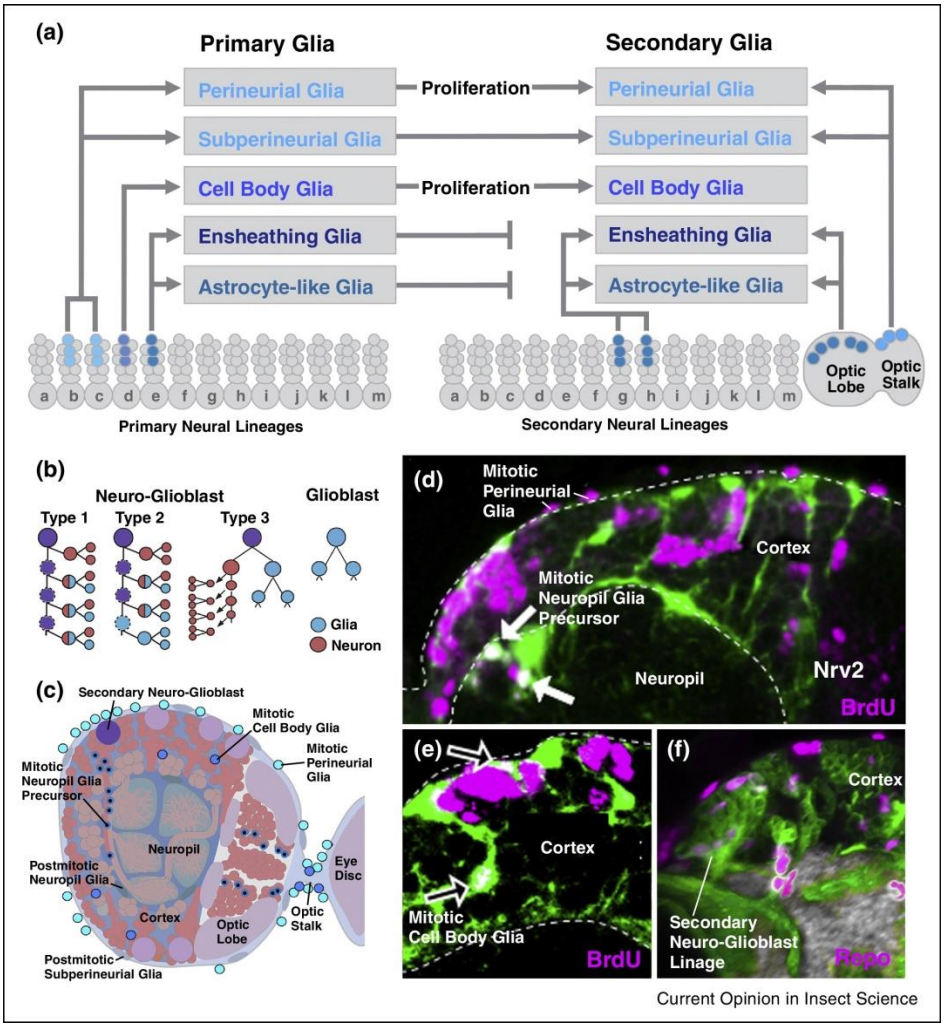

Figure Intro-2: Origin of primary (larval) and secondary (adult) glia. (a) In the embryo, primary glia arise from a small subset ('b, c, d, e') of proliferating, neural lineages ('a–m'). Primary perineurial glia and cell body glial cells remain mitotically active in the larva and generate secondary glia. Primary neuropil glial cells undergo programmed cell death during metamorphosis and are replaced by glial precursor cells generated from a different set of neural lineages ('g, h') that, along with all other neural lineages, undergo a secondary phase of proliferation during the larval period. Primary subperineurial glial cells most likely are retained into the adult period. The primordia of the optic lobe and eye, which proliferate in the larva, contribute a large number of secondary glia of all

types. (b) Proliferation pattern of glial progenitors as glioblasts, and type 1–3 neuro glioblasts (after [10,53]). (c) Schematic frontal section of late larval brain hemisphere, showing spatial relationship between differentiated primary glia and secondary glial progenitors. (d, e) Frontal confocal sections of part of late larval brain hemisphere showing proliferating (BrdU-positive; magenta) perineurial glia (d) and cell body glia (e), as well neuropil glia progenitors (d). Nrv-2-Gal4-activated GFP labels cell body glia and neuropil glia (green). (f) Repo-positive neuropil glia progenitors (magenta) form part of secondary lineages, labeled by anti-Neurotactin (green; modified from [13]).

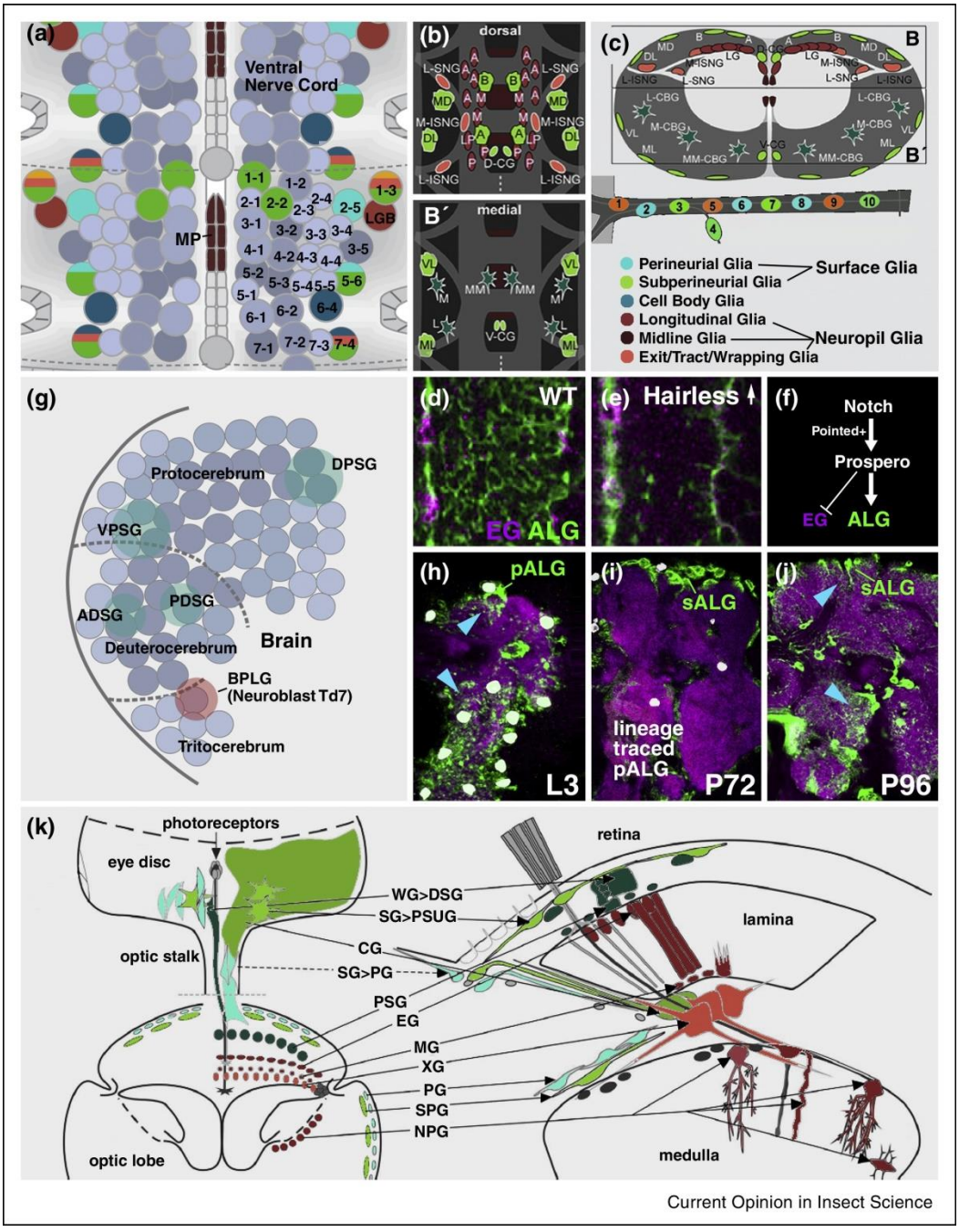

Figure Intro-3: Fatemap of glial progenitors. (a–c, g) Progenitors of primary glia of the larval ventral nerve cord and peripheral nerves (a–c), and brain (g). (a) Map of the ventral nerve cord with glioblasts and neuro-glioblasts identified by different coloring (after [40]). Neuroblasts and neuro-glioblasts of one hemineuromere are identified

alphanumerically. Lateral glioblast (LGB), Midline progenitors (MP). (b,c) Schematic horizontal sections (b, b0) and cross section (c) of late embryonic ventral nerve cord and peripheral nerve, showing location of glial cells, identified by same colors as their corresponding progenitors in (a), relative to the boundaries of neuromere, neuropil, and peripheral nerves (modified from [9,30,40]). Boxed areas in (c) indicate dorso-ventral levels of corresponding horizontal sections shown in (b, b0). Bottom of (c) color key for types of glia used in schematic drawings of panels (a–c, g, k). (d–f) Fate decision between astrocyte-like glia (ALG, green) and ensheathing glia (EG, magenta) depends on Notch activity. Antagonism of the Notch pathway with Hairless overexpression (e) changes structural phenotype of ALG into that of EG (from [20], with permission). (g) Schematic neuroblast map of the brain, indicating boundaries between the brain neuromeres protocerebrum, deuterocerebrum, and tritocerebrum, and approximate location of glial progenitor clusters giving rise to surface and cell body glia in the protocerebrum (DPSG, VPSG) and deuterocerebrum (ADSG, PDSG), and to neuropil glia (BPLG; neuroblast Td7) (after [13]). (h–j) Frontal confocal section of brain hemisphere of late larva (h), mid-stage pupa (i), and pharate adult (j), showing development of astrocyte-like glia. Primary astrocyte-like glia (pALG) are lineage-traced from larva onward (white nuclei); these cells are no longer detectable in adult. Secondary astrocyte-like glia (sALG), produced in the larva, spread out over the neuropil surface (i) and differentiate in the late pupa (j; reticular processes of pALG and sALG indicated by cyan arrowheads) (from [13]). (k) Fatemap of glia in the optic lobe. Schematic cross sections of larval optic lobe and eye disc (left) and adult optic lobe (right). Nomenclature of optic lobe glia and relationship between larval progenitors and

adult glial types is indicated by coloring and arrows. For color code see (c). Abbreviations: CG, carpet glia; DSG, distal satellite glia; EG, epithelial glia; MG, marginal glia; NPG, neuropil glia; PG, perineurial glia; PSUG, pseudocartridge glia; SG, surface glia; SPG, subperineurial glia; XG, outer optic chiasm glia (modified with permission from [33]).

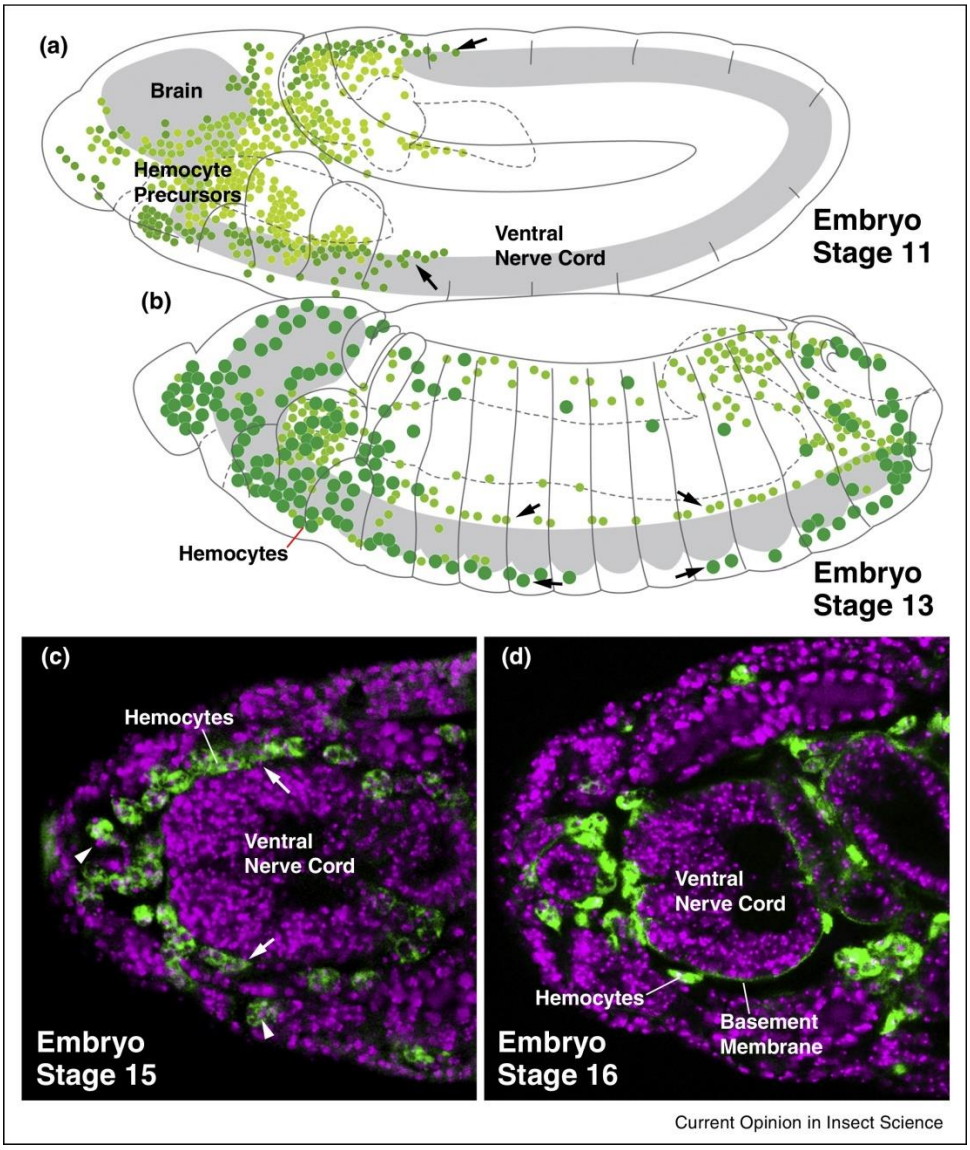

Figure Intro-4: Origin and migration of hemocytes. (a,b) Drawings of embryos (lateral view) at stage 11 (a) and 13 (b). Profiles of interior structures are shaded (brain, ventral nerve cord) or given as dashed lines (gut primordia). The distribution of hemocyte precursors (small light green circles) and differentiated, phagocytotic hemocytes (large, dark green circles) is indicated, based on camera lucida drawings of anti-Peroxidasin labeled whole mount of representative embryo. Hemocytes migrate along the surface of the CNS (arrows) and other organs (from [41], with permission). (c,d) Horizontal

confocal sections of anterior ventral nerve cord at embryonic stage 15 (c) and 16. Nuclei of all cells labeled by Sytox (magenta). Differentiated hemocytes are labeled by anti-Peroxidasin; they contain phagolysomes with cellular debris (arrowhead) and are associated with the surface of the ventral nerve cord. By stage 16, hemocytes have deposited a Peroxidasin-positive basement membrane around nerve cord (d).

References

Altenhein B: Glial cell progenitors in the Drosophila embryo. *Glia* 2015, 63:1291-1302. DOI: 10.1002/glia.22820

Avet-Rochex A, Kaul AK, Gatt AP, McNeill H, Bateman JM: Concerted control of gliogenesis by InR/TOR and FGF signalling in the Drosophila post-embryonic brain. *Development* 2012, 139:2763-2772. DOI: 10.1242/dev.074719

Avet-Rochex A, Maierbrugger KT, Bateman JM: Glial enriched gene expression profiling identifies novel factors regulating the proliferation of specific glial subtypes in the Drosophila brain. *Gene Expr Patterns* 2014, 16:61-68. DOI: 10.1016/j.gep.2014.09.001

Awad TA, Truman JW: Postembryonic development of the midline glia in the CNS of Drosophila: proliferation, programmed cell death, and endocrine regulation. *Dev Biol* 1997, 187:283-297. DOI: 10.1006/dbio.1997.8587

Awasaki T, Lai SL, Ito K. Lee T: Organization and postembryonic development of glial cells in the adult central brain of Drosophila. *J Neurosci* 2008, 28:13742-13753. DOI: 10.1523/JNEUROSCI.4844-08.2008

Bauke AC, Sasse S, Matzat T, Klämbt C: A transcriptional network controlling glial development in the Drosophila visual system. *Development* 2015, 142:2184-2193. DOI: 10.1242/dev.119750

Bayraktar OA, Fuentealba LC, Alvarez-Buylla A, Rowitch DH: Astrocyte development and heterogeneity. *Cold Spring Harb Perspect Biol* 2014, 7:a020362. DOI: 10.1101/cshperspect.a020362

Beckervordersandforth RM, Rickert C, Altenein B, Technau GM: Subtypes of glial cells in the Drosophila embryonic ventral nerve cord as related to lineage and gene expression. *Mech Dev* 2008, 125:542-557. DOI: 10.1016/j.mod.2007.12.004

Bernardoni R, Vivancos V, Giangrande A: glide/gcm is expressed and required in the scavenger cell lineage. *Dev Biol* 1997, 191:118-130. DOI: 10.1006/dbio.1997.8702

Bossing T, Technau GM: The fate of the CNS midline progenitors in Drosophila as revealed by a new method for single cell labeling. *Development* 1994, 120:1895-1906.

Cantera R: Glial cells in adult and developing prothoracic ganglion of the hawk moth Manduca sexta. *Cell Tissue Res* 1993, 272:93-108.

Chell JM, Brand AH: Nutrition-responsive glia control exit of neural stem cells from quiescence. *Cell* 2010, 143:1161-1173. DOI: 10.1016/j.cell.2010.12.007

Chotard C, Salecker I: Glial cell development and function in the Drosophila visual system. *Neuron Glia Biol* 2007, 3:17-25. DOI: 10.1017/S1740925X07000592

Colonques J, Ceron J, Tejedor FJ: Segregation of postembryonic neuronal and glial lineages inferred from a mosaic analysis of the Drosophila larval brain. *Mech Dev* 2007, 124:327-340. DOI: 10.1016/j.mod.2007.01.004

Doherty J, Logan MA, Tasdemir OE, Freeman MR: Ensheathing glia function as phagocytes in the adult Drosophila brain. *J Neurosci* 2009, 29:4768-4781. DOI: 10.1523/JNEUROSCI.5951-08.2009

Edwards TN, Nuschke AC, Nern A, Meinertzhagen IA: Organization and metamorphosis of glia in the Drosophila visual system. *J Comp Neurol* 2012, 520:2067-2085. DOI: 10.1002/cne.23071

Fischbach KF, Hiesinger PR: Optic lobe development. *Adv Exp Med Biol* 2008, 628:115-136. DOI: 10.1007/978-0-387-78261-4_8

Freeman MR: Drosophila central nervous system glia. *Cold Spring Harb Perspect Biol* 2015, 7: pii:a020552. DOI: 10.1101/cshperspect.a020552

Hartenstein V, Nassif C, Lekven A: Embryonic development of the Drosophila brain. II. Pattern of glial cells. *J Comp Neurol* 1998, 402:32-47.

Hartenstein V: Morphological diversity and development of glia in Drosophila. *Glia* 2011, 59:1237-1252. DOI: 10.1001/glia.21162

Hartline DK: The evolutionary origins of glia. *Glia* 2011, 59:1215-1236. DOI: 10.1002/glia.21149

Hoyle G: Glial cells of an insect ganglion. *J Comp Neurol* 1986, 246:85-103. DOI: 10.1002/cne.902460106

Huang Y, Ng FS, Jackson FR: Comparison of larval and adult Drososphila astrocytes reveals stage-specific gene expression profiles. *G3 (Bethesda)* 2015, 5:551-558. DOI: 10.1534/g3.114.016162

Ito K, Urban J, Technau GM: Distribution, classification, and development of Drosophila glial cells in the late embryonic and early larval ventral nerve cord. *Roux's archives of developmental biology* 1995, 204:284-307. DOI: 10.1007/BF02179499

Izergina N, Balmer, J, Bello B, Reichert H: Postembryonic development of transit amplifying neuroblast lineages in the Drosophila brain. *Neural Dev* 2009, 4:44. DOI: 10.1186/1749-8104-4-44

Kriegstein A, Alvarez-Buylla A: The glial nature of embryonic and adult neural stem cells. *Annu Rev Neurosci* 2009, 32:149-184. DOI: 10.1146/annurev.neuro.051508

Lavin Y, Mortha A, Rahman A, Merad M: Regulation of macrophage development and function in the peripheral tissues. *Nat Rev Immunol* 2015, 15:731-744. DOI: 10.1038/nri3920

Lebestky T, Chang T, Hartenstein V, Banerjee U: Specification of Drosophila hematopoietic lineage by conserved transcription factors. *Science* 2000, 288:146-149. DOI: 10.1126/science.288.5463.146

Limmer S, Weiler A, Volkenhoff A, Babatz F, Klämbt C: The Drosophila blood-brain barrier: development and function of a glial endothelium. *Front Neurosci* 2014, 8:365. DOI: 10.3389/fnins.2014.00365

Liu H, Zhou B, Yan W, Lei Z, Zhao X, Zhang K, Guo A: Astrocyte-like glial cells physiologically regulate olfactory processing through the modification of ORN-PN synaptic strength in Drosophila. *Eur J Neurosci* 2014, 40:2744-2754. DOI: 10.1111/ejn.12646

Macnamee SE, Liu KE, Gerhard S, Tran CT, Fetter RD, Cardona A, Tolbert LP, Oland LA: Astrocytic glutamate transport regulates a Drosophila CNS synapse that lacks astrocyte ensheathment. *J Comp Neurol* 2016, 524:1979-1998. DOI: 10.1002/cne.24016

Melom JE, Littleton JT: Mutation of a NCKX eliminates glial microdomain calcium oscillations and enhances seizure susceptibility. *J Neurosci* 2013, 33:1169-1178.

Miller RH: Regulation of oligodendrocyte development in the vertebrate CNS. *Prog Neurobiol* 2002, 67:451-467. DOI: 10.1016/S0301-0082(02)00058-8

Ngo KT, Wang J, Junker M, Kriz S, Vo G, Asem B, Olson JM, Banerjee U, Hartenstein V: Concomitant requirement for Notch and Jak/Stat signaling during neuro-epithelial differentiation in the Drosophila optic lobe. *Dev Biol* 2010, 346:284-295. DOI: 10.1016/j.ydbio.2010.07.036

Olofsson B, Page DT: Condensation of the central nervous system in embryonic Drosophila is inhibited by blocking hemocyte migration or neural activity. *Dev Biol* 2005, 279:233-243. DOI: 10.1016/j.ydbio.2004.12.020

Omoto JJ, Yogi P, Hartenstein V: Origin and development of neuropil glia of the Drosophila larval and adult brain: Two distinct glial populations derived from separate progenitors. *Dev Biol* 2015, 404:2-20. DOI: 10.1016/j.ydbio.2015.03.004

Peco E, Davla S, Camp D, M Stacey S, Landgraf M, van Meyel DJ: Drosophila astrocytes cover specific territories of the CNS neuropil and are instructed to differentiate by Prospero, a key effector of Notch. *Development* 2016, 143:1170-1181. DOI: 10.1242/dev.133165

Pereanu W, Shy D, Hartenstein V: Morphogenesis and proliferation of the larval brain glia in Drosophila. *Dev Biol* 2005, 283:191-203. DOI: 10.1016/j.ydbio.2005.04.024

Reddy BV, Irvine KD: Regulation of Drosophila glial cell proliferation by Merlin-Hippo signaling. *Development* 2011, 138:5201-5212. DOI: 10.1242/dev.069385

Sears HC, Kennedy CJ, Garrity PA: Macrophage-mediated corpse engulfment is required for normal Drosophila CNS morphogenesis. *Development* 2003, 130:3557-3565. DOI: 10.1242/dev.00586

Sonnenfeld MJ, Jacobs JR: Macrophages and glia participate in the removal of apoptotic neurons from the Drosophila embryonic nervous system. *J Comp Neurol* 1995, 359:644-652. DOI: 10.1002/cne.903590410

Spindler SR, Ortiz I, Fung S, Takashima S, Hartenstein V: Drosophila cortex and neuropile glia influence secondary axon tract growth, pathfinding, and fasciculation in the developing larval brain. *Dev Biol* 2009, 334:355-368. DOI: 10.1016/j.ydbio.2009.07.035

Stork T, Sheehan A, Tasdemir-Yilmaz OE, Freeman MR: Neuron-glia interactions through the Heartless FGF receptor signaling pathway mediate morphogenesis of Drosophila astrocytes. *Neuron* 2014, 83:388-403. DOI: 10.1016/j.neuron.2014.06.026

Stratoulias V, Heino TI: MANF silencing, immunity induction or autophagy trigger an unusual cell type in metamorphosing Drosophila brain. *Cell Mol Life Sci* 2015, 72:1989-2004. DOI: 10.1007/s00018-014-1789-7

Tasdemir-Yilmaz OE, Freeman MR: Astrocytes engage unique molecular programs to engulf pruned neuronal debris from distinct subsets of neurons. *Genes Dev* 2014, 28:20-33. DOI: 10.1101/gad.229518.113

Tepass U, Fessler LI, Aziz A, Hartenstein V: Embryonic origin of hemocytes and their relationship to cell death in Drosophila. *Development* 1994, 120:1829-1837.

Unhavaithaya Y, Orr-Weaver TL: Polyploidization of glia in neural development links tissue growth to blood-brain barrier integrity. *Genes Dev* 2012, 26:31-36. DOI: 10.1101/gad.177436.111

Urbach R, Schnabel R, Technau GM: The pattern of neuroblast formation, mitotic domains and proneural gene expression during early brain development in Drosophila. *Development* 2003, 130:3589-3606. DOI: 10.1242/dev.00528

Viktorin G, Riebli N, Popkova A, Giangrande A, Reichert H: Multipotent neural stem cells generate glial cells of the central complex through transit amplifying intermediate progenitors in Drosophila brain development. *Dev Biol* 2011, 356:553-565. DOI: 10.1016/j.ydbio.2011.06.013

Volkenhoff A, Weiler A, Letzel M, Stehling M, Klämbt C, Schirmeier S: Glial glycolysis is essential for neuronal survival in Drosophila. *Cell Metab* 2015, 22:437-447. DOI: 10.1016/j.cmet.2015.07.006

Von Hilchen CM, Beckervordersandforth RM, Rickert C, Technau GM, Altenhein B: Identity, origin, and migration of peripheral glial cells in the Drosophila embryo. *Mech Dev* 2008, 125:337-352. DOI: 10.1016/j.mod.2007.10.010

Von Hilchen CM, Bustos AE, Giangrande A, Technau GM, Altenhein B: Predetermined embryonic glial cells form the distinct glial sheaths of the Drosophila peripheral nervous system. *Development* 2013, 140:3657-3668. DOI: 10.1242/dev.093245

Chapter 1 - Origin and development of neuropil glia of the *Drosophila* larval and adult brain: Two distinct glial populations derived from separate progenitors

Abstract

Glia comprise a conspicuous population of non-neuronal cells in vertebrate and invertebrate nervous systems. *Drosophila* serves as a favorable model to elucidate basic principles of glial biology in vivo. The *Drosophila* neuropil glia (NPG), subdivided into astrocyte-like (ALG) and ensheathing glia (EG), extend reticular processes which associate with synapses and sheath-like processes which surround neuropil compartments, respectively. In this paper we characterize the development of NPG throughout fly brain development. We find that differentiated neuropil glia of the larval brain originate as a cluster of precursors derived from embryonic progenitors located in the basal brain. These precursors undergo a characteristic migration to spread over the neuropil surface while specifying/differentiating into primary ALG and EG. Embryonically-derived primary NPG are large cells which are few in number, and occupy relatively stereotyped positions around the larval neuropil surface. During metamorphosis, primary NPG undergo cell death. Neuropil glia of the adult (secondary NPG) are derived from type II lineages during the postembryonic phase of neurogliogenesis. These secondary NPG are much smaller in size but greater in number than primary NPG. Lineage tracing reveals that both NPG subtypes derive from intermediate neural progenitors of multipotent type II lineages. Taken together, this study reveals previously uncharacterized dynamics of NPG development and provides a framework for future studies utilizing *Drosophila* glia as a model.

Introduction

Drosophila glial cells have become a genetically-tractable in vivo system to understand fundamental aspects of glial cell biology. Glial cells are divided into three basic classes defined by topology, cell morphology, and function (Awasaki et al., 2008; Ito et al., 1995; Pereanu et al., 2005; Xiong et al., 1994). (1) Surface glia, further subdivided into subperineurial and perineurial glia, have cell bodies which lie on the brain surface. These glia extend flattened processes which encapsulate the entire outer brain surface and together form a structure analogous to the blood–brain–barrier (DeSalvo et al., 2011; Stork et al., 2008). (2) Cortex glia (or cell body-associated glia), of which there is only one subtype, possess cell bodies located within the cellular cortex amongst the somata of differentiated neurons. This class extends processes which encapsulate neuronal cell bodies and neuroblasts, forming the so-called “trophospongium” (Dumstrei et al., 2003; Hoyle, 1986; Hoyle et al., 1986). (3) Neuropil glia have somata at the neuropil-cortex interface and associate with the various neuropil compartments of the fly brain. Two distinct neuropil glia subtypes have been identified (Awasaki et al., 2008; Doherty et al., 2009; Pereanu et al., 2005). One subtype, known as reticular or astrocyte-like glia (ALG), extends processes that extend into the neuropil. These extensively branched processes are in close association with terminal neurites and synapses, situating them in a position to modulate neurotransmission, similarly to the vertebrate astrocyte. The second subtype, known as ensheathing glia (EG), extends sheath-like processes around the neuropil and some of the major axon tracts, but lack processes which penetrate into the neuropil.

A number of recent studies have shown that neuropil glia (ALG in particular) express amino acid transporters important for the reuptake of neurotransmitters, such as glutamate and γ-aminobutyric acid transporter (GABA) (Stacey et al., 2010; Stork et al., 2014). As a result, neuropil glia play a crucial role in controlling the encoding of specific behaviors. The concentration of transmitters, that in turn depends on re-uptake by glial cells, will either strengthen or weaken synaptic transmission and/or neurotransmitter tone (Grosjean et al., 2008; Jackson and Haydon, 2008; Sinakevitch et al., 2010; Stork et al., 2014). In addition to their physiological role in mature brain function, ALG and EG also appear to play multiple roles during neural development. Interestingly, different neuropil glia subtypes phagocytose accumulating neuronal debris in a context dependent manner. EG, which express the engulfment receptor Draper and dCed-6, are important for clearing axonal debris due to injury in adult brains (Doherty et al., 2009), whereas ALG, also expressing Draper, are responsible for the uptake of pruned axons from neurons that are remodeled during metamorphosis (Tasdemir-Yilmaz and Freeman, 2014). Furthermore, neuropil glia also play a part in the construction of neuronal circuitry, by aiding in axonal guidance, terminal branching, and synaptogenesis (Hidalgo et al., 1995; Muthukumar et al., 2014; Spindler et al., 2009).

Studies of the developmental origin, migration patterns and morphogenesis of glia are essential in understanding the role of glia during nervous system development. Such studies will also provide the genetic tools to selectively eliminate groups of glial cells, by, for example, ablating the progenitor type that produces them.

The embryonic origin of glia has been mapped in detail for the embryonic ventral nerve cord (VNC) (Beckervordersandforth et al., 2008; Ito et al., 1995; Schmidt et al.,

1997). Here, neuropil glia (also known as longitudinal glia), derive from a single lateral glioblast (LGB). The LGB progeny migrate towards the longitudinal connectives, undergo several rounds of mitotic divisions to produce a cluster of 9 cells per hemineuromere, and subsequently migrate around and encapsulate the neuropil (Beckervordersandforth et al., 2008; Ito et al., 1995; Jacobs et al., 1989). Late during embryogenesis, longitudinal glia are thought to be differentially specified by a largely unknown mechanism to generate ensheathing and astrocyte-like glia. Neuropil glia of the brain originate from one or a small set of neuroblasts at the deutero-tritocerebral boundary, from where they migrate over the brain neuropil surface while likely undergoing several rounds of divisions (Hartenstein et al., 1998).

Studies of postembryonic glial development are restricted to the brain. Pereanu et al. (2005) observed that all glial classes increase in number during late larval stages and attributed this growth primarily to secondary proliferation of neuroblasts, as well as mitotic divisions of differentiated glia and/or persistent glial precursors generated in the embryo. Consistent with this notion, posteriorly-located type II neuroblasts, which generate large lineages via intermediate neural progenitors (INPs), have been shown to generate glia during the early phase of postembryonic proliferation (Bayraktar and Doe, 2013; Izergina et al., 2009; Viktorin et al., 2011; Yu et al., 2013). As they spread out around the neuropil in the pupa, these glial cells continue to proliferate. The molecular mechanisms, such as the FGF, InR/TOR, and Merlin-Hippo signaling pathways, which mediate subtype-specific, post-embryonic gliogenesis are just beginning to be elucidated (Avet-Rochex et al., 2012; Reddy and Irvine, 2011).

In the present study we address several fundamental aspects of neuropil glial origin and development which have remained elusive. Astrocyte-like and ensheathing glia have been described in both the larval and adult brain (Awasaki et al., 2008; Pereanu et al., 2005). At least in the larva, both classes of differentiated neuropil glia comprise a relatively small number of cells (this study). Are these primary glia fixed in number, similar to primary neurons? Is their location, in relation to specific neuropil compartments, invariant? Do both classes contribute equally to the neuropil sheath? In terms of development, a crucial question is how, if at all, are the larval and adult neuropil glia related? Are both derived from the same embryonic progenitor pool? Do larval glial cells proliferate to give rise to adult glia? Does the same class of progenitors produce both ALG and EG? Here, using specific markers for ALG (*NP3233-Gal4*; *alrm-Gal4*; anti-GAT) and EG (*NP6520-Gal4*) (Awasaki et al. 2008; Doherty et al., 2009; Stork et al., 2014) in conjunction with lineage tracing experiments, we have reconstructed the origin and developmental fate of neuropil glia of the *Drosophila* brain. This analysis demonstrates that a small population of approximately 30 primary ALG and EG originates in the basal brain from where they spread out to occupy stereotyped positions around the neuropil by the early larva. These primary ALG and EG do not proliferate during the larval period, but increase in nuclear/cytoplasmic size and process length to accommodate the increase in neuropil volume. During metamorphosis, primary ALG lose their branched morphology and subsequently undergo programmed cell death. Secondary neuropil glia originate from a different progenitor pool than primary glia, which includes several of the dorsomedial type II lineages. Secondary neuropil glia increase in number while spreading out around the neuropil surface and

the emerging compartments of the central complex during the late larval and early pupal period. They extend processes into the neuropil starting around P60–72 (hrs after puparium formation), a developmental time period which corresponds to synaptic maturation.

Materials and methods

Fly Stocks

Flies were grown at 25 °C using standard fly media unless otherwise noted. The following fly stocks were used (sources in parentheses): *NP3233-Gal4* and *NP6520-Gal4* (Awasaki et al., 2008) (Kyoto *Drosophila* Genetic Resource Center), *alrm (astrocytic leucine-rich repeat molecule)-Gal4* (Doherty et al., 2009) (kind gift from M. Freeman, University of Massachusetts Medical School, Worcester, MA), *MZ1407 (inscuteable)-Gal4* (kind gift from H. Reichert, Biozentrum, University of Basel, Basel, Switzerland), *tub-Gal80^{ts}, UAS-Redstinger6, UAS-mCD8-GFP, UAS-FLP^{JD1}, hs-FLP^{1}, UAS-mCD8-GFP.nls, R9D11 (earmuff)-Gal4* (Bayraktar et al., 2010), *acj6-Gal4, sine oculis-Gal4, UAS-EGFR^{DN}, engrailed-Gal4, Act5C>Stop>lacZ (Act5C promoter-FRT-phl[+]-FRT-lacZ.nls), tub-FRT-GAL80-FRT-GAL4* (Zecca and Struhl, 2002) (Bloomington Stock Center).

Clonal analysis and lineage tracing experiments

Single cell, primary neuropil glia flp-out clones were generated using flies bearing the genotype: *hs-FLP^{1}, UAS-mCD8-GFP/+; UAS-mCD8-GFP/+; tub-FRT-GAL80-FRT-GAL4* (Zecca and Struhl, 2002). Briefly, embryos were heat-shocked at 38 °C for 5 min and raised in 18 °C until wandering third instar larva; third instar larval brains were dissected and processed for immunohistochemistry (see below). Flies bearing the genotype *UAS-FLP^{JD1}; tub-Gal80^{ts}/Act5C>Stop>lacZ; alrm-Gal4/+* were used to determine the fate of primary astrocyte-like glia in the pupa. Briefly, embryos were collected for 48 h in 18 °C; freshly hatched larvae were raised in 29 °C for 24 h, and placed back in 18 °C until specified extrapolated pupal time points (development in 18

°C is roughly twice as long as 25 °C). *UAS-FLP^{JD1}, Act5C>Stop>lacZ* flies were also crossed to appropriate Gal4 lines and stained with anti-GAT antibody at P48 or stained with anti-Repo antibody in the wandering third instar larva, to determine the lineage of secondary astrocyte-like glia or secondary neuropil glia precursors, respectively.

Immunostaining and TUNEL assay

Samples were fixed in 4% methanol-free formaldehyde in phosphate buffered saline (PBS, Fisher-Scientific, pH=7.4; Cat No. #BP399-4). Tissues were permeabilized in PBT (PBS with 0.1% or 0.3% Triton X-100, pH=7.4) and immunohistochemistry was performed using standard procedures (Ashburner, 1989). Embryos were dechorionated in 50% bleach, fixed in equal ratio PEMS (0.1 M Pipes, 2 mM MgSO4, 1 mM EGTA, pH 7.0) buffered 4% formaldehyde and heptane. Embryos were then devitellinized in methanol, rehydrated in PBT and stained using standard procedures (Ashburner, 1989). The following antibodies were provided by the Developmental Studies Hybridoma Bank (Iowa City, IA): mouse anti-Repo (repo, 1:10), mouse anti-Neurotactin (BP106, 1:10), rat anti-DN-cadherin (DN-EX #8, 1:20), and mouse anti-Bruchpilot (nc82, 1:30). For third instar larval staining of Neurotactin, samples were subjected to a methanol dehydration series (25, 50, and 100% for 20 min each) after fixation, prior to staining. We also used mouse or rabbit anti-β-galactosidase (1:100, Promega), rabbit anti- C-terminus γ-aminobutyric acid transporter (GAT, 1:3000) (kind gift from M. Freeman, University of Massachusetts Medical School, Worcester, MA) and rabbit anti-Labial (1:200) (kind gift from H. Reichert, Biozentrum University of Basel, Basel, Switzerland). Secondary antibodies, IgG1 (Jackson ImmunoResearch; Molecular Probes) were used at the following dilutions: Alexa 546-conjugated anti-mouse (1:500), Cy3-conjugated anti-

mouse (1:500), Cy5-conjugated anti-rat (1:400), Alexa 568-conjugated anti-mouse (1:500), Alexa 568-conjugated anti-rabbit (1:400), Alexa 488-conjugated anti-mouse (1:400). For terminal deoxynucleotidyl transferase dUTP nick end labeling (TUNEL), we used the In Situ Cell Death Detection Kit, Fluorescein (Roche). Briefly, P24 brains were dissected directly in cold 4% methanol-free formaldehyde and fixed for 45 min, followed by cold PBS washes and an ethanol dehydration series (5, 10, 20, 40, 75, 100% for 5 min each). After an overnight incubation in 100% EtOH at 4 °C, samples were rehydrated in 0.3% PBT and stained with antibodies using standard procedures. Immunostained samples were incubated in 1:10 TUNEL reaction mixture for 1 h and 15 min and prepared for imaging.

Confocal microscopy and analysis

Staged *Drosophila* embryonic, larval, pupal, and adult brains labeled with suitable markers were viewed as whole-mounts by confocal microscopy [LSM 700 Imager M2 using Zen 2009 (Carl Zeiss Inc.); lenses: 40× oil (numerical aperture 1.3)]. Complete series of optical sections were taken at 2-µm intervals. Captured images were processed by ImageJ or FIJI (National Institutes of Health, http://rsbweb.nih.gov/ij/ and http://fiji.sc/) and figures assembled in Adobe Photoshop. Cell counts and nuclear size measurements were carried out manually using the “Cell Counter” and “Measure” plugins in ImageJ. All error bars represent ±Stdev. Neuropil glia counts for embryonic brains were carried out for one hemisphere from the deutero-tritocerebral boundary to the supraesophageal commissure. Neuropil glia counts for larval brains were carried out for the supraesophageal ganglion specifically.

Registration and generation of three-dimensional models

Digitized images of confocal sections were processed in ImageJ and imported into FIJI (Schindelin et al., 2012; http://fiji.sc/). Surface renderings of first and third instar larval brains stained with anti-DN-cadherin and anti-Bruchpilot, respectively, were generated as volumes in the 3-dimensional viewer in FIJI. Particularly well oriented samples (for both L1 and L3) in which the peduncles were aligned with the z-axis of the stack, were chosen as the "standard" brains for registration. In FIJI, using the "Name Landmarks and Register" plugin (http://fiji.sc/Name_Landmarks_and_Register), fiducial markers were placed at spatially reproducible landmarks on the standard brain throughout the neuropil surface (ex. entry points for specific lineages). The digitized confocal section images of *alrm-Gal4, UAS-mCD8-GFP* brains were registered to the standard brains, imported using the TrakEM2 plugin in FIJI software (Cardona et al., 2012), and glial cell bodies were indicated (as spheres) on surface renderings using TrakEM2.

Results

Astrocyte-like and ensheathing glia of the larval and adult brain

The *Drosophila* larval and adult brains contain populations of Repo-positive ensheathing and astrocyte-like glia which can be labeled by the neuropil glia subtype-specific Gal4 drivers, *NP6520-Gal4* and *NP3233* or *alrm-Gal4*, respectively (Fig. 1A–F). Similarly to neurons, these populations are derived from primary and secondary neuroblast lineages and therefore we classify them as primary (larval) and secondary (adult) neuropil glia (pNPG and sNPG) (see later sections). However, unlike primary neurons, many of which are remodeled and retained into adulthood, pNPG are not retained into adulthood (see later sections). EG extend sheath-like processes around neuropil compartments and axon tracts (Fig. 1A–C; see Table 1 for abbreviations). Single cell clonal analysis in the third instar larva demonstrates that primary EG (pEG) typically have enlarged, flattened cell bodies (Fig. 1B and G). The processes of a single primary ensheathing glial cell can ensheath the border of a neuropil compartment and incoming secondary axon tracts simultaneously (Fig. 1B; inset). Secondary EG (sEG) are prominent around major tracts and central complex of the adult brain (Fig. 1C). ALG extend highly branched processes with dendritic/reticular morphology into neuropil compartments (Fig. 1D–F). Flp-out clonal analysis of a single, primary astrocyte-like glial cell in the third instar larva reveals details of their complex morphology. Primary astrocyte-like glia (pALG) have very large, rounded cell bodies and nuclei in comparison to neurons, and even in comparison to pEG (Fig. 1E and G). They extend a variable number of processes which are relatively thick where they branch off the soma (“root processes”), but branch distally into a dense network of fine fibers (“distal processes”)

(Fig. 1E1 and H). The processes of a single primary astrocyte-like glial cell typically infiltrates more than one neuropil compartment (e.g., the antennal lobe and anterior peri-esophageal compartment as shown in Fig. 1E2 and E2′), and often traverses a large neuropil volume. sALG of the adult brain are smaller in size and far more numerous than the pALG of the larval brain (Fig. 1F and G). We utilized double labeling of the two pNPG subpopulations in order to assess the spatial relationship between the pALG and pEG at the neuropil surface (Fig. 1I). ALG stably express the γ-aminobutyric acid transporter (GAT) on their soma as well as on their membrane protrusions; this serves as a specific, reliable marker for ALG (Stork et al., 2014; Supp. Info. Fig. S1). The entire neuropil surface is encapsulated by the membrane contributions of the two NPG subtypes. Most of the neuropil surface is covered with the large, flattened pEG (Fig. 1J and J′). This EG sheath is disrupted by gaps which are filled by the cell bodies of ALG (Fig. 1J and J′). The processes emanating from pALG somata most frequently extend directly into the neuropil, however, they occasionally grow tangentially along the neuropil surface, passing over pEG sheaths before entering the neuropil through a gap in the pEG (Fig. 1K–M).

Development of neuropil glia around the embryonic brain

Progenitors of the primary neuropil glia form part of the population of neuroglioblasts/glioblasts that have been described for the embryo. In the thoracic and abdominal neuromeres of the ventral nerve cord, as well as the gnathal neuromeres, neuropil (longitudinal) glia are derived from a single paired cell, the lateral glioblast (Beckervordersandforth et al., 2008; Jacobs et al., 1989). Brain neuropil glial progenitors form a small cluster of Repo-positive cells, called the basal procephalic

longitudinal glia (BPLG), located at the boundary between the tritocerebrum and deuterocerebrum (Hartenstein et al., 1998) (Fig. 2A and B). The glial determinant *glial cells missing* (*gcm*) is known to be required and sufficient for gliogenesis and is expressed early in glial lineages (Hosoya et al., 1995; Jones et al., 1995; Vincent et al., 1996). The brain neuroblast map by Urbach and Technau, 2003 demonstrated that there is a single *gcm*-positive neuroblast amongst the tritocerebral neuroblasts which is likely to represent the neuroglioblast (or glioblast) that generates the BPLG (Fig. 2C). It has been shown (Beckervordersandforth et al., 2008; Ito et al., 1995) that neuropil glia of the VNC migrate towards the dorsal surface of the nascent neuropil; by stage 14, they form a continuous double row of Repo-positive cells along the dorsal surface of the VNC (Fig. 2D). Likewise, neuropil glia of the brain derived from the BPLG cluster, assemble at the medial surface of the brain neuropil, reaching dorsally to a level where the brain commissure will appear (Fig. 2E). 53±9% (n=5) of the Repo-positive neuropil glia expresses *alrm*/GAT, attesting to the fate of these cells as presumptive pALG. During stages 15 and 16, a subpopulation of neuropil glia migrates around the entire neuropil surface: ventrally in the VNC, laterally and dorsally in the brain (Fig. 2F–F”, G–G”). As the neuropil becomes structured into distinct compartments (e.g., antennal lobe, mushroom body, lateral accessory lobe), neuropil glia adopt their final position relative to these compartments (Fig. 2H–H”).

Pattern of primary astrocyte-like and ensheathing glia in the larval brain

The neuropil of the hatching larva is surrounded by approximately 15 pALG and 12 pEG per brain hemisphere (Fig. 3M). These figures do not increase throughout the larval period (Fig. 3M). Similarly to the pALG of the VNC (Stork et al., 2014), pALG of

the brain are distributed in an almost invariant pattern which does not change from early to late larva (Fig. 3). Due to their topological reproducibility, we adopted a nomenclature system for individual or clusters of pALG based on the adjacent neuropil compartment (Table 2). At the anterior neuropil surface we typically find three individual cells flanking the antennal lobe (ALm), the lateral accessory lobe (LALa), and the superior lateral protocerebrum (SLPl; Fig. 3A–D, N), respectively. In addition, a cluster of 3–4 pALG borders the anterior surface of the ventrolateral protocerebrum (VLPa; Fig. 3A–D, O). Further posteriorly, one primary astrocyte-like glial cell flanks the crown of the superior medial protocerebrum (SMPm) and 1–2 pALG are grouped around the tip of the vertical lobe of the mushroom body (VLd; Fig. 3E–H). Lastly, the pALG around the posterior neuropil surface include two cells bordering the calyx medially (CAm) and ventrally (CAv), one cell adjacent to the posterior inferior protocerebrum (IPpm), and a group of 2–3 cells covering the ventromedial cerebrum (PSl; Fig. 3I–L, P,Q).

pEG exhibit a higher degree of spatial variability than pALG (Fig. 4). As shown in Fig. 4E–I, even though the overall number of pEG is in the same, low range as pALG, the location of pEG cell bodies and nuclei in relationship to compartments, or nearby pALG, changes between different specimens. We therefore did not establish a specific nomenclature for individual cell clusters in this glial subclass.

The relatively invariant pattern of pALG somata suggests that the central processes of pALG may also associate with neuropil compartments in a similar, relatively invariant fashion. Single cell clonal analysis of equivalent pALG of different brains demonstrates that this is indeed the case. However, the exact trajectory of pALG root processes and the neuropil volume invested by their distal processes, similarly to

the topology of somata, can exhibit subtle variability. For example, the cell ALm, shown for two different brains in Fig. 5A–C and Fig. 5D–F, extends processes laterally into the antennal lobe (AL) and medially/posteriorly towards the adjacent neuropil. Distal processes of this cell fill the entire AL. A subtle, but significant difference between the two ALm cells exists in regard to the processes directed towards the neuropil flanking the AL medially. The cell shown in the top row (Fig. 5A–C) branches predominantly in the ventromedial cerebrum (VMC), located posteriorly adjacent to the AL; most extra-antennal processes of the other ALm (Fig. 5D–F) are focused further anteriorly in the peri-esophageal neuropil (PENPa). Note the abundance of ALm processes surrounding the loVM fascicle (penetrating the VMC compartment) in Fig. 5C, and the virtual absence of such processes in Fig. 5F. Shown as the second example in Fig. 5G–I and Fig. 5J–L, respectively, are CAm clones from two different brains. In both cases, CAm sends a major branch laterally into the superior lateral protocerebrum (SLP; Fig. 5G and H, J and K), and another branch postero-medially into the superior medial protocerebrum (SMP) and medial inferior protocerebrum (IPm; Fig. 5H and K). At a posterior level, the branching pattern of both cells differs subtly, in that one projects more prominently into the calyx (CA; Fig. 5I; arrowhead), whereas the other projects into the posterior inferior protocerebrum (IPp; Fig. 5L; arrow).

Morphogenesis of primary astrocyte-like glia: progressive densification of processes in the larva, followed by regression and programmed cell death in the pupa

In order to accommodate for the several-fold expansion of the larval neuropil during development, pALG increase in size (Fig. 6), indicating that pALG, as seen for

most other differentiated *Drosophila* cell types, undergo endoreplication (Unhavaithaya and Orr-Weaver, 2012). Concomitant with the increase in cytoplasmic and nuclear volume, there is an increase in density of pALG processes filling the neuropil compartments. In the late embryo, pALG are spindle-shaped cells restricted to the neuropil surface (Fig. 6A and A′). After hatching, pALG project small protrusions which fill the neuropil volume (Fig. 6B and B′). Processes are added continuously throughout the larval period (Fig. 6C–D′). During the third larval instar (Fig. 6E–F), a conspicuous pattern of neuropil domains with high pALG density, separated by domains lacking pALG processes altogether (arrowheads in Fig. 6E–E′′′), evolves. The domains lacking pALG processes are positive for Neurotactin (BP106; Fig. 6F), which labels secondary neurons, as well as for DN-cadherin (Fig. 6E and E′′′), but they are negative for the synaptic marker Bruchpilot (nc82; Fig. 6E′′ and E′′′). We therefore interpret the pALG-negative domains as the massive bundles of secondary axon tracts (SATs), tipped by growth cones and filopodia, that, as described in previous works (Pereanu and Hartenstein, 2006; Pereanu et al., 2010), invade the primary neuropil and generate wide gaps between larval synaptic compartments. Several of the domains filled by SATs form distinctive primordia of adult neuropil compartments, such as the compartment of the fan-shaped body (FBp; Fig. 6E–E′′′), or (in the ventral nerve cord) the primordia of the leg neuropils (Supp. Info. Fig. S4A-A′). pALG processes are virtually excluded from these primordia (Fig. 6E–E′′). The only compartment that is rich in synapses but contains a low amount of pALG processes are the lobes (ML medial lobe; VL vertical lobe) and peduncle (PED) of the mushroom body (MB; Fig. 6E–E′′). At the onset of metamorphosis, from P0–P6, the distal processes of the pALG begin to fragment (Fig.

7A–F). The network of fine processes disappears, and is replaced by dense spherical bodies (visualized with mcd8-GFP; Fig. 7B′ and E). These spherical bodies correspond to the pALG vacuoles that, according to previous studies, are involved in the phagocytosis of neuronal debris (Cantera and Technau, 1996; Hakim et al., 2014; Singh and Singh, 1999; Tasdemir-Yilmaz and Freeman, 2014). By P12, the neuropil is virtually free of any *NP3233/alrm-Gal4*-driven mcd8-GFP signal (Fig. 7C and C', F). pALG somata are also difficult to detect after this point, suggesting that they undergo programmed cell death (Fig. 7C and C′, F). This conclusion was confirmed by two experiments, lineage tracing of pALG and TUNEL labeling. We performed lineage tracing experiments, where an *Act5C >Stop >lacZ* construct was specifically and stably activated in pALG during the early larval period, and not activated in sALG due to the presence of *tub-Gal80^{ts}* (see Material and Methods). Third instar larvae expressed LacZ only in pALG, confirmed by co-staining with GAT antibody (data not shown). LacZ-positive pALG were still present at relatively normal numbers at P24 (Fig. 7G and J), but became rare around P72 (Fig. 7H and J), and were absent by P96 (Fig. 7I and J). GAT antibody first labels primary ALG and their processes until P24 (Fig. 7G), is absent around P36 (data not shown), and turns back on in secondary ALG by P48 onward (Fig. 7H and I; Muthukumar et al., 2014). Importantly, lineage traced pALG were GAT-positive at P24 (Fig. 7G), but GAT-positive secondary ALG were not LacZ-positive (Fig. 7H and I), demonstrating that pALG undergo cell death and that they do not give rise to sALG. TUNEL staining of pupal brains, double labeled with anti-GAT and anti-Repo, showed that TUNEL positive cells are detectable during early to mid-pupal stages (Fig. 7K and L).

Pattern and morphogenesis of secondary neuropil glia throughout metamorphosis

Until mid-larval development (48 h after hatching (ah), late first/early second instar), most, if not all Repo-positive neuropil glia express markers for differentiated pALG or pEG (GAT or *NP6520*-positive) (Supp. Info. Fig.S2A). During the third larval instar, an increasing number of small, Repo-positive cells, clearly distinguishable from the polyploid primary NPG, appear on the surface of neuropil compartments (Fig. 7A; Supp. Info. Fig.S2B). These cells, which are initially negative for *alrm/NP3233*/GAT and *NP6520*, constitute the precursors of secondary ALG and EG. In the late larva/early pupa, they are clustered at the posterior and lateral surface of the neuropil and, inside the neuropil, around the primordium of the central complex (Fig. 7A; Supp. Info. Fig.S2B). During early metamorphosis, a subset of these secondary neuropil glia precursors become *NP3233*-positive and, somewhat later, *alrm*-positive, demonstrating that they are secondary astrocyte-like glia (sALG) precursors (Fig. 7B and C′; Supp. Info. Fig.S3). *NP3233*-positive sALG precursors are small, spindle-shaped cells which are much more numerous than pALG (Fig. 7B and C′) and can also be observed in the VNC (Supp. Info. Fig.S4).

As metamorphosis proceeds, between P12 and P48, secondary NPG precursors increase in number and become evenly distributed over the outer neuropil surface (Fig. 8A–H). During later pupal stages, sNPG also spread within the neuropil, migrating along major axon bundles, including the great commissure, antennal lobe tract, peduncle, longitudinal ventral fascicle, and longitudinal superior medial fascicle (Fig. 8F–H). Counts of sNPG precursors around the enlarging compartments of the central complex

(fan-shaped body, ellipsoid body, noduli) demonstrate that, although proliferation of neuroblasts has terminated (Ito and Hotta, 1992), a nearly 3-fold increase in sNPG precursors occurs during this time (99 to 270 cells) (Fig. 8I). This implies that following Repo expression, neuropil glia precursors proliferate, confirming the descriptions of Viktorin et al. (2011). Morphogenesis of sALG proceeds similar to the pattern described for pALG in the larva. As reported previously (Muthukumar et al., 2014), up until around P48, sALG are flat or spindle-shaped cells (Fig. 8F′). From P48-P72, sALG elaborate a few primary processes that radiate into the neuropil (Fig. 8G′); during the last day of the pupal period, these processes form branches of increasing density in the neuropil (Fig. 8H′). High magnification images of the developing antennal lobe clearly illustrate the dynamics of sALG morphogenesis (Supp. Info. Fig. S5). Oland et al. (2008) demonstrated that primary processes of sALG form from P60-P72 around the glomeruli, which had appeared much earlier (Supp. Info. Fig. S5 B–C′). The interior of glomeruli becomes penetrated by the fine branches of sALG between P72 and P96 (Supp. Info. Fig.S5 D–D’).

Expression of the EG marker *NP6520* begins later and shows a different dynamic than that of *NP3233*. *NP6520* expression decreases steadily from late larva to around P12 (Fig. 8J). No expression is visible during mid-metamorphosis (Fig. 8K). Around P60–P72, *NP6520* appears in centrally located neuropil glia surrounding the central complex, and only later, from P96 onward, in glia at the neuropil surface (Fig. 8M). At this stage, most of the external neuropil surface, in addition to the compartments of the central complex, mushroom body and adjoining major tracts, are covered by sEG. Only at the dorsal neuropil surface the sEG sheath remains thin, and small gaps appear at

locations where there is a high concentration of (*NP6520*-negative) sALG (arrow in inset of Fig. 8M).

Origin and fate of secondary neuropil glia from gliogenic type II lineages

Primary neuropil glia do not divide, and undergo cell death during the pupal period (see above). This prompts the question for the origin of secondary NPG. Previous studies had suggested that these cells are formed as part of secondary neuro-(glio)blast lineages (Pereanu et al., 2005); the formation of putative central complex-associated sEG by a subset of type II lineages, utilizing lineage tracing and MARCM analysis, had been followed in detail (Izergina et al., 2009; Viktorin et al., 2011). To systematically address the origin and migration of sNPG, in particular sALG, we followed the association of Repo-positive sNPG with secondary lineages at different larval stages, and carried out lineage tracing experiments to confirm the origin of these cells.

As expected, using the secondary lineage-specific driver, *insc-Gal4*, we could identify Repo-positive nuclei of sNPG precursors as part of the type II lineages DPMm1 (DM1), DPMpm1 (DM2), DPMpm2 (DM3), CM1 (DM5), and CP2/3 (DL1/2), from about 60hr after hatching onward (Fig. 8A–C). This confirms the findings of Izergina et al. (2009) and Viktorin et al. (2011), and in part, the analysis of secondary lineage clones in the adult brain by Yu et al. (2013). Sparse Repo-positive nuclei were also occasionally observed in lineages CM4 (DM4) and CM3 (DM6). None of the type I lineages showed Repo labeling, corroborating the findings of Izergina et al. (2009). Repo-positive sNPG precursors are located distally within their respective lineages, indicating that they are among the first born cells (Fig. 9L). As development proceeds, lineages add new cells

at the periphery (i.e., close to the neuroblast and intermediate progenitors). These newly born cells turn on the *insc* marker, whereas earlier born cells, including sNPG precursors, lose *insc* expression (Fig. 9L). Among the later born cells, none expressed Repo, excepting in one lineage, CM1 (DM5), which continued to produce new Repo-positive sNPG until the late larval stage (Fig. 9J). Throughout larval development, sNPG precursors remain close to the neuropil surface, clustered around the entry points of lineage tracts into the neuropil (Fig. 9A, D, L). Starting around 84 h ah, sNPG precursors invade the neuropil and spread out around the posterolateral neuropil surface and emerging neuropil compartments (e.g., primordia of the protocerebral bridge and fan-shaped body; Fig. 9G–I, J–L). The contribution of each lineage to the total sNPG population becomes difficult to assess due to the subsequent distribution of glial cells over the neuropil surface (Fig. 9F and I). However, one can, at least initially, roughly categorize sNPG precursors into dorsomedial (DM), posterolateral (PL), and lateral (L) groups (Fig. 9F). The DPM lineages appear to make significant contributions to the DM group which populate the central complex primordium, the CM lineages to the PL group which splay across the posterior lateral protocerebrum, and the CP lineages to the L group which cluster around the lateral regions of the brain neuropil (Fig. 9F and I).

To critically address the question whether both types of sNPG, sALG and sEG, are derived from type II lineages, we traced intermediate precursors (INPs) of type II lineages, using the INP-specific driver *9D11(erm)-Gal4*, and determined their fate using the ALG-specific marker, GAT. We find that, as expected, many neurons located in the posterior cortex are LacZ positive (Fig. 10A). We also find many GAT-positive and GAT-

negative nuclei surrounding the central complex, suggesting that type II lineages can indeed generate both sNPG subtypes (Fig. 10B and C). To further support the notion that type I lineages do not give rise to sNPG, we used a number of drivers expressed in sets of type I lineages, among them *acj6-Gal4* [expressed in secondary lineages BAmv3, BLD5, BLD6, BLP3, BLP5, BLVp1, BLVp2 (Supp. Info. Fig. 6)] and *engrailed-Gal4* [expressed in secondary lineages BAla3, DALv2, DALv3, DPLam (Kumar et al., 2009a; Kumar et al., 2009b)]. Lineage tracing using both lines revealed predictably distributed neuronal progeny (Fig.10D and E, H and I). However, neither line produced any sALG or sEG (Fig. 10F and G, J and K).

The optic lobe primordium does not contribute to the neuropil glia of the central brain

The optic lobe generates numerous specialized populations of glia (Edwards and Meinertzhagen, 2010; Hartenstein, 2011). Distinguished in Fig. 10L are the conspicuous bands of glial precursors produced at an early stage by the inner and outer optic anlage [subsumed as lateral optic lobe glial precursors (OLl)], and the medial glial precursors (OLm), born later over a long period of time from the large number of lineages that form the medulla. An increasing population of lateral Repo-positive sNPG of the central brain neuropil ("L" in Fig. 9C, F, I) exhibits a continuity with the Repo-positive cells within the optic lobe, specifically, with the cells of the Olm. This observation is consistent with Viktorin et al., (2013) which demonstrated that the type II lineage CP2/3, specifically DL1, gives rise to Repo-positive cells which migrate from the central brain into the optic lobe to form a subpopulation of optic lobe glia. It is also possible that a subpopulation of the large numbers of glial cells born in the optic lobe migrate into the opposite direction,

contributing to the glial population of the central brain. To address this possibility, we lineage-traced using *sine oculis-Gal4* to identify all cells derived from the optic lobe placode of the embryo (Chang et al., 2003). Although a large number of neurons and glia (OLl and OLm) were derived from *sine oculis-Gal4* expressing progenitors, lateral sNPG were not (Fig. 10M and N). This finding indicates that glia born in the optic lobe primordium remains confined to this domain and does not contribute to central brain neuropil glia.

Discussion

Glia are intimately associated with neurons and represent a major cellular constituent of both vertebrate and invertebrate nervous systems. Invertebrate model organisms such as *Drosophila*, with their wealth of genetic tools, are gaining momentum to elucidate fundamental aspects of glial biology. A number of recent studies (Avet-Rochex et al., 2012; Awasaki et al., 2008; Beckervordersandforth et al., 2008; Doherty et al., 2009; Muthukumar et al., 2014; Stork et al., 2008; Stork et al., 2014; Tasdemir-Yilmaz and Freeman, 2014), emphasize the ample heterogeneity of *Drosophila* glia, and initiated questions regarding their origin and developmentally changing patterns. In the present study, we establish a developmental/morphological framework for neuropil glia of the brain, the glial class most intimately associated with neurites. We demonstrate that the larval brain is associated with large, primary neuropil glia which are few in number and relatively stereotyped in position. These cells undergo programmed cell death and do not contribute to neuropil glia of the adult. The adult brain is invested with a much larger population of secondary neuropil glia which is generated during larval stages from a relatively small set of neuroglioblasts, the type II lineages, different from those that gave rise to primary neuropil glia (Fig. 11).

Origin and morphogenesis of primary neuropil glia

Primary NPG has been reconstructed for the embryonic ventral nerve cord in a number of previous studies. Jacobs and Goodman (1989) originally classified glia associated with the neuropil of the embryonic VNC as longitudinal, midline, and nerve root glia (Jacobs and Goodman, 1989). Longitudinal glia, also called “interface glia”, envelop the connectives, midline glia the commissures, and nerve root glia the points of

exit of peripheral nerves (Beckervordersandforth et al., 2008; Ito et al., 1995; Jacobs and Goodman, 1989). It was shown that the longitudinal glia consist of 9 cells per hemineuromere and are produced by a dedicated glioblast termed, the “lateral glioblast” (LGB) (Beckervordersandforth et al., 2008; Jacobs et al., 1989). Progeny of the LGB migrate from their lateral point of origin to the location where the longitudinal axons pioneering the connectives appear, and subsequently undergo multiple rounds of equal mitoses to produce the longitudinal glia (Griffiths and Hidalgo, 2004). Longitudinal glia likely comprise an equivalence group which differentially specifies into primary astrocyte-like and ensheathing glia (Stork et al., 2014; this study). Although a more descriptive term such as the previously suggested “reticular glia” for ALG may be more suitable considering they may or may not be homologous to vertebrate astrocytes by definition, we adopt this terminology to maintain consistency in the field (Hartenstein, 2011 and Hartline, 2011). Midline glia (the only type of glia in *Drosophila* that does not express Gcm or Repo) comprises 3–4 cells in each hemineuromere and has its origin from among the so-called midline progenitors, peculiar cells which divide only once before differentiating (Bossing and Technau, 1994). Nerve root glia originates from one of the lateral neuroglioblasts, Nb1-3 (Beckervordersandforth et al., 2008). The origin and fate of embryonic midline and nerve root glia are not addressed in this study, although they were defined as members of the embryonic “neuropil-associated glia” class. A dedicated (neuro)-glioblast which generates neuropil glia precursors of the brain, the BPLG, has yet to be identified. However, a strong candidate includes Td7 based on its expression of glial-specific genes and proximity to the emerging BPLG cluster (Hartenstein et al., 1998; Urbach and Technau, 2003).

Previous counts of Repo-positive neuropil glia throughout larval development demonstrates that the number of NPG remains relatively constant (<30) until the early third larval instar, at which point the number of NPG nearly triples (Pereanu et al., 2005). Our analysis using markers of differentiated NPG subtypes demonstrates that the number of differentiated neuropil glia does not change throughout larval development in the VNC (data not shown) or brain. In addition, double labeling experiments demonstrate that all NPG of the second instar larval brain (prior to this massive increase in number) are pEG and pALG. Therefore, the newly generated NPG in the third larval instar represent recently born secondary neuropil glia precursors (see later section). We propose that a more or less invariant number of pNPG in the CNS which undergo a late embryonic migration to stereotyped positions around the neuropil are generated by dedicated primary glioblasts.

Although the number of pNPG does not change throughout development, they exhibit significant morphogenetic changes. Both neuropil glial subtypes exhibit an increase in nuclear size and progressive elaboration of their membranous processes. These changes are likely carried out to accommodate the many-fold expansion of the larval neuropil volume. Previous studies examining incorporation of BrdU during larval development suggested that neuropil glia of the third instar VNC, confirmed to represent mature longitudinal glia, replicate DNA content without cellular division (Prokop and Technau, 1994). Subperineurial glia (SPG), which, similarly to pNPG do not execute cytokinesis, also undergo polyploidization (Unhavaithaya and Orr-Weaver, 2012). In this case, polyploidization is required to sustain the massive increase in cell size necessary

to maintain the blood–brain barrier around a progressively expanding larval brain. Interestingly, SPG evidently increase ploidy in response to an increase in neuronal mass, suggesting a feedback mechanism to sustain coordinate growth during organogenesis (Unhavaithaya and Orr-Weaver, 2012). It will be interesting to address the possibility that endoreplication in pNPG is required in a similar way for the expanding larval neuropil.

At the onset of metamorphosis, pALG drastically change morphology. Tasdemir-Yilmaz and Freeman (2014) demonstrated that the processes of primary ALG (called “larval astrocytes” in their study) vacuolate in an ecdysone-dependent manner at the onset of metamorphosis and become sparser as metamorphosis proceeds, consistent with our findings. However, it was suggested that the same population of cells re-extends their processes into the neuropil during late metamorphosis, prior to adulthood. Our analysis suggests that pALG do not re-infiltrate the neuropil, and in fact they are lost by programmed cell death. This represents, to our knowledge, the first description of cell death of an entire cellular class in the *Drosophila* brain. A similar developmental scenario is likely to be true of ensheathing glia based on expression of the *NP6520-Gal4* driver. Similarly to *alrm-Gal4, NP6520-Gal4* is expressed throughout larval development in a small number of primary EG with progressively enlarging nuclei and turns off during mid-metamorphosis (P24-P48). However, further lineage tracing experiments of pEG must be conducted to confirm this hypothesis.

Origin and morphogenesis of secondary neuropil glia

Previous studies in the developing larval brain suggest that all three glial classes increase in number, particularly during the third instar (Pereanu et al., 2005). The

observed increase in Repo-positive neuropil glia can be due to either (or a combination of) (1) mitotic divisions of differentiated primary glia, (2) proliferation of secondary multipotent neural/glial progenitors (neuroglioblasts), (3) mitotic divisions of undifferentiated, secondary NPG precursors. Based on our comprehensive analysis of various neuropil glia-subtype specific markers throughout development in combination with lineage tracing, we suggest that the increase in neuropil glia number is primarily due to proliferation of neuroglioblast lineages rather than division of differentiated pNPG. In addition, mitotic divisions of sNPG precursors are also thought to contribute to the final population (Pereanu et al., 2005; Viktorin et al., 2011). Thus, after the Repo-positive sNPG precursors have separated from their lineages of origin and started to spread around the neuropil, there is a further, substantial increase in their number during the early pupal period, (Fig. 8I), even though proliferation of neuroblasts and neuroglioblasts has ceased (Ito and Hotta, 1992). Therefore, clonal expansion of sNPG precursors likely contributes greatly (up to 75%) of the mature population (Viktorin et al., 2011; this study). The molecular mechanisms which dictate proliferation, although elucidated for other glial subtypes, require further investigation for sALG and sEG (Avet-Rochex et al., 2012). Therefore, we are currently pursuing the role of FGF signaling in mediating proliferation of post-embryonic sALG precursors (Gibson et al., 2012; unpublished data).

As previously reported (Izergina et al., 2009; Viktorin et al., 2011) and confirmed in this study, a subset of the posteriorly located type II lineages constitute the source of central complex-associated sNPG. Our data suggests that type I lineages do not give

rise to any sNPG. Based on cell morphology at P20, type II lineages were suggested to exclusively give rise to ensheathing glia (Viktorin et al., 2011). However, we have demonstrated, using NPG subtype-specific markers, that type II lineages can give rise to both sNPG subtypes. We surmise that this discrepancy is based on the fact that one cannot fully distinguish sALG and sEG at this stage in metamorphosis, given that sALG have not fully elaborated their processes. It remains to determined, however, if sALG and sEG are derived from specific, distinct type II neuroblasts or potentially from distinct INPs from individual type II neuroblasts.

MARCM analysis suggested that precursors of sNPG (postembryonic neuropil glia) proliferate in stereotyped regions in the larval brain (posteromedial, lateral, and dorsal interface), followed by migration during metamorphosis (Awasaki et al., 2008). We documented this migration with preparations representing multiple discrete time windows throughout metamorphosis. Our results suggest that sNPG, albeit more complex in nature in comparison to pNPG, also exhibit a stereotyped migratory pattern emanating from the previously described posteromedial, lateral, and dorsal loci. This pattern is characterized by Repo-positive sNPG gradually distributing equally over the neuropil surface and invading crevices between neuropil compartments. Interestingly, sALG retain a spindle-shaped morphology until late metamorphosis (P48-P72), at which point they infiltrate the neuropil and remain for the rest of adulthood. Recent work has demonstrated that primary ALG require fibroblast growth factor receptor signaling in order to extend processes into the late embryonic neuropil (Stork et al., 2014). However, the molecular mechanisms responsible for prompting sALG processes to infiltrate the neuropil during metamorphosis have yet to be determined. Notably, the

developmental time windows when synaptogenesis and elaboration of sALG processes occurs are coincident (Muthukumar et al., 2014; Singh and Singh, 1999). Although specific sALG-derived synaptogenic molecules remain to be determined, recent work has demonstrated that sALG influence synaptogenesis of adult-specific neurons during metamorphosis, akin to what has been described for vertebrate astrocytes (Clarke and Barres, 2013; Muthukumar et al., 2014).

Relationship between astrocyte-like and ensheathing glia

A morphological distinction among the neuropil glia between ensheathing glia, whose processes largely remain confined to the neuropil surface, and astrocyte-like glia with neuron-like, highly branched morphology was prompted by clonal labeling of, and specific markers for these cells (Awasaki et al., 2008; Pereanu et al., 2005). It appears likely that for both brain and VNC, both cell types are derived from the same progenitors. Thus, as shown in the present study, a small number of type II lineages in the posterior brain generate the large majority of sEG and sALG. In the embryonic VNC, the lateral glioblast generates both pEG and pALG.

What is the significance of two different NPG cell types, and how is the differentiation between EG and ALG specified? In the embryonic VNC, it appears that initially, all descendants of the lateral glioblast express the ALG marker *alrm-Gal4* (Stork et al., 2014; this study), and that the separation between the two NPG subtypes, manifested by the restriction of *alrm* to just anterior longitudinal glia, occurs secondarily. Presumptive primary ALG can be distinguished from EG by the expression of Prospero (Pros) (Griffiths and Hidalgo, 2004). Notch signaling appears likely to be involved in this separation, since Notch activity is required independently for the expression of Pros and

the glutamate transporter, excitatory amino acid transporter 1 (Eaat1), in the anterior longitudinal glia (presumptive pALG) (Stacey et al., 2010; Thomas and van Meyel, 2007). Therefore, longitudinal glia are initially equivalent cells which require environmental cues such as fringe-mediated serrate/delta-notch signaling to promote pNPG subtype-specific gene expression. It is currently unknown whether similar mechanisms dictate the differential specification of brain primary neuropil glia. In addition, nothing is known about the corresponding specification of type II-derived secondary ALG and EG. The concept of the longitudinal glia as an equivalence group prompts the question of the true identity of ensheathing glia. For example, are EG and ALG actually different cells, or is EG the "default" fate? Is it possible that EG are simply a reserve population which are competent to elaborate processes into the neuropil, but do not because they lack appropriate environmental cues during a specific phenocritical period? Further studies ablating ALG populations need to be conducted to answer this question.

Neuropil glia in *Drosophila* and other insects

In this study, we provide a developmental framework for the study of neuropil glia in *Drosophila*. Neuropil glia are defined by their somata location (located at neuropil boundaries) and morphology (dendritic and invested in the neuropil or sheath-like and surrounding neuropil boundaries for ALG and EG, respectively). We describe two disparate glial strategies for "supporting" the neuropil of the insect nervous system. The larval brain is associated with few, large pNPG which likely undergo endoreplication to accommodate the growing CNS rather than proliferate. The adult brain is associated with many more, small sNPG which derive from secondary lineages and clonally

expand to generate the final population. Do other insects have analogous neuropil glia subtypes? If so, what is their cellular origin? What “strategy” do various insects use, especially considering many are hemimetabolous and do not undergo a metamorphosis?

Studies in moth (*Manduca sexta*) larvae have described “glia of the neuropil cover” which consisted of multiple subtypes roughly corresponding to *Drosophila* primary NPG (Cantera, 1992). Although primary NPG in *Manduca* have not been followed throughout larval development, a recent study demonstrated GAT (*Mas*GAT in *Manduca*) immunoreactivity exclusively in the “complex” glial cells (analogous to pALG) and absent in the “simple” glial cells (analogous to pEG) of the late larval and early metamorphosing antennal lobe (Oland et al., 2010). Although not comprehensively investigated, the striking phenomena of glial process vacuolization (likely corresponding to clearance of neuronal debris) and clearance has been documented (Fig. 4 in Oland et al., 2010). In addition, the presence of what are most likely secondary neuropil glia analogous in morphology to the subtypes we observe in *Drosophila* have been described in the developing adult *Manduca* antennal lobe (Oland et al., 1999). This demonstrates the striking similarity between glial morphology and gene expression between holometabolous insects.

Studies of neuropil glia in the hemimetabolan grasshopper *Schistocerca americana* have shown the presence of “primitive” glia (“glia of the connective”) associated with the early embryonic longitudinal connectives. These glia, similarly to *Drosophila*, are thought to be required for establishing reciprocal cellular interactions with neurons imperative for normal development of the longitudinal connectives

(Bastiani and Goodman, 1986; Hidalgo and Booth, 2000). However, the fate of the grasshopper “glia of the connective” or their unknown brain counterparts, which likely correspond to *Drosophila* primary NPG, is unknown. Large glial cells reminiscent of pNPG have thus far, not been reported. Unlike *Drosophila*, the grasshopper *Schistocerca gregaria*, like other hemimetabolan insects, generates brain structures required for complex adult motor control such as the central complex in the embryo. This structure has been shown to be associated with neuropil glia strikingly similar to the secondary neuropil glia which we have described during metamorphosis (Boyan et al., 2013). In fact, like *Drosophila* sALG, these glia first migrate to the central complex from other brain regions and only elaborate their processes into the central complex neuropil after the columnar neuroarchitecture has formed (Boyan et al., 2011). In addition, Repo-positive cells have been shown to intermingle with neurons within developing central complex lineages and proliferate, thus demonstrating the presence of multipotent neuroglioblasts in the grasshopper (Liu and Boyan, 2013). Thus, we hypothesize that grasshoppers and other hemimetabolans likely generate (primary) NPG at an early stage for the purpose of establishing early neuroarchitecture, but in contrast to holometabolans, do not maintain and enlarge these cells for functional use in a larval stage that is lacking in these insects.

Figures

Table 1-1.
List of abbreviations of neuropil brain compartments (left), fascicles (right), optic lobe-specific terms (right, and other (right).

Brain compartments	Abbr.	Brain fascicles	Abbr.
Antennal lobe	AL	Antennal lobe tract	ALT
Anterior optic tubercle	AOTU	Great commissure	GC
Anterior periesophageal neuropil	PENPa	Longitudinal superior medial fascicle	loSM
Ellipsoid Body	EB	Longitudinal ventral fascicle	loV
Fan-shaped body	FB	Medial loV	loVM
Fan-shaped body primordium	FBp	Medial equatorial fascicle	MEF
Inferior protocerebrum	IP	Posterior lateral ellipsoid fascicle	LEp
Medial IP	IPm	Supraellipsoid body commissure	SEC
Posterior IP	IPp	Transverse super intermediate fascicle	trSI
Lateral accessory lobe	LAL	Optic Lobe	Abbr.
Lateral appendix of the medial lobe	LAML	Inner Optic Anlage	IOA
Mushroom body	MB	Lobula neuropil	LOnp
Calyx of MB	CA	Medula cortex	MEco
Medial lobe of MB	ML	Medulla neuropil	MEnp
Peduncle of MB	PED	Optic Lobe	OL
Vertical lobe of MB	VL	Outer Optic Anlage	OOA
Protocerebral bridge	PB	Other	Abbr.
Superior lateral protocerebrum	SLP	Abdominal ganglia	ABD
Superior lateral protocerebrum/Lateral horn primordium	SLPp/LHp	leg neuropil primordium	lnp
Superior medial protocerebrum	SMP	Subesophageal ganglion	SEG
Ventro-lateral protocerebrum	VLP		
Ventro-medial cerebrum	VMC		
Postcommissural/Posterior VMC	VMCpo		

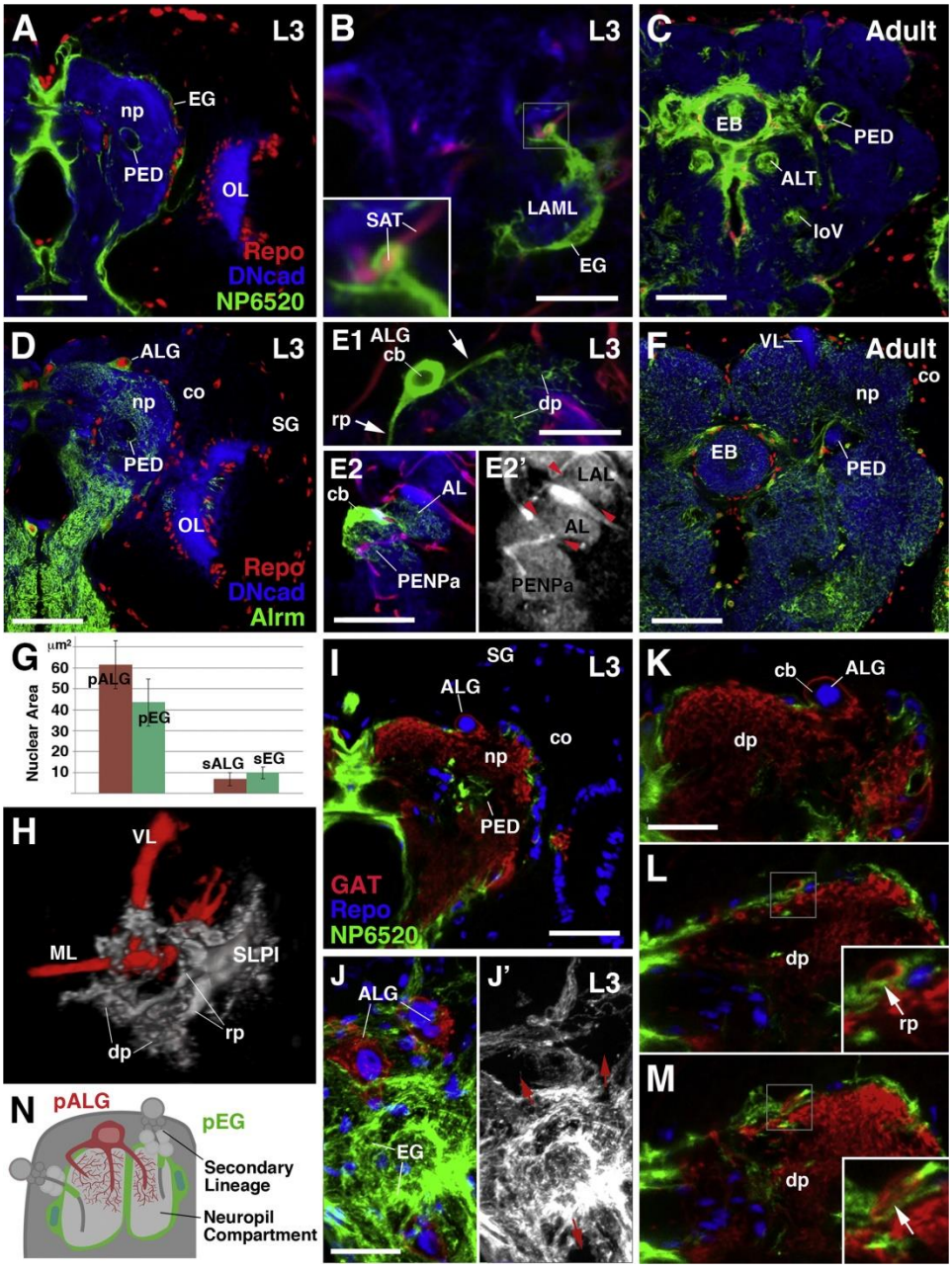

Figure 1-1: Cytology of mature Drosophila neuropil glia. (A–C): Ensheathing glia (EG). Frontal confocal sections (dorsal, up; lateral, right) of late third instar larval (A and B) and adult brain hemispheres (C) depicting mature primary ensheathing glia (pEG) (A), a high magnification image of a representative GFP-labeled pEG single cell clone (B), and mature secondary ensheathing glia (sEG) (C). pEG and sEG are labeled in green by NP6520-Gal4 (A and C). (B) pEG single cell clone associated with the neuropil

compartment, lateral appendix of the medial lobe (LAML) and is simultaneously associated with a secondary axon tract (SAT) labeled by anti-Neurotactin (red) (boxed inset). (D–F): Astrocyte-like glia (ALG). Equivalent stages depicting mature primary astrocyte-like glia (pALG) in late larval brain (D), representative pALG single cell clones (E1, E2–E2′), and mature secondary astrocyte-like glia (sALG) in adult (F). pALG and sALG are labeled in green by alrm-Gal4 (D and F). (E1) pALG single cell clone demonstrates that pALG have a large nucleus and soma. A single pALG cell extends multiple primary “root processes” (rp, arrows), each with reticular “distal processes” (dp). (E2–E2’) A second pALG single cell clone demonstrating extension of processes into two distinct neuropil compartments labeled by anti-DN-cadherin (E2, blue; E2’, gray) bordered by SATs [anti-Neurotactin (red), red arrowheads]; the antennal lobe and the anterior peri-esophageal neuropil. Compartment definitions have been described previously (Pereanu et al., 2010). The nuclei of all glial cells are labeled by anti-Repo (red) (A, C, D, F). The larval and adult neuropil (np) is labeled with anti-DN-cadherin (blue) (A–F). (G) Nuclear mean area quantifications of primary and secondary neuropil glia (n=39). (H) 3D volume rendering of a spatially identifiable pALG single cell clone, representing the SLPl (gray color; see Fig. 3); the mushroom body is shown for spatial reference (red). (I–M) Frontal (or tangential; J–J’) confocal sections of third instar larval brains in which pEG are labeled by NP6520-Gal4 (green), and pALG are labeled by anti-GAT (red); glial nuclei marked with anti-Repo (blue). (J–J’) Tangential section of the neuropil surface demonstrating that the neuropil surface is predominantly ensheathed by the membranes of pEG; the somata of pALG occupy gaps in the pEG (red arrows) and contribute to the sheath as well. pALG processes predominantly extend directly into

the neuropil (K) or stay superficial relative to pEG prior to penetrating through the pEG into neuropil (boxed inset; arrows) (L–M). (N) Schematic depicting the morphology of, and spatial relationship between, astrocyte-like (red) and ensheathing (green) glia relative to other brain structures such as secondary lineages and neuropil compartments. Anatomical abbreviations found in Table 1. Other abbreviations: cb, cell body; co, cortex; SG, surface glia. Bars: 50 μm (A, C, D, F, I); 20 μm (B, E); 10 μm (J; K–M).

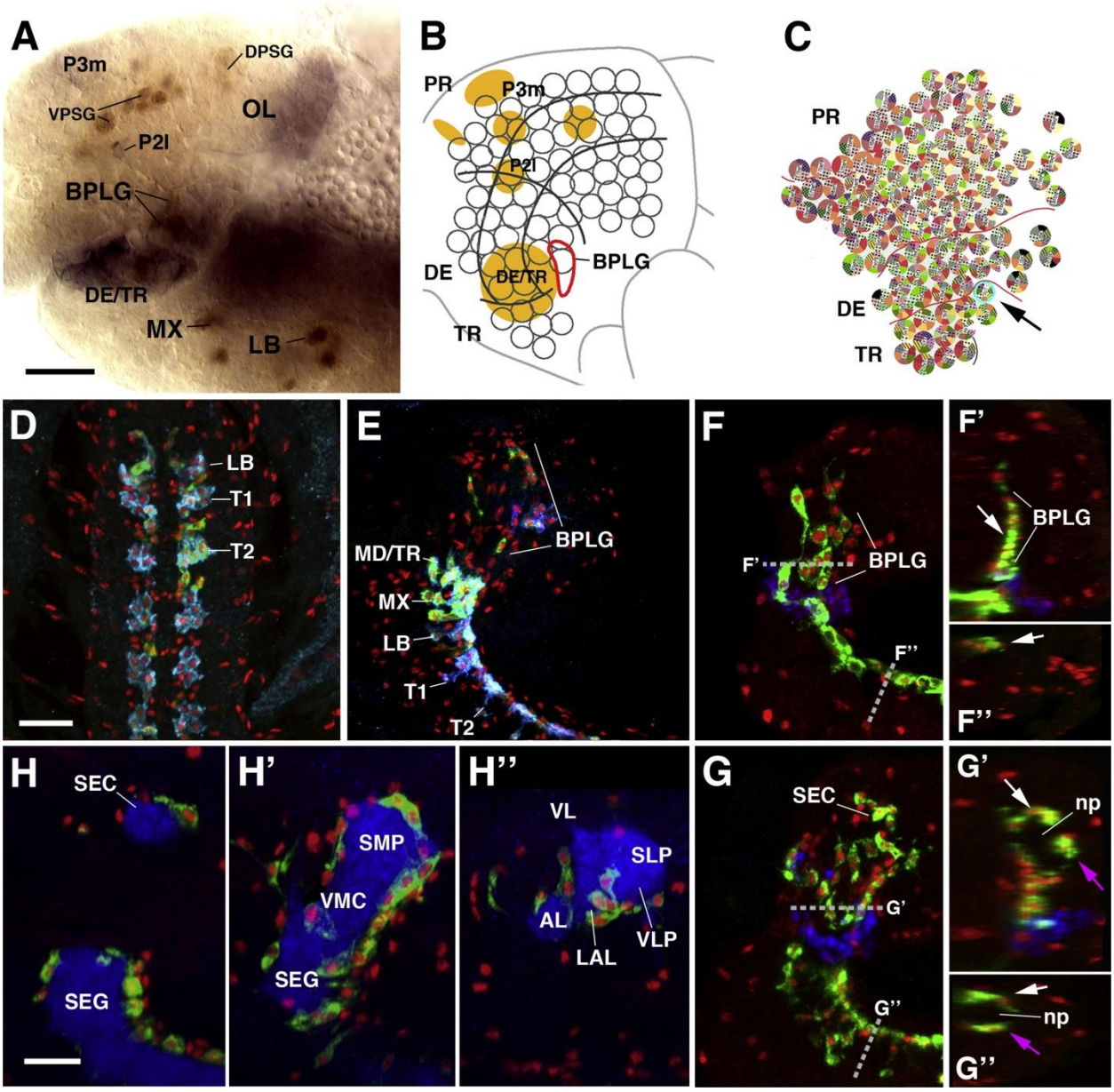

Figure 1-2: Embryonic development of primary neuropil glia. (A) Early stage 12 embryo labeled with anti-Repo (brown) and anti-FasII (purple), depicting specific immature glial clusters. (B) Schematic representation of the brain neuroblast map. (C) Brain neuroblast map of Urbach and Technau (2003). FasII-positive cells shown in (A), and depicted as orange domains in (B), represent clusters of pioneer neurons that serve as reference markers to follow cell movements in the brain primordium. Gray lines in (B) subdivide

the brain neuroblast map into a protocerebral domain (PR), deuterocerebral domain (DE), and tritocerebral domain (TR); the same subdivisions are indicated in (C). Progenitors of brain neuropil glia form the basal procephalic longitudinal glia (BPLG) cluster, outlined by red line in (B). Arrow and cyan circle in (C) points at the only gcm-positive neuro-(glio)blast (Td7) of the neuroblast map. This cell is situated at the location where the BPLG develops, and therefore is most likely the progenitor of the brain neuropil glia. (D–H) Z-projections of confocal sections of stage 15–17 embryonic ventral nerve cords (VNC) and brains labeled with anti-Repo (red) and marker of astrocyte-like glia (alrm-Gal4, green). (D) horizontal section of stage 15 embryonic VNC. Astrocyte-like glia are marked by the expression of GAT (blue), in addition to alrm-Gal4 (green), and appear in cyan color. (F): parasagittal sections of stage 15 brain and VNC. (F', F"): digital rotations of z-projection shown in (F), showing virtual horizontal section of brain, and frontal section of VNC [see dashed lines in (F) for plane of section of F' and F"]. Labeling with anti-Labial (blue) was used to delineate the tritocerebral domain, from where the brain neuropil glia originates (see panel (C) above). At the stage shown, cells of the alrm-positive BPLG cluster have spread out dorsally along the emerging brain neuropil; cells are still clustered at the medial surface of the neuropil (arrow in F'). VNC neuropil glia are located at the dorsal surface of the VNC neuropil (arrow in F''). (G–G''): z-projection and digital rotations thereof of parasagittal sections of late stage 16; labeled and oriented like panels (F–F''). The alrm-positive brain neuropil glia have further spread dorsally (G), and also laterally/anteriorly, surrounding the neuropil (np) on all sides (from white to magenta arrow in G'). The spreading of VNC glia around the neuropil also occurs at this stage (from white to magenta arrow in G"). For clarity, non-

CNS staining was manually removed (E–G′′). (H–H′′) Three parasagittal sections of a stage 17 brain, representing level close to the midline (H), level along center of neuropil (H′) and level of lateral neuropil (H′′). Neuropil is labeled by anti-DN-cadherin (blue). Alrm-positive glia have reached final position around neuropil compartments. Anatomical abbreviations found in Table 1. Other abbreviations: DPSG, dorsal procephalic subperineurial glia; P2l and P3m, fiber tract founder clusters of the protocerebrum; LB, labial segment; MX, maxillary segment; MD/TR mandibular segment/tritocerebrum; T1, T2, Thoracic segments 1 and 2; VPSG, ventral procephalic subperineurial glia. Bars: 10 μm.

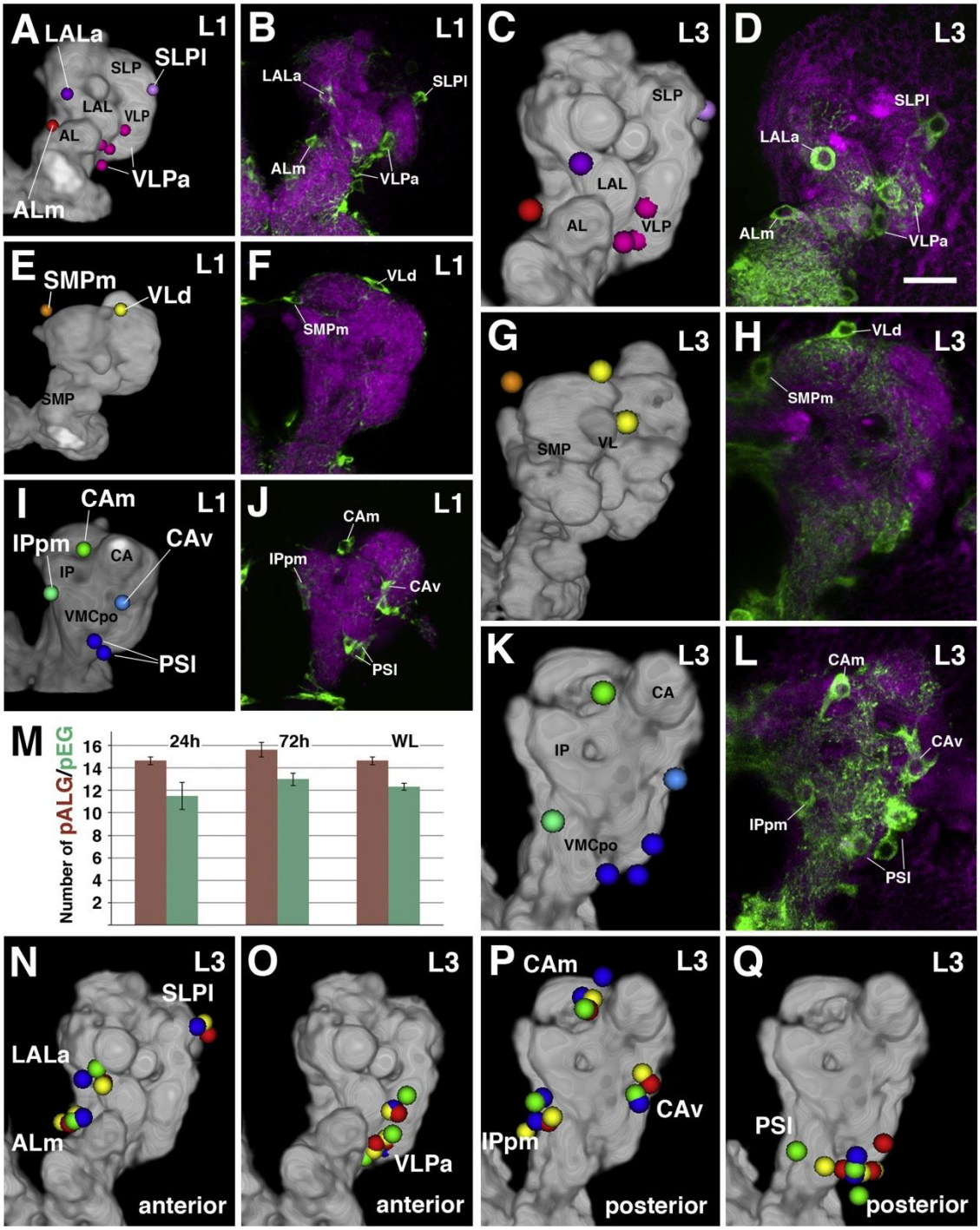

Figure 1-3: Primary neuropil glia exhibit a relatively stereotyped topological pattern around the larval neuropil. Anterior pALG clusters (A–D), intermediate clusters (E–H), and posterior clusters (I–L) are shown in the first larval instar (left two columns) and in the third larval instar (right two columns); (dorsal up, lateral right). The first and the third

column represent digital 3D models of the first instar (A, E, I) and third instar (C, G, K) larval brain. The neuropil surface is rendered in gray (annotated with black lettering) surrounded by color coded pALG clusters (annotated with white lettering). Panels of the second column (B, F, J) and fourth column (D, H, L) show frontal confocal z-projections of first instar and third instar brains, respectively. The same pALG clusters modeled in (A, E, I) and (C, G, K), respectively, are visualized by alrm-Gal4 in green; the neuropil is labeled by anti-DN-cadherin (magenta). (A–D) Anterior view reveals the anterior clusters of astrocyte-like glial cells, including the ALm (antennal lobe medial; red), LALa (lateral accessory lobe anterior; purple), SLPl (superior lateral protocerebrum lateral; light purple), and VLPa (ventro-lateral protocerebrum anterior; magenta). (E–H) Anterior dorsal view reveals the intermediate clusters; VLd (vertical lobe dorsal; yellow) and SMPm (superior medial protocerebrum medial; orange). (I–L) Posterior view reveals the posterior clusters; CAm (calyx medial; green), CAv (calyx ventral; cyan), PSl (posterior slope lateral; blue), and IPpm (inferior protocerebrum posterior medial; green blue). (M) Numbers of pALG and pEG at early larval stage (24 h ah), mid larval stage (72 h ah), and at wandering larva stage (WL) (n≥3 for each timepoint). (N–Q) 3D volume renderings of third instar larval brain neuropils (gray) depicting anterior (N–O) and posterior (P–Q) primary astrocyte-like glial clusters. Corresponding pALG from four representative brain hemispheres were registered to a standard brain and are shown in red, blue, yellow, and green. Note the low degree of spatial variability of pALG between samples. Primary astrocyte-like glia nomenclature can be found in Table 2. Bar: 25 μm.

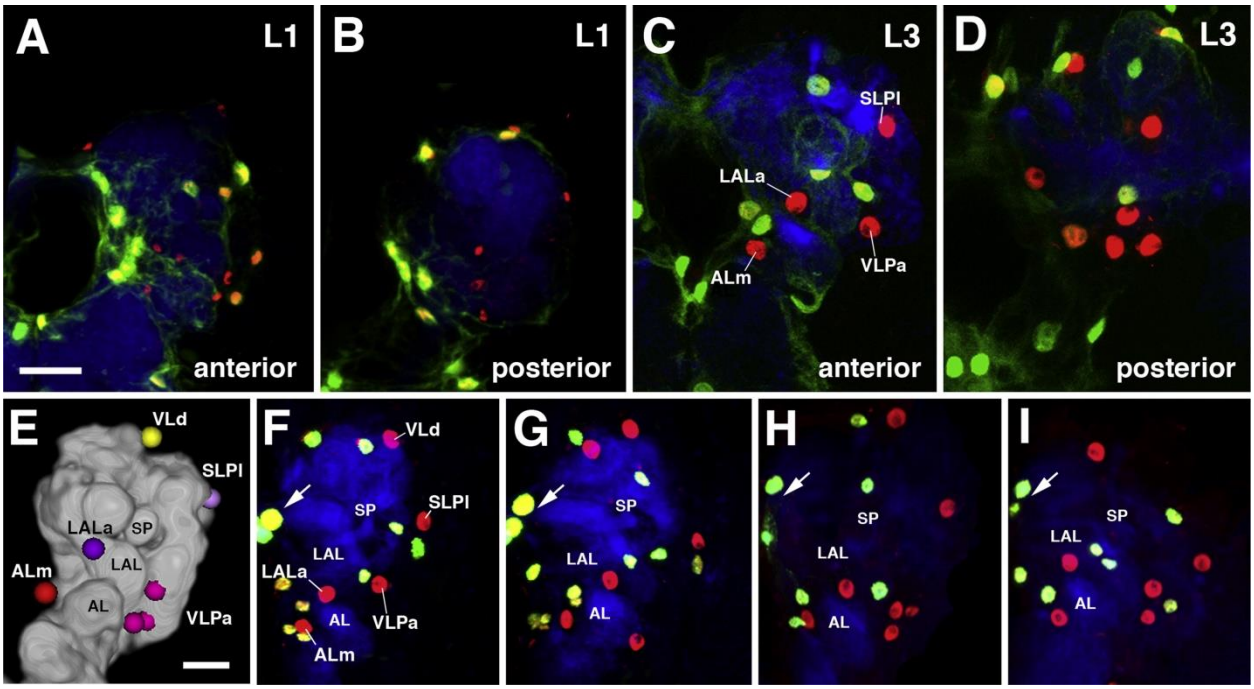

Figure 1-4: Pattern of primary ensheathing glia (pEG). Frontal confocal z-projections of first instar (A–B) and third instar (C–D) larval brains depicting anterior (A, C) and posterior (B, D) clusters of primary ensheathing glia labeled by NP6520-Gal4 driving nuclear GFP in green relative to the semi-stereotyped primary astrocyte-like glia, astrocyte-like glia labeled by anti-Repo in red, and the neuropil labeled by anti-DN-cadherin in blue. Anatomical abbreviations found in Table 1. (E) 3D digital model of anterior surface of third instar larval brain hemisphere (medial to the left), depicting five pALG clusters. (F–I) Confocal sections of four brain hemispheres, labeled with anti-Repo (red) and NP6520-Gal4 (green). For clarity, non-CNS and non-primary neuropil glial staining was manually removed (A–I). Note invariant pattern of pALG (Repo-positive; NP6520-negative), corresponding to the cells shown in model (E). One cell,

ALm, can be always associated with the antennal lobe (AL), another one, LALa, with the lateral accessory lobe (LAL); one, SLPl, with the anterior surface of the SLP compartment; one or two (VLd) with the vertical lobe. By contrast, NP6520-positive pEG, with the exception of the four interhemispheric glia (arrow; two nuclei in focus), show more variability. For example, two pEG are close to the anterior SLP in the hemisphere shown in (F); one in (G); none in (H), and one in (I). Two pEG are close to the vertical lobe in (F), one in (G) and (H), and none in (I). Other abbreviations: SP spur of mushroom body. Bars: 25 μm.

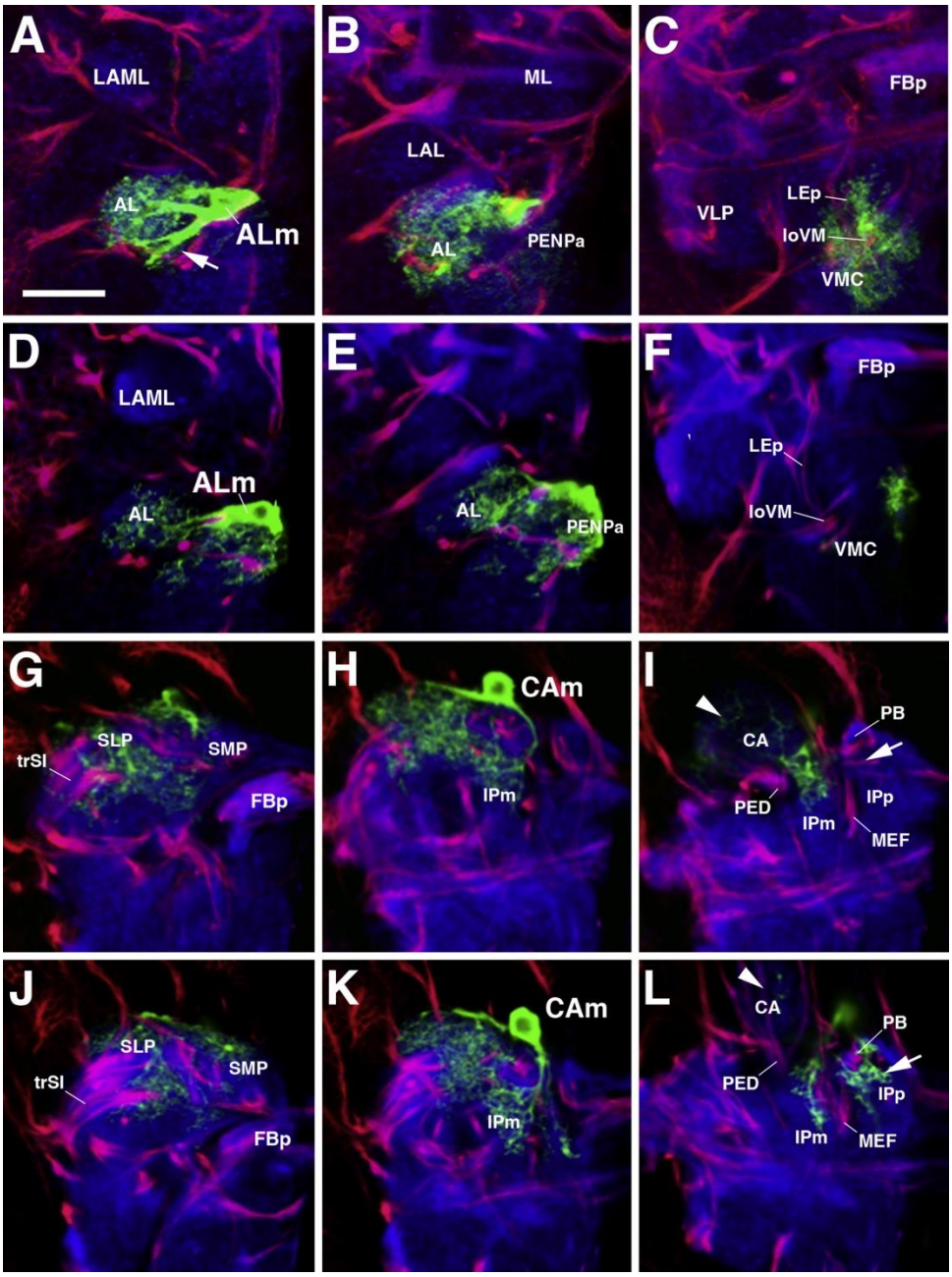

Figure 1-5: Branching pattern of primary astrocyte-like glial cells. (A–L) Z-projections of frontal confocal sections (dorsal, up; lateral, left) of late third instar larval brain hemispheres. GFP-labeled single-cell flp-out pALG clones in green, neuropil labeled by anti-DN-cadherin in blue, and secondary axon tracts labeled by anti-Neurotactin in red. (A–C) and (D–F): Antennal lobe medial (ALm) cell in two different brains. Z-projections

represent brain slices of 10–16 µm thickness at three different antero-posterior levels (A, D): anterior part of antennal lobe (AL); (B, E): posterior part of antennal lobe; (C, F): ventromedial cerebrum (VMC), posterior of antennal lobe. Even though both cells are located at the same position, the example shown in (A–C) projects more thick root branches towards the ventrolateral antennal lobe [arrow in (A)] and covers a larger part of the VMC (C) than the second example shown in (D–F). (G–I) and (J–L): Calyx medial (CAm) cell in two different brains. Z-projections taken at three antero-posterior levels [level of fan-shaped body primordium (FBp) (G, J); posterior of FBp, at the level of the medial inferior protocerebrum (IPm) (H, K); calyx (CA) (I, L)]. The projections of both examples of the CAm glia are very similar; note, however, more extensive arborizations of the cell shown in (G–I) in the calyx (CA; arrowheads in I, L) and the cell shown in (J–L) in the posterior inferior protocerebrum (IPp; arrows in I, L). Anatomical abbreviations found in Table 1. Bar: 20 µm.

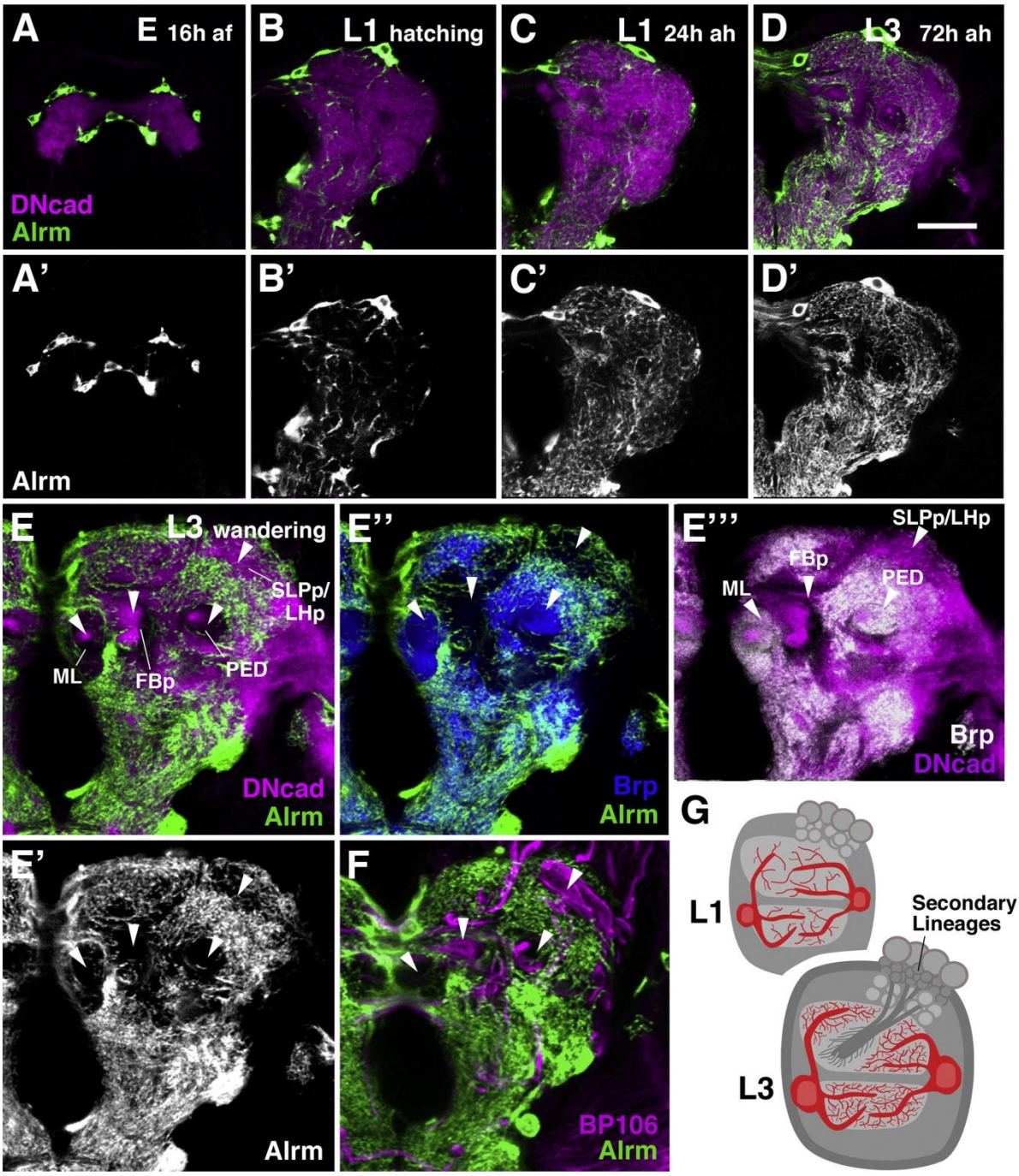

Figure 1-6: Morphogenesis of primary astrocyte-like glia. (A–F') Developmental time course of astrocyte-like glia from late embryo (16 h after fertilization) to the third instar wandering larva. pALG are labeled by alrm-Gal4 in green (A–F) and in grayscale (A′–D′, E′′). The neuropil is labeled by anti-DN-cadherin in magenta (A–E, E′′′). pALG

processes extend initially around the surface of the late embryonic neuropil (A–A′), followed by the formation of branches that penetrate into the neuropil in the freshly hatched larva (B–B′). Neuropil branches increase in density throughout larval development (C–E'). The third instar larval neuropil contains "gaps" in the density of pALG processes [arrowheads in (E–F)], which correspond to domains where fiber bundles of secondary neurons labeled by Neurotactin (BP106) penetrate into the neuropil (F). These undifferentiated fibers form the primordia of adult neuropil compartments; they lack synapses [see absence of blue and white Brp signal in (E" and E"'), respectively], but are positive for DN-cadherin [magenta signal in (E, E"')]. Processes of pALG are restricted to the Brp-positive (synapse-rich) neuropil domains (E"). (G) Schematic depicting the coordinate morphogenesis (increase in cell size and process density) of primary astrocyte-like glia and the increasing neuropil volume from early to late larva. Anatomical abbreviations found in Table 1. Other abbreviations: af, after fertilization; ah, after hatching. Bar: 25 μm.

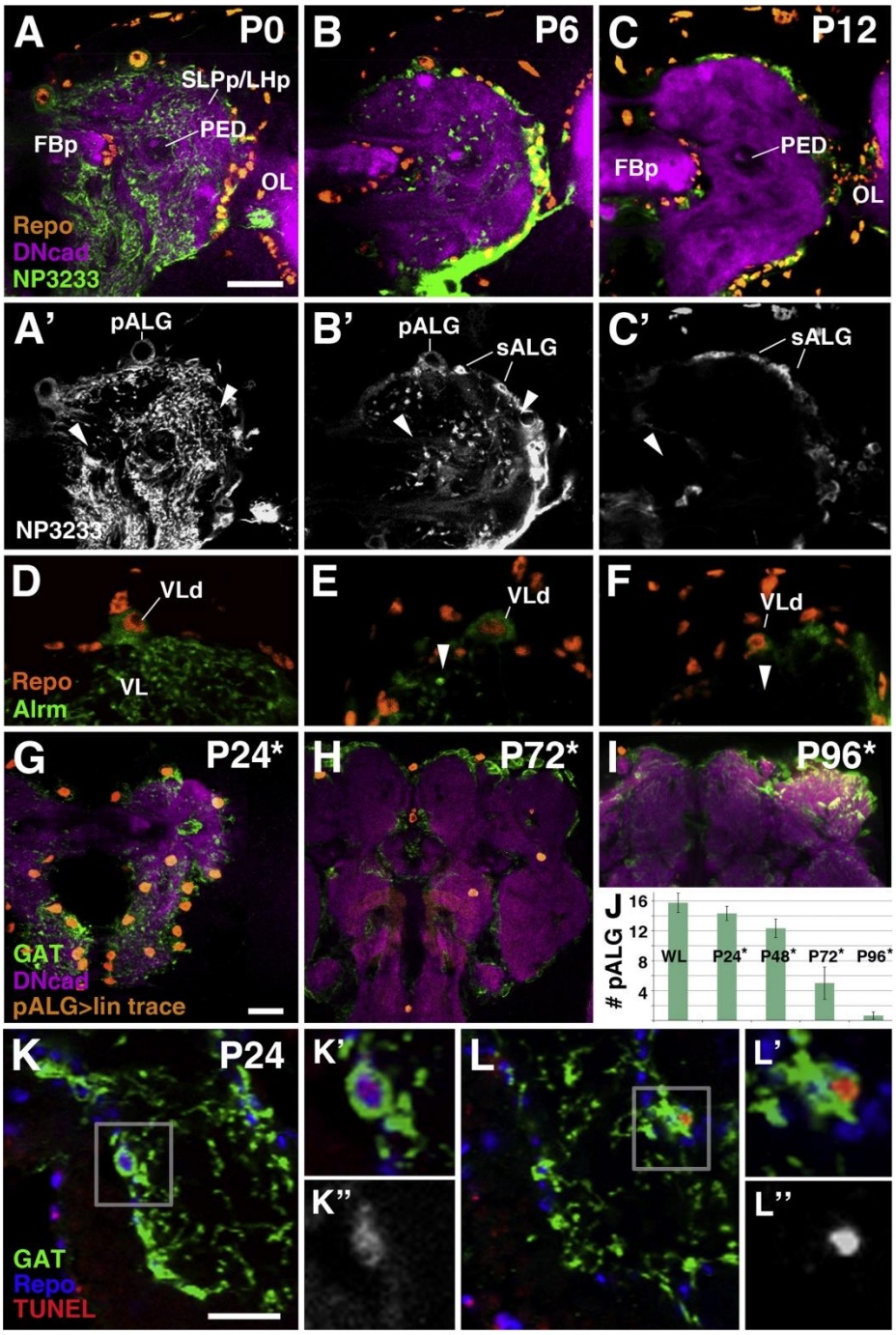

Figure 1-7: Primary astrocyte-like glia undergo programmed cell death during metamorphosis. (A–F) Developmental time course of astrocyte-like glia from white prepupa (P0) to P12. ALG are labeled by NP3233-Gal4 in green (A–C) and in grayscale (A′–C′). The neuropil is labeled by anti-DN-cadherin in magenta and glial cell nuclei are

labeled by anti-Repo in orange in (A–C). (D–F) High magnification images of the dorsal neuropil in context of the vertical lobe (VL, arrowheads); pALG in green labeled by alrm-Gal4 and glial cell nuclei labeled by anti-Repo in orange [looking specifically at the vertical lobe dorsal cell (VLd)] at equivalent stages as (A–C). At P0 (A–A′, D) highly branched pALG processes are seen throughout the neuropil. During the first six hours of metamorphosis, pALG processes start to undergo fragmentation and vacuolization (B–B′, E). At P12, pALG processes are almost undetectable in the neuropil using Gal4 drivers (C–C′, F). Note also small, NP3233 and Repo-positive sALG precursors emerging at the neuropil-cortex interface (B–C′). (G–I) Lineage tracing of alrm-Gal4 expressing pALG. Nuclei of lineage traced cells are labeled in orange, anti-GAT in green, and anti-DN-cadherin in magenta. Asterisk indicates estimated time points based on rate of development at 18 °C. (G) Lineage traced pALG are still relatively present at P24. (H–I) By the mid-pupal stage, the number of lineage traced nuclei declines and remaining nuclei appear atrophied; no pALG can be detected in the late pupa or adult. (J) Quantification of lineage traced pALG throughout metamorphosis. pALG numbers steadily decline until mid-metamorphosis, and quickly decline during late metamorphosis (n≥3 for each time point). (K–L) TUNEL labeling of pALG at P24. pALG somata at this stage can still be detected, unlike the Gal4 drivers, using anti-GAT (green). Sparse TUNEL labeling (red) can be observed in pALG (gray in K′′ and L′′) at this stage. Anti-Repo is shown in blue. Anatomical abbreviations found in Table 1. Bar: 25 μm.

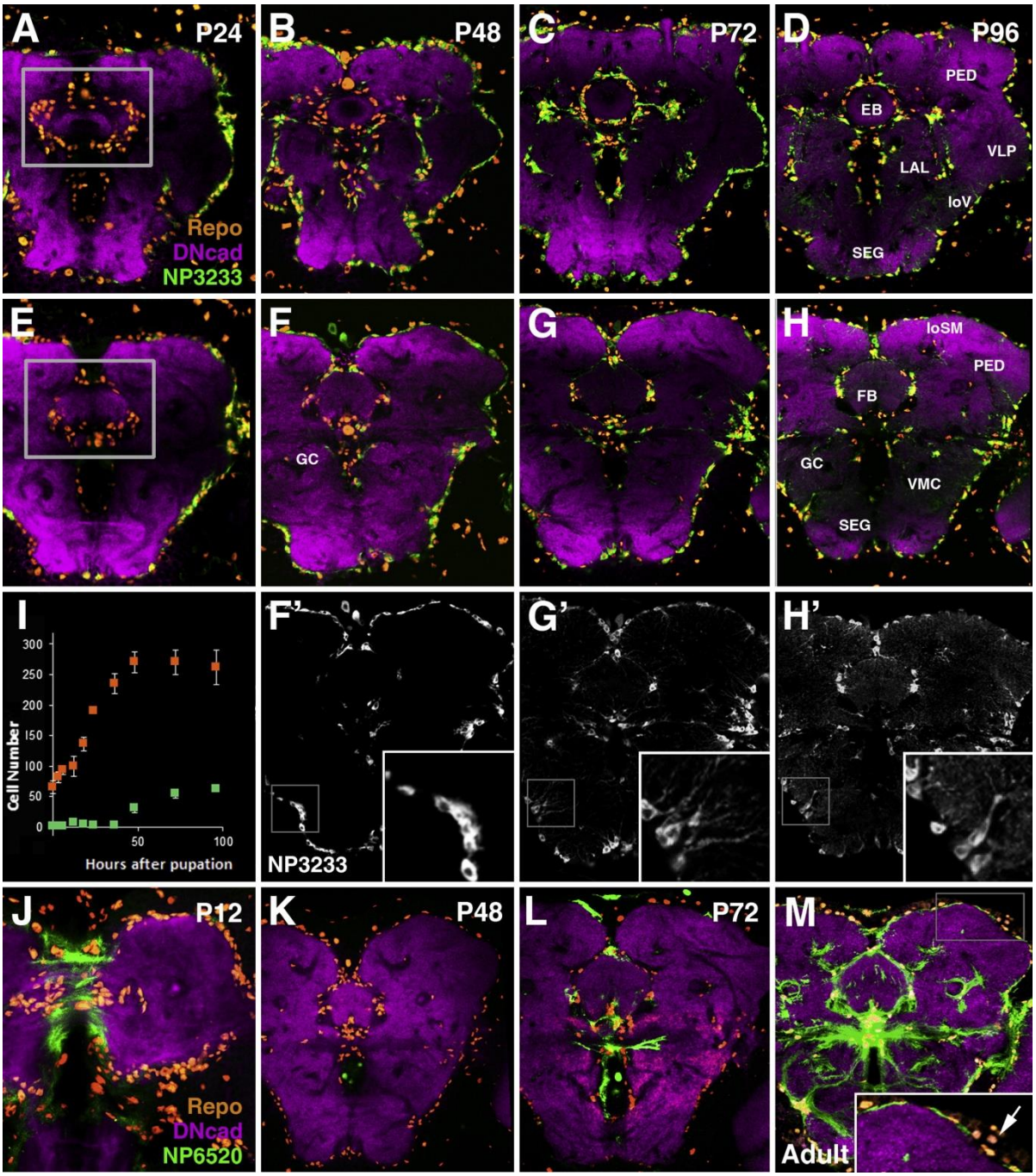

Figure 1-8: Pattern of secondary neuropil glia throughout metamorphosis. (A–H) Z-projections of frontal confocal sections of pupal brains in which sALG are labeled by NP3233-Gal4 (green); the neuropil is visualized by anti-DN-cadherin (magenta), and glial cell nuclei are labeled by anti-Repo (orange). sALG from (F–H) are shown in grayscale with high magnification insets of boxed regions in (F'–H'). Panels of first row

(A–D) show z-projections at level of ellipsoid body (EB); panels of second and third row (E–H, F′–H′) show slightly more posterior level at fan-shaped body (FB). Boxed regions in (A, E) depict the domains in which cell counts were conducted (I); (I) total Repo-positive cells associated with the central complex (i.e. EB, FB, noduli) are shown in orange, fraction of Repo-positive cells which co-express NP3233-Gal4 is shown in light green (n≥3 for each time point). At early and mid-pupal stages, sALG spread out around neuropil surface and central complex primordium while at the same time increasing in number (A, E, B, F–F′). sALG processes do not yet enter the neuropil at significant numbers (see inset in F′). During the second half of the pupal stage (C, G–G′), radial processes emanate from the sALG into the neuropil (see inset in G'). Glial processes form a rich network of branches during the last day of metamorphosis (D, H–H'; see inset in H'). (J–M) Developmental time course of primary and secondary ensheathing glia (sEG) from P12 to adult at the level of the fan-shaped body (FB) and great commissure (GC). EG are labeled by NP6520-Gal4 in green, neuropil is labeled by anti-DN-cadherin in magenta, and glial cell nuclei are labeled by anti-Repo in orange. At P12 (J) primary EG of the larva are still present. During mid-metamorphosis (K), NP6520-positive pEG are no longer seen. NP6520 expression in secondary EG appears first around the central complex (L), followed by expression at the neuropil surface (M). Clusters of NP6520-Gal4 negative neuropil glia, interpreted as sALG, occupy regions of low sEG density at the adult neuropil surface (M, inset; arrow). Anatomical abbreviations found in Table 1. Bar: 50 µm.

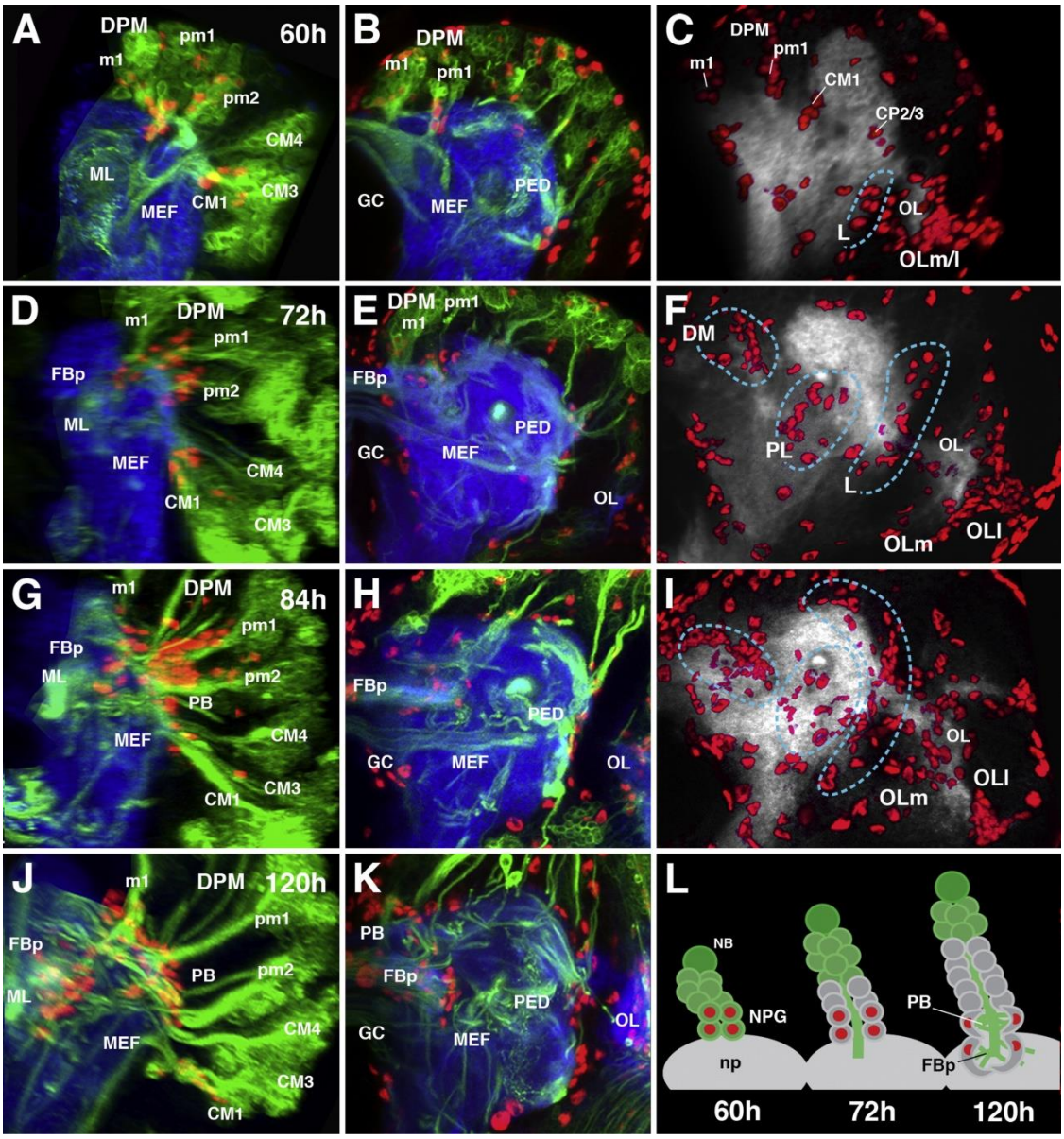

Figure 1-9: Origin and migration of secondary neuropil glial precursors throughout larval development. (A–K) Confocal z-projections depicting parasagittal views (first column) frontal view at the level of the fan-shaped body primordium (second column) and frontal view of anti-Repo volume renderings (third column) of larval development from 60 h ah (A–C) to 120 h ah (J–K). Neuro-(glio)blast lineages are labeled by insc-Gal4 in green, glial nuclei by anti-Repo in red, and the neuropil by anti-DN-cadherin in blue (A–B, D–E, G–H, J–K). (C, F, I) Neuropil is labeled by anti-DN-cadherin in gray and

volume renderings of glial nuclei labeled by anti-Repo in red. For clarity, in parasagittal views (A, D, G, J), type I lineages were manually erased, along with cortex and surface glia. Secondary neuropil glia emerge within identifiable type II lineage clusters (A–C, L). Secondary neuropil glia remain associated with the axon tracts of the lineages from which they emerge and reach the neuropil surface (D–E, L), followed by invasion into the brain to associate with emerging neuropil compartments such as the fan-shaped body primordium (G–H, J–K, L), and spread out onto the posterior lateral surface of the neuropil (I–L). Neuropil glia can initially be identified as constituents of specific lineages (C), and subsequently distribute into rough categories (demarcated by cyan hashed lines): dorsomedial (DM), postero-lateral (PL), and lateral (L) clusters (F). Anatomical abbreviations found in Table 1. Other abbreviations: np, neuropil; OLm/l, medial and lateral optic lobe glia.

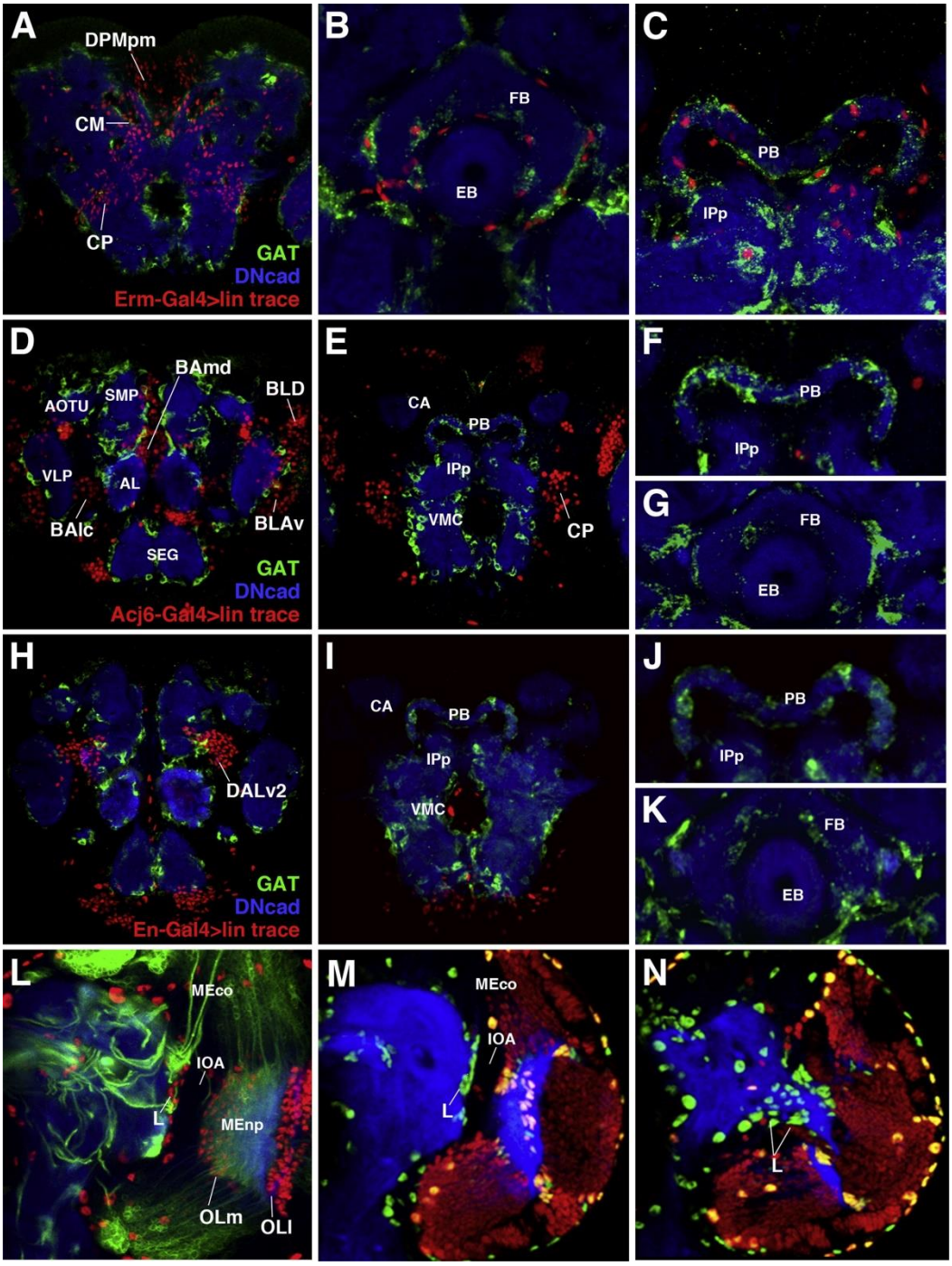

Figure 1-10: Both neuropil glia subtypes of the central complex derive from intermediate progenitors of multipotent type II neuroglioblasts, but do not derive from the optic lobe (A–K) Frontal confocal z-projections of P48 brains. The neuropil is labeled by anti-DN-cadherin in blue, secondary astrocyte-like glia by GAT in green, and lineage

traced cells from specific progenitor populations by anti-β-gal in red. Progeny of type II lineage intermediate progenitors (INPs) (A–C), and the type I neuroblast lineages BLD, BAmd, BALc, BLAv (D–G), and DALv2 (H–K), were labeled by erm-Gal4, acj6-Gal4, and engrailed-Gal4, respectively. Neuronal progeny of INPs can be observed by a z-projection of posterior brain (A), and neuropil glial progeny can be observed around compartments of the central complex [(ellipsoid body and fan-shaped body, B; protocerebral bridge, C)]. Neuronal progeny of acj6- and engrailed-positive lineages can be observed in anterior (D, H) and posterior (E, I) z-projections of the brain, but no glial progeny are associated with the compartments of the central complex (F–G, J–K). (L) Frontal confocal z-projection of a third instar larval brain at the level of the inner optic anlage (IOA) depicting medial (OLm) and lateral (OLl) populations of optic lobe glia. Neuro-(glio)blast lineages are labeled by insc-Gal4 in green, glial nuclei by anti-Repo in red, and the neuropil by anti-DN-cadherin in blue. Lateral population of secondary neuropil glia precursors (L) is indicated and, posteriorly (not shown), exhibits a continuity with medial glial cells of the optic lobe (OLm). Confocal z-projections of the intermediate (M) and posterior (N) neuropil of a third instar larval brain. Glial nuclei labeled by anti-Repo in green, the neuropil by anti-DN-cadherin in blue, and neuronal/glial progeny of sine oculis-positive progenitors (optic lobe placode) labeled in red. Optic lobe placode-derived neurons (red) and glia (orange) revealed by sine oculis lineage tracing reveals that the lateral population (L) of secondary neuropil glia are not optic lobe-derived. Anatomical abbreviations found in Table 1.

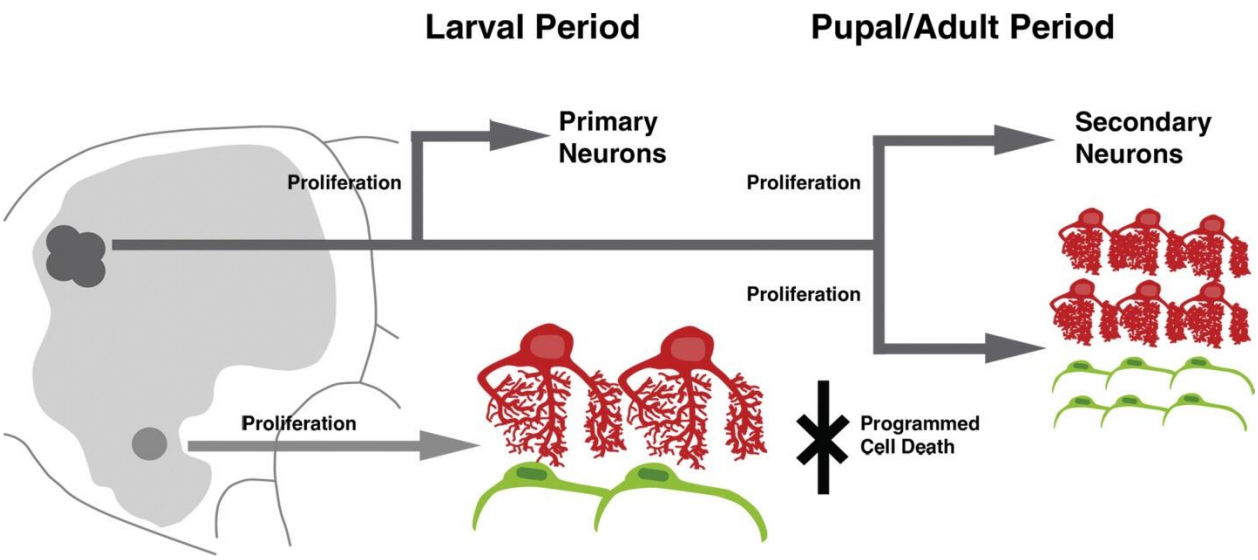

Figure 1-11: Working model for the lineage and development of neuropil glia throughout Drosophila brain development. Primary neuropil glia of the brain [pALG (red) and pEG (green)] are derived from dedicated glioblasts located in the basal brain located at the tritocerebrum and deuterocerebrum boundary. Primary neuropil glia are large cells which are few in number; they increase cellular size likely via endoreplication to account for the expanding neuropil. Primary neuropil glia undergo programmed cell death and do not contribute to neuropil glia of the adult. Type II lineages, which likely give rise solely to neurons during the embryonic (primary) phase of progenitor proliferation, undergo a secondary phase of multipotent proliferation in which they give rise to secondary neurons and secondary neuropil glia precursors. Secondary neuropil glia precursors are small, spindle-shaped cells which greatly expand in number around the developing neuropil compartments and ultimately differentiate into secondary astrocyte-like and ensheathing glia [sALG (red) and sEG (green)] of the adult brain.

References

Ashburner, M., 1989. Drosophila. A laboratory manual. Cold Spring Harbor Laboratory Press, Cold Spring Harbor, NY, pp. 214–217.

Avet-Rochex, A., Kaul, A.K., Gatt, A.P., McNeill, H., Bateman, J.M., 2012. Concerted control of gliogenesis by InR/TOR and FGF signalling in the Drosophila postembryonic brain. Development 139, 2763–2772.

Awasaki, T., Lai, S.L., Ito, K., Lee, T., 2008. Organization and postembryonic development of glial cells in the adult central brain of Drosophila. J. Neurosci. 28, 13742–13753.

Bastiani, M.J., Goodman, C.S., 1986. Guidance of neuronal growth cones in the grasshopper embryo. III. Recognition of specific glial pathways. J. Neurosci. 6, 3542–3551.

Bayraktar, O.A., Boone, J.Q., Drummond, M.L., Doe, C.Q., 2010. Drosophila type II neuroblast lineages keep Prospero levels low to generate large clones that contribute to the adult brain central complex. Neural Dev. 5, 26.

Bayraktar, O.A., Doe, C.Q., 2013. Combinatorial temporal patterning in progenitors expands neural diversity. Nature 498, 449–455.

Beckervordersandforth, R.M., Rickert, C., Altenhein, B., Technau, G.M., 2008. Subtypes of glial cells in the Drosophila embryonic ventral nerve cord as related to lineage and gene expression. Mech. Dev. 125, 542–557.

Bossing, T., Technau, G.M., 1994. The fate of the CNS midline progenitors in Drosophila as revealed by a new method for single cell labelling. Development 120, 1895–1906.

Boyan, G., Loser, M., Williams, L., Liu, Y., 2011. Astrocyte-like glia associated with the embryonic development of the central complex in the grasshopper Schistocerca gregaria. Dev. Genes Evol. 221, 141–155.

Boyan, G., Williams, L., Götz, S., 2013. Postembryonic development of astrocyte-like glia of the central complex in the grasshopper Schistocerca gregaria. Cell Tissue Res. 351, 361–372.

Cantera, R., 1992. Glial cells in adult and developing prothoracic ganglion of the hawk moth Manduca sexta. Cell Tissue Res. 272, 93–108.

Cantera, R., Technau, G.M., 1996. Glial cells phagocytose neuronal debris during the metamorphosis of the central nervous system in Drosophila melanogaster. Dev. Genes Evol. 206, 277–280.

Cardona, A., Saalfeld, S., Schindelin, J., Arganda-Carreras, I., Preibisch, S., Longair, M., Tomancak, P., Hartenstein, V., Douglas, R.J., 2012. TrakEM2 software for neural circuit reconstruction. PLoS ONE 7 (6), e38011. http://dx.doi.org/10.1371/journal.pone.0038011.

Chang, T., Shy, D., Hartenstein, V., 2003. Antagonistic relationship between Dpp and EGFR signaling in Drosophila head patterning. Dev. Biol. 263, 103–113.

Clarke, L.E., Barres, B.A., 2013. Emerging roles of astrocytes in neural circuit development. Nat. Rev. Neurosci. 14, 311–321.

DeSalvo, M.K., Mayer, N., Mayer, F., Bainton, R.J., 2011. Physiologic and anatomic characterization of the brain surface glia barrier in Drosophila. Glia 59, 1322–1340.

Doherty, J., Logan, M.A., Taşdemir, O.E., Freeman, M.R., 2009. Ensheathing glia function as phagocytes in the adult Drosophila brain. J. Neurosci. 29, 4768–4781.

Dumstrei, K., Wang, F., Hartenstein, V., 2003. Role of DE-cadherin in neuroblast proliferation, neural morphogenesis, and axon tract formation in Drosophila larval brain development. J. Neurosci. 23, 3325–3335.

Edwards, T.N., Meinertzhagen, I.A., 2010. The functional organisation of glia in the adult brain of Drosophila and other insects. Prog. Neurobiol. 90, 471–497.

Gibson, N.J., Tolbert, L.P., Oland, L.A., 2012. Activation of glial FGFRs is essential in glial migration, proliferation, and survival and in glia-neuron signaling during olfactory system development. PLoS ONE 7 (4), e33828. http://dx.doi.org/10.1371/journal.pone.0033828.

Griffiths, R.L., Hidalgo, A., 2004. Prospero maintains the mitotic potential of glial precursors enabling them to respond to neurons. EMBO J. 23, 2440–2450.

Grosjean, Y., Grillet, M., Augustin, H., Ferveur, J.F., Featherstone, D.E., 2008. A glial amino-acid transporter controls synapse strength and courtship in Drosophila. Nat. Neurosci. 11, 54–61.

Hakim, Y., Yaniv, S.P., Schuldiner, O., 2014. Astrocytes play a key role in Drosophila mushroom body axon pruning. PLoS ONE 9 (1), e86178. http://dx.doi.org/10.1371/journal.pone.0086178.

Hartenstein, V., 2011. Morphological diversity and development of glia in Drosophila. Glia 59, 1237–1252.

Hartenstein, V., Nassif, C., Lekven, A., 1998. Embryonic development of the Drosophila brain. II. Pattern of glial cells. J. Comp. Neurol. 402, 32–47.

Hartline, D.K., 2011. The evolutionary origins of glia. Glia 59, 1215–1236.

Hidalgo, A., Booth, G.E., 2000. Glia dictate pioneer axon trajectories in the Drosophila embryonic CNS. Development 127, 393–402.

Hidalgo, A., Urban, J., Brand, A.H., 1995. Targeted ablation of glia disrupts axon tract formation in the Drosophila CNS. Development 121, 3703–3712.

Hosoya, T., Takizawa, K., Nitta, K., Hotta, Y., 1995. Glial cells missing: a binary switch between neuronal and glial determination in Drosophila. Cell 82, 1025–1036.

Hoyle, G., 1986. Glial cells of an insect ganglion. J. Comp. Neurol. 246, 85–103.

Hoyle, G., Williams, M., Phillips, C., 1986. Functional morphology of insect neuronal cell-surface/glial contacts: the trophospongium. J. Comp. Neurol. 246, 113–128.

Ito, K., Hotta, Y., 1992. Proliferation pattern of postembryonic neuroblasts in the brain of Drosophila melanogaster. Dev. Biol. 149, 134–148.

Ito, K., Urban, J., Technau, G.M., 1995. Distribution, classification, and development of Drosophila glial cells in the late embryonic and early larval ventral nerve cord. Roux's Arch. Dev. Biol. 204, 284–307.

Izergina, N., Balmer, J., Bello, B., Reichert, H., 2009. Postembryonic development of transit amplifying neuroblast lineages in the Drosophila brain. Neural. Dev. 4, 44.

Jackson, F.R., Haydon, P.G., 2008. Glial cell regulation of neurotransmission and behavior in Drosophila. Neuron Glia Biol. 4, 11–17.

Jacobs, J.R., Goodman, C.S., 1989. Embryonic development of axon pathways in the Drosophila CNS. I. A glial scaffold appears before the first growth cones. J. Neurosci. 9, 2402–2411.

Jacobs, J.R., Hiromi, Y., Patel, N.H., Goodman, C.S., 1989. Lineage, migration, and morphogenesis of longitudinal glia in the Drosophila CNS as revealed by a molecular lineage marker. Neuron 2, 1625–1631.

Jones, B.W., Fetter, R.D., Tear, G., Goodman, C.S., 1995. Glial cells missing: a genetic switch that controls glial versus neuronal fate. Cell 82, 1013–1023.

Kumar, A., Bello, B., Reichert, H., 2009a. Lineage-specific cell death in postembryonic brain development of Drosophila. Development 136, 3433–3442.

Kumar, A., Fung, S., Lichtneckert, R., Reichert, H., Hartenstein, V., 2009b. Arborization pattern of engrailed-positive neural lineages reveal neuromere boundaries in the Drosophila brain neuropil. J. Comp. Neurol. 517, 87–104.

Liu, Y., Boyan, G., 2013. Glia associated with central complex lineages in the embryonic brain of the grasshopper Schistocerca gregaria. Dev. Genes Evol. 223, 213–223.

Muthukumar, A.K., Stork, T., Freeman, M.R., 2014. Activity-dependent regulation of astrocyte GAT levels during synaptogenesis. Nat. Neurosci. 17, 1340–1350.

Oland, L.A., Biebelhausen, J.P., Tolbert, L.P., 2008. Glial investment of the adult and developing antennal lobe of Drosophila. J. Comp. Neurol. 509, 526–550.

Oland, L.A., Gibson, N.J., Tolbert, L.P., 2010. Localization of a GABA transporter to glial cells in the developing and adult olfactory pathway of the moth Manduca sexta. J. Comp. Neurol. 518, 815–838.

Oland, L.A., Marrero, H.G., Burger, I., 1999. Glial cells in the developing and adult olfactory lobe of the moth Manduca sexta. Cell Tissue Res. 297, 527–545.

Pereanu, W., Hartenstein, V., 2006. Neural lineages of the Drosophila brain: a three dimensional digital atlas of the pattern of lineage location and projection at the late larval stage. J. Neurosci. 26, 5534–5553.

Pereanu, W., Kumar, A., Jennett, A., Reichert, H., Hartenstein, V., 2010. Development based compartmentalization of the Drosophila central brain. J. Comp. Neurol. 518, 2996–3023.

Pereanu, W., Shy, D., Hartenstein, V., 2005. Morphogenesis and proliferation of the larval brain glia in Drosophila. Dev. Biol. 283, 191–203.

Prokop, A., Technau, G.M., 1994. BrdU incorporation reveals DNA replication in non dividing glial cells in the larval abdominal CNS of Drosophila. Roux's Arch. Dev. Biol. 204, 54–61.

Reddy, B.V., Irvine, K.D., 2011. Regulation of Drosophila glial cell proliferation by Merlin-Hippo signaling. Development 138, 5201–5212.

Schindelin, J., Arganda-Carreras, I., Frise, E., Kaynig, V., Longair, M., Pietzsch, T., Preibisch, S., Rueden, C., Saalfeld, S., Schmid, B., Tinevez, J.Y., White, D.J.,

Hartenstein, V., Eliceiri, K., Tomancak, P., Cardona, A., 2012. Fiji: an open source platform for biological-image analysis. Nat. Methods 9, 676–682.

Schmidt, H., Rickert, C., Bossing, T., Vef, O., Urban, J., Technau, G.M., 1997. The embryonic central nervous system lineages of Drosophila melanogaster. II. Neuroblast lineages derived from the dorsal part of the neuroectoderm. Dev. Biol. 189, 186–204.

Sinakevitch, I., Grau, Y., Strausfeld, N.J., Birman, S., 2010. Dynamics of glutamatergic signaling in the mushroom body of young adult Drosophila. Neural Dev. 5, 10.

Singh, K., Singh, R.N., 1999. Metamorphosis of the central nervous system of Drosophila melanogaster Meigen (Diptera: Drosophilidae) during pupation. J. Biosci. 24, 345–360.

Spindler, S.R., Ortiz, I., Fung, S., Takashima, S., Hartenstein, V., 2009. Drosophila cortex and neuropile glia influence secondary axon tract growth, pathfinding, and fasciculation in the developing larval brain. Dev. Biol. 334, 335–368.

Stacey, S.M., Muraro, N.I., Peco, E., Labbé, A., Thomas, G.B., Baines, R.A., van Meyel, D.J., 2010. Drosophila glial glutamate transporter Eaat1 is regulated by fringemediated notch signaling and is essential for larval locomotion. J. Neurosci. 30, 14446–14457.

Stork, T., Engelen, D., Krudewig, A., Silies, M., Bainton, R.J., Klämbt, C., 2008. Organization and function of the blood-brain barrier in Drosophila. J. Neurosci. 28, 587–597.

Stork, T., Sheehan, A., Tasdemir-Yilmaz, O.E., Freeman, M.R., 2014. Neuron-glia interactions through the Heartless FGF receptor signaling pathway mediate morphogenesis of Drosophila astrocytes. Neuron 83, 388–403.

Tasdemir-Yilmaz, O.E., Freeman, M.R., 2014. Astrocytes engage unique molecular programs to engulf pruned neuronal debris from distinct subsets of neurons. Genes Dev. 28, 20–33.

Thomas, G.B., van Meyel, D.J., 2007. The glycosyltransferase Fringe promotes Delta Notch signaling between neurons and glia, and is required for subtype-specific glial gene expression. Development 134, 591–600.

Unhavaithaya, Y., Orr-Weaver, T.L., 2012. Polyploidization of glia in neural development links tissue growth to blood-brain barrier integrity. Genes Dev. 26, 31–36.

Urbach, R., Technau, G.M., 2003. Molecular markers for identified neuroblasts in the developing brain of Drosophila. Development 130, 3621–3637.

Viktorin, G., Riebli, N., Popkova, A., Giangrande, A., Reichert, H., 2011. Multipotent neural stem cells generate glial cells of the central complex through transit amplifying intermediate progenitors in Drosophila brain development. Dev. Biol. 356, 553–565.

Viktorin, G., Riebli, N., Reichert, H., 2013. A multipotent transit-amplifying neuroblast lineage in the central brain gives rise to optic lobe glial cells in Drosophila. Dev. Biol. 379, 182–194.

Vincent, S., Vonesch, J.L., Giangrande, A., 1996. Glide directs glial fate commitment and cell fate switch between neurones and glia. Development 122, 131–139.

Xiong, W.C., Okano, H., Patel, N.H., Blendy, J.A., Montell, C., 1994. repo encodes a glial-specific homeo domain protein required in the Drosophila nervous system. Genes Dev. 8, 981–994.

Yu, H.H., Awasaki, T., Schroeder, M.D., Long, F., Yang, J.S., He, Y., Ding, P., Kao, J.C., Wu, G.Y., Peng, H., Myers, G., Lee, T., 2013. Clonal development and organization of the adult Drosophila central brain. Curr. Biol. 23, 633–643.

Zecca, M., Struhl, G., 2002. Subdivision of the Drosophila wing imaginal disc by EGFR-mediated signaling. Development 129, 1357–1368.

Chapter 2 - Visual input to the *Drosophila* central complex by developmentally and functionally distinct neuronal populations

Abstract

The *Drosophila* central brain consists of stereotyped neural lineages, developmental-structural units of macrocircuitry formed by the sibling neurons of single progenitors called neuroblasts. We demonstrate that the lineage principle guides the connectivity and function of neurons providing input to the central complex, a collection of neuropil compartments important for visually-guided behaviors. One of these compartments is the ellipsoid body (EB), a structure formed largely by the axons of ring (R) neurons, all of which are generated by a single lineage, DALv2. Two further lineages, DALcl1 and DALcl2, produce neurons that connect the anterior optic tubercle, a central brain visual center, with R neurons. Finally, DALcl1/2 receive input from visual projection neurons of the optic lobe medulla, completing a three-legged circuit we call the anterior visual pathway (AVP). The AVP bears fundamental resemblance to the sky-compass pathway, a visual navigation circuit described in other insects. Neuroanatomical analysis and two-photon calcium imaging demonstrates that DALcl1 and DALcl2 form two parallel channels, establishing connections with R neurons located in the peripheral and central domains of the EB, respectively. Although neurons of both lineages preferentially respond to bright objects, DALcl1 neurons have small ipsilateral, retinotopically-ordered receptive fields, whereas DALcl2 neurons share a large excitatory receptive field in the contralateral hemifield. DALcl2 neurons become inhibited when the object enters the ipsilateral hemifield, and display an additional

excitation after the object leaves the field of view. Thus, the spatial position of a bright feature, such as a celestial body, may be encoded within this pathway.

Introduction

The central complex (CX) is an evolutionarily conserved domain in the insect brain that has a highly ordered, modular neuronal architecture. In *Drosophila*, it comprises several compartments that are situated across the brain midline, including (from anterior to posterior), the ellipsoid body (EB), fan-shaped body (FB) with noduli (NO), and protocerebral bridge (PB) (Hanesch et al., 1989; Ito et al., 2014, Strausfeld, 1976). The ellipsoid body is flanked laterally by two compartments of the lateral complex, the bulb (BU) and lateral accessory lobe (LAL), which act as portals for input to and output from the central complex.

Numerous anatomical, functional, and genetic studies conducted in the past suggest that the central complex is involved, among other functions, in the control of motor output and spatial orientation. Stimulation of the CX alters a large number of behaviors that require fine motor control, including stridulation, walking, and escape (Huber 1960; Otto 1971). Genetic lesions of the CX affect walking and flight (Ilius et al., 1994; Strauss and Heisenberg, 1993; Strauss et al., 1992). Silencing specific classes of ring neurons innervating the ellipsoid body of the CX causes deficits in visual place learning and spatial orientation memory in *Drosophila* (Neuser et al., 2008; Ofstad et al., 2011). Along these lines, functional imaging studies in behaving flies suggest that populations of columnar neurons in the CX encode the fly's spatial orientation relative to its environment (Seelig and Jayaraman, 2015), suggesting that the CX could play a navigational role similar to that one of the hippocampus and entorhinal cortex in mammals (Poucet et al., 2015; Rowland et al., 2016).

Similar to the mushroom body, another highly structured neuropil domain of the insect brain known for its pivotal function in olfactory learning and memory, the central complex does not receive direct input from peripheral sense organs. Processed sensory information is relayed from the primary olfactory center (antennal lobe) to the mushroom body via antennal lobe projection neurons. These anatomically and functionally specialized neurons are derived from four developmentally defined classes, so called lineages (Lai et al., 2008). A lineage comprises all neurons produced by a single neural progenitor (neuroblast). The fly brain is generated by approximately 100 pairs of such neuroblasts, each of which defined by a unique pattern of gene expression that dictates the morphology and function of the cells within the lineage (Hartenstein et al., 2008). Its lineage-based composition provides great conceptual and technical advantages to analyze the structure and development of the antennal lobe projection in great detail, making this input pathway one of the preeminent model systems to study the genetic mechanism controlling the assembly of a central brain circuit (Jefferis et al., 2001; Marin et al., 2002; Wong et al., 2002).

By comparison to the antennal lobe input pathway towards the mushroom body, very little is known about the circuitry providing input to the *Drosophila* central complex. It must receive input from the visual system; dendrites of ellipsoid body ring (R) neurons, located in the bulb, are sensitive to visual stimuli and form a retinotopically-ordered arrangement (Seelig and Jayaraman, 2013). In other insects, neurons conducting visual information from the optic lobe to the CX have been characterized, using anatomical and electrophysiological methods, in considerable detail (el Jundi et al., 2014). This circuit, called the sky-compass pathway, is thought to encode skylight

cue information relevant for navigation, such as the spatial position of bright celestial bodies, the pattern of polarized light in the sky, or the sky's spectral gradient. It is a pathway consisting of multiple layers; neurons of the optic lobe medulla project to a known domain of visual input in the central brain called the anterior optic tubercle (AOTU). From there, information is relayed by another neuronal population to the bulb, the input domain of tangential neurons of the central body lower division (homologous to *Drosophila* ring neurons and ellipsoid body). In this paper, we have investigated the visual input pathway to the central complex in *Drosophila*. Which, if any, lineages form the "building blocks" of this pathway? Does the lineage principle guide the structural connectivity and thus, the function of neuronal circuit elements within this pathway?

Using clonal analysis, we and others previously identified the projection pattern for the majority of neuroblast lineages in the *Drosophila* brain (Ito et al., 2013; Lovick et al., 2013; Wong et al., 2013; Yu et al., 2013). This analysis revealed that ring (R) neurons of the ellipsoid body are derived from a single paired lineage (DALv2). Two additional lineages (DALcl1 and 2) were identified; similarly to neurons in the sky-compass pathway, they project from the anterior optic tubercle to the bulb, and we thus call them tuberculo-bulbar (TuBu) neurons. Identification of Gal4 drivers which reflect the projection pattern of neurons within these lineages allowed us to demonstrate a parallel pattern of topographically-ordered connectivity within this pathway. Double labeling and GFP reconstitution across synaptic partners (GRASP) demonstrates that TuBu neurons provide direct input to R neurons. Two-photon calcium imaging of TuBu neuron presynaptic terminals further corroborates this notion; TuBu neuron outputs from DALcl1, which predominantly innervate the superior domain of the bulb, exhibit similar

response properties as R neuron dendrites from the same region, based on previous studies (Seelig and Jayaraman, 2013). However, DALcl2 TuBu neuron outputs, which predominantly innervate the inferior domain of the bulb, do not respond in the same fashion, demonstrating that the lineage principle determines not only the structure, but also the function of neuronal populations.

Materials and Methods

Drosophila stocks

Flies were reared at 25°C using standard fly media unless otherwise noted. The *Drosophila* driver lines utilized in this study, as well as more specific genotype information, are listed in the Supplemental Experimental Procedures. The following general transgenic fly stocks were used: *UAS-DenMark::mCherry, UAS-Syt::GFP* [29], *su(Hw)attP8:HA_V5_FLAG_1* [31], *10xUAS-mCD8::GFP, 10XUAS-IVS-mCD8::RFP, 13XLexAop2-mCD8::GFP, LexAop-CD2::RFP, UAS-CD4::spGFP1-10, LexAop-CD4::spGFP11, 20xUAS-GCAMP6m* (Bloomington Stock Center, Bloomington, Indiana).

Clonal analysis

GFP-labeled adult neuroblast MARCM clones were induced at the late first instar/early second instar stage by heat-shocking in a water bath at 38 °C for 30-60 min. Larvae were approximately 12-44 hours old. Heat-shocked larvae were grown to adult for analysis.

Single cell analysis of neurons in the AVP pathway was conducted using the multicolor flip-out (MCFO) method described previously [31,33]. Briefly, depending on the cell density of a given Gal4 line, 1-3 day old flies were dissected to obtain single cell labeling.

Immunostaining, confocal microscopy, and image analysis

Immunohistochemistry was performed using standard procedures with some modifications [62], details for staining procedures and list of antibodies are in Supplemental Experimental Procedures. *Drosophila* adult brains labeled with antibody

markers were viewed as whole-mounts in Vectashield mounting medium H-1000 (Vector Laboratories), by confocal microscopy [LSM 700 Imager M2 using Zen 2009 (Carl Zeiss Inc.); lenses: 40× oil (numerical aperture 1.3)]. Complete series of optical sections were taken from preparations between 1.2 and 2-μM intervals. Preparations were mounted anteriorly or dorsally. Dorsally-oriented preparations were acquired by sliding the brain dorsal-side up, inside the crevice between two closely apposed cover slips. Captured images were processed by ImageJ or FIJI (National Institutes of Health, http://rsbweb.nih.gov/ij/ and http://fiji.sc/). In some panels, such as panel E of Fig.1, background labeling was manually removed to improve clarity of specific neuronal morphologies. In this case, ventral hemilineages of DALcl1/2 were digitally removed, and z-projections of the labeled dorsal hemilineages were registered digitally with z-projections of a standard brain at the corresponding antero-posterior plane using the scaling and warping tool in the NIH ImageJ and Adobe Photoshop software programs. Easily recognizable landmarks, including the center of the peduncle and ellipsoid body, and the tips of the mushroom body lobes were used as fiduciary points. For multicolor flip-out experiments, anti-Brp labeled neuropil compartments were outlined with hatched lines from the same sample. Schematics were made in Adobe Illustrator and figures assembled in Adobe Photoshop.

Two-photon calcium imaging, visual stimuli, and two-photon imaging analysis

Calcium imaging was conducted as previously described [63]. Briefly, calcium-dependent fluorescent signals were detected using a two-photon excitation scanning microscope (3i, Boulder, CO) with Slidebook 6 software (3i, CO), at an image acquisition rate of 10 frames/sec. 3-7 day old female flies expressing *20xUAS-*

GCAMP6m under the control of a specific Gal4 driver labeling tuberculo-bulbar neuron subpopulations were used; all recordings were conducted from the microglomerular presynaptic terminals of these neurons. Flies were immobilized in a custom holder and bathed in physiological saline; neurons of interest were made optically accessible by dissecting the posterior cuticle of the head capsule. Visual stimuli were presented to the fly using a 96x32 pixel LED arena. Specific details of two-photon imaging setup, visual stimuli, and imaging analysis are provided in Supplemental Experimental Procedures.

Results

Discrete neural lineages form input pathways of the ellipsoid body

The pathway providing input from the optic lobe to the ellipsoid body, called the anterior visual pathway (AVP) in the following (Fig.1A), represents a circuit whose central part is formed by the neurons of three lineages. As known from previous works and summarized above, ring (R) neurons of lineage DALv2 project from the bulb to the ellipsoid body. Cell bodies of this lineage are located in the anterior brain cortex, surrounding the spur of the mushroom body. The bulb receives the short, proximal neurites of DALv2 neurons; DALv2 axons form a fiber tract, termed the anterior lateral ellipsoid body tract (LEa), which extends medially towards the EB (Fig.1B) (Pereanu et al., 2010; Strausfeld, 1976).

We identified two hemilineages, DALcl1d and DALcl2d, which interconnect the bulb with the anterior optic tubercle (AOTU) via tuberculo-bulbar (TuBu) neurons (Fig.1C, D). The identified neurons resemble likely homologues, called tubercle-lateral accessory lobe type 1 neurons (TuLAL1 neurons), from the sky-compass pathway. The AOTU consists of a large, spherical medial compartment (AOTUm) to which two smaller domains [intermediate AOTU (AOTUin) and lateral AOTU (AOTUl)] are attached (Fig.1A; Ito et al., 2014). In many other insects, the AOTU is oriented such that the larger domain is located dorsally of the smaller domains, and are therefore called the upper unit (AOTU-UU) and lower unit, or lower unit complex (AOTU-LU, AOTU-LUC), respectively. DALcl1d TuBu neurons appear to have short, proximal processes in the lateral AOTU (AOTUl), and distal terminals in the superior and anterior BU (BUs; BUa; Fig.1C, E). DALcl2d TuBu neurons innervate complementary regions, connecting the

intermediate domain of the AOTU (AOTUin) with the inferior BU (BUi; Fig.1D, E). We did not identify neurons projecting directly from the large AOTUm compartment to the CX.

Visual interneurons of the medulla provide input to the AOTUl and AOTUin via a thick fiber bundle, the anterior optic tract (AOT). Gal4 driver lines reveal several discrete subpopulations of such medullo-tubercular (MeTu) neurons with proximal dendrites extending in medulla layer m6-8 (Fig.1F, G) and distal axonal branches confined to the lateral and intermediate AOTU. Putative homologies between neurons of the AVP and the sky-compass pathway from other insects are summarized in Table 1.

By expressing reporter proteins specifically targeted to presynaptic terminals (*UAS-syt.GFP*) and postsynaptic membranes (*UAS-DenMark*) we can show that the anterior visual pathway is directed from the medulla to the anterior optic tubercle and, from there, towards the ellipsoid body. Thus, projections of DALv2 R neurons are mostly axonal in the EB, and dendritic in the BU (Fig.1H). Likewise, projections of DALcl1/2 TuBu neurons have mostly presynaptic, axonal sites in the bulb, and postsynaptic, dendritic sites in the AOTU (Fig.1I). Proximal neurites of MeTu neurons in the medulla are exclusively dendritic; distal projections in the AOTU appear to possess intermingled presynaptic and postsynaptic sites (Fig.1J).

Ring neuron subclasses of DALv2 establish a topographically ordered connectivity between the bulb and ellipsoid body

Global markers for neuropil [antibodies against DN-cadherin (DNcad) or Bruchpilot (Brp)] in conjunction with specific Gal4 driver lines reveal more detail about the intricate anatomy and connectivity within the anterior visual pathway. In the EB, five

discrete domains can be distinguished based on different expression levels of DN-cadherin (Fig.2A-C). These comprise an inner posterior domain (EBip) and inner central domain (EBic) with low DNcad signal, an outer central domain (EBoc) with moderate DNcad signal, and an anterior domain (EBa) and outer posterior domain (EBop) with high signal. The bulb consists of three major domains defined by their position relative to the LEa fiber bundle formed by DALv2-derived ring (R) neuron axons. The superior and inferior domains of the bulb are located dorsally and ventrally of the LEa, respectively; the anterior bulb is attached to the lateral surface of the LEa at a position where it bends medially (Fig.2A, B). DNcad labeling reveals the individual, large input synapses, called microglomeruli, formed by R neuron dendrites (Fig.2B, arrowheads).

We screened the expression patterns of several Gal4 driver lines which label subpopulations of R neurons (Jenett et al., 2012). This analysis, in conjunction with single-cell labeling using the multicolor flip-out method (MCFO) (Nern et al., 2015), reveals that the ring domains of the ellipsoid body are connected in a topographically ordered pattern to the bulb, consistent with previous reports (Renn et al., 1999). R neurons innervating the anterior domain (Fig.2D-F) and outer central domain (Fig.2G-I) have dendrites in the superior bulb; other R neurons innervating the outer central domain are connected to the anterior bulb (Fig.2J-L). R neurons innervating the inner central and inner posterior domain possess dendrites in the inferior bulb (Fig.2M-O). These and additional ring neurons will be classified according to an expanded form of the current *Drosophila* ring neuron nomenclature system in a future anatomical report (Omoto et al., in prep).

We did not identify any ring neurons which form axons in the outer posterior domain of the ellipsoid body. This domain, as well as the other domains of the EB, is innervated by two main classes of columnar neurons that interconnect the different compartments of the central complex, PB-EB-gall (“wedge”) neurons (Fig.2P, Q) and PB-EB-NO (“tile”) neurons (Fig.2R) (Wolff et al., 2015). Both represent sublineages of four large type II lineages (DM1/DPMm1, DM2/DPMpm1, DM3/DPMpm2, DM4/CM4) (Wong et al., 2013; Yang et al., 2013), whose cell bodies are located in the posterior brain. Wedge neurons have proximal branches in the protocerebral bridge; from here they extend forward, through the fan-shaped body, into the EB where they presumably receive R neuron input. Collateral branches of wedge neurons project further forward into the gall of the lateral accessory lobe (Fig.2P, Q; Ito et al., Wolff et al., 2015), a known premotor area of the fly brain (Namiki and Kanzaki, 2016). Tile neurons have a more restricted projection to the outer posterior EB (Fig.2R), and therefore overlap extensively with wedge neurons but not R neurons.

Tuberculo-bulbar neurons of DALcl1 and DALcl2 form a topographically ordered projection between the anterior optic tubercle and bulb

In view of the ordered connectivity between bulb and ellipsoid body, it stands to reason that neurons of DALcl1 and DALcl2, which connect the anterior optic tubercle to the bulb, are also topographically organized. Based on DNcad expression, three subdomains (medial, intermediate, lateral) can be defined for the AOTU (Ito et al., 2014). Closer inspection of DNcad-labeled brains revealed that the intermediate domain is further subdivided into two narrow, vertical slices, named (from lateral to medial), AOTUil and AOTUim (Fig.3A, B). The lateral domain, AOTUl, is divided into three

finger-like processes (AOTUla, AOTUlc, AOTUlp) that are most easily revealed in horizontal sections of the tubercle (Fig.3B).

We identified multiple Gal4 driver lines expressed in subpopulations of medullo-tubercular (MeTu) neurons and DALcl1 and 2-derived tuberculo-bulbar (TuBu) neurons whose projection is predominantly restricted to specific subdomains of the AOTU, additionally corroborated by MCFO-labeled single cell clones. The DALcl1-derived TuBu subpopulation with axons terminating primarily in the superior bulb ($TuBu_s$), has dendrites enriched in all three process of the lateral subdomain (AOTUla/c/p), and can be labeled by *R88A06-Gal4* (Fig.3D-F). TuBu neurons terminating in the anterior bulb ($TuBu_a$), also derived from DALcl1, actually exhibit dendrites filling the lateral slice of the intermediate AOTU subdomain (AOTUil) (Fig.3G-I). Dendrites of inferior bulb tuberculo-bulbar neurons ($TuBu_i$), derived from DALcl2, are concentrated in the medial intermediate subdomain (AOTUim) and express *R49E09-Gal4* (Fig.3J-L). The parallel pathways connecting the anterior optic tubercle with the bulb and ellipsoid body are schematically summarized in Fig.4.

MeTu neurons from the medulla (previously described (Otsuna et al., 2014) as medullar columnar 61 neurons; MC61) also terminate in specific subdomains of the lateral and intermediate AOTU defined by the dendrites of TuBu neurons. The AOTUm receives input from the lobula (lobula columnar 10; LC10) (Otsuna and Ito, 2006; Panser et al., 2016). Numerous driver lines expressed in MeTu neurons have been identified; three representative examples are depicted in Fig.3M-T. Dendrites fill predominantly layer m7, with sparser branches reaching up into m6 (the layer contacted by photoreceptors R7) and deeper into m8. Single cell clones reveal that the dendritic

tree covers 10-15 contiguous medulla columns (Fig.3O-O''), identifying MeTu neurons as special subclasses of multicolumnar medullary visual projection neurons. Their cell body location and projection pattern is reminiscent of *Drosophila* transmedullary neurons but, instead of targeting the lobula complex, directly project to the central brain. Most MeTu neurons are restricted to the dorsal half of the medulla, as shown here for neurons innervating the AOTUil domain ($MeTu_{il}$; Fig.3Q, R) and the AOTUim domain ($MeTu_{im}$; Fig.3S, T). Some MeTu neurons, such as those innervating AOTUl ($MeTu_{l}$; Fig.3M, N), are spread out over the entire medulla.

Concomitant labeling of DALcl1 or DALcl2 TuBu neurons and DALv2 R neurons demonstrates that the endings of the former fully overlap with the proximal branches of the latter in the bulb (Fig.4B, C). Given the large size of the pre-and postsynaptic endings, forming microglomeruli of approximately 2μm diameter, it was evident that individual R neuron dendrites were directly contacted by TuBu neuron axons. To provide further evidence for a direct synaptic contact, we carried out a GRASP analysis, in which the post-synaptic cells are expressing CD2-RFP and split-GFP11, whereas the presynaptic cells express split-GFP1-10. As shown in Fig.4D and E, a strong GRASP signal is detected specifically in the bulb within the expected target region. DALcl1-derived $TuBu_{s}$ neurons innervate EBoc R neurons with microglomerular dendrites in the superior bulb, whereas DALcl2-derived $TuBu_{i}$ neurons innervate EBic R neurons in the inferior bulb, confirming the presence of parallel, superior and inferior bulb pathways.

Lineally-organized input channels to the ellipsoid body form parallel neural ensembles that are functionally-distinct

Previous studies utilizing pan-neuronal or ring neuron-specific (R2 and R4d) two-photon calcium imaging in the superior bulb demonstrated that a subpopulation of R neuron dendrites respond to visual features. Visually-responsive dendritic microglomeruli typically exhibit ipsilateral receptive fields, bright (ON)-selectivity, and vertical orientation tuning (Seelig and Jayaraman, 2013). Our anatomical data demonstrate that TuBu neurons provide direct input to R neuron dendrites; we therefore tested the hypothesis that the microglomerular presynaptic terminals of TuBu neurons exhibit similar physiological properties as R neuron dendrites. We expressed the genetically-encoded calcium indicator GCAMP6m under the control of *R88A06-Gal4* (Fig.5B), which predominantly labels $TuBu_s$, the superior bulb-innervating neurons of DALcl1 (Fig.3D-F and 4B). Quiescent flies were placed in front of a curved visual display of LEDs and presented with different visual stimuli while conducting two-photon calcium imaging from the microglomerular axonal outputs of these neurons (Fig.5A). Recordings were conducted in two planes to maximally detect microglomerular activity (see Supplemental Experimental Procedures). Responsive superior bulb microglomeruli from both planes exhibited qualitatively homogenous characteristics and were therefore analyzed collectively, in contrast to inferior bulb microglomeruli (see below).

Receptive field mapping with a small bright (ON) object revealed that $TuBu_s$ outputs in the superior bulb exhibit small, retinotopically-organized receptive fields that are localized to, and provide wide coverage of, the ipsilateral visual hemifield (Fig.5B-G). The average receptive field size was 29.2° and 44.2° (±3.5° and ±2.8° standard deviation, minor axis and major axis lengths respectively), suggesting that individual $TuBu_s$ neurons might be pooling information from 6-9 photoreceptors. The relative

positioning of microglomeruli roughly corresponds to the positioning of the spatial receptive fields along the animal's visual elevation (Fig.5E and F, top panels) and azimuth (Fig.5E and F, bottom panels). In other words, microglomeruli with receptive fields located on the lower part of the visual field cluster in the ventrolateral part of the superior bulb, whereas microglomeruli located in the dorsomedial portion of the superior bulb have receptive fields located on the upper part of the visual field. Similarly, medially located microglomeruli tend to respond to visual stimulation on the medial portion of the ipsilateral visual field, whereas laterally located microglomeruli respond on the lateral portion of it (Fig.5E and F). Spatial receptive fields of individual presynaptic microglomeruli were similar in size within and between animals (Fig.5H). As R neuron dendrites are tuned to vertically-oriented features, we next presented a horizontally moving bright (ON) bar spanning the full vertical extent of the display. In most microglomeruli, the ON bar elicited strong calcium responses close or equal to the peak amplitude response generated by the small ON object (Fig.5J, K), indicating that $TuBu_s$ neurons do not exhibit robust size tuning in the vertical axis. Furthermore, presentation of the ON object outside the excitatory receptive field generated no measurable decreases in fluorescence (Fig.5K), which would be expected by inhibitory interactions between $TuBu_s$ neuron microglomeruli. Inverting the contrast polarity to a moving dark (OFF) bar on a bright background resulted in a diminished response, suggesting that $TuBu_s$ neurons, like their downstream ring neurons, are ON-selective (Fig 5I) (Seelig and Jayaraman, 2013). As a population, $TuBu_s$ neurons respond equally well to motion in either horizontal direction and are only weakly excited by a wide-field grating (Fig.5J). Taken together, the response properties of $TuBu_s$ neuron presynaptic terminals

resemble those of superior bulb-associated ring neuron dendrites from previous reports (Seelig and Jayaraman, 2013), corroborating their role as direct presynaptic inputs.

We hypothesized that due to their distinct developmental origin, DALcl2-derived $TuBu_i$ neurons, which innervate the inferior bulb, should exhibit functional dissimilarity to superior bulb innervating, DALcl1 $TuBu_s$ neurons (Fig.1C-E). Flies expressing GCAMP6m under the control of the predominantly $TuBu_i$ neuron driver, *R49E09-Gal4*, were presented with the same battery of visual stimuli as shown for $TuBu_s$ neuron microglomeruli. Unlike superior bulb $TuBu_s$ neurons, responses in the inferior bulb $TuBu_i$ neurons were heterogenous and variable (see Supplemental Experimental Procedures, Fig S1); yet we identified one consistent response type for at least one microglomerulus in both imaging planes for every fly. The responses in the first imaging plane typically showed excitation to objects in the contralateral visual hemifield and inhibition when the object entered the ipsilateral visual hemifield (Fig.6A and D, mint green). Interestingly, microglomeruli showed strong secondary excitation as the object left the ipsilateral visual field and no stimulation was present (Fig.6D, mint green, black arrow). Qualitatively similar responses were observed from microglomeruli in the second imaging plane (Fig.6C and D, light orange), yet these responses were smaller in amplitude. In addition, we observed microglomerular structures that did not respond to any of our stimuli (Fig.6C, only drawn microglomeruli showed significant responses). When an object moved from the ipsilateral visual hemifield towards the contralateral one, microglomeruli responded by slight excitation followed by inhibition (Fig.6D'). We observed a strong response when the object entered the contralateral visual field (Fig.6D'). Inferior bulb response characteristics were consistent across 104

microglomeruli in 15 flies (Fig.6E and E') and they were distinct from superior bulb responses. In contrast to the superior bulb, the physiological responses of ring neurons that extend dendrites into the inferior bulb (R3) have not been systematically characterized, preventing us from making direct input-output comparisons. Nevertheless, the optophysiological analysis of separate TuBu neuron populations derived from DALcl1 and DALcl2 confirm the notion that different lineages form functionally-distinct neuronal ensembles.

In addition to the distinct temporal dynamics of inferior and superior bulb TuBu neuron object responses, we noted that the inferior bulb microglomeruli have larger spatial receptive fields that cover the entire contralateral visual hemifield and are very similar across microglomeruli, showing strongest responses to visual stimuli presented on the upper portion of the display (Fig.6B). Whereas the spatial receptive fields and temporal response properties are distinct between superior bulb and inferior bulb, the preference for ON objects is similar (Fig.6F). Also, like superior bulb $TuBu_s$ neurons, the inferior bulb $TuBu_i$ neurons do not show strong directional selectivity on the horizontal axis and responds to wide-field gratings with only slight excitation (Fig.6G, see above). Our results indicate that both superior and inferior bulb-innervating TuBu neurons are sensitive to bright objects but sample unique hemifields; ipsilateral and contralateral fields, respectively, with distinct receptive field structure and temporal dynamics.

Discussion

In both vertebrates and many invertebrates, luminance signals detected by photoreceptors are processed in sequential neural layers to extract visual features from the visual panorama. Neurons carrying information about visual features project to higher brain centers; this function is accomplished by approximately 20 retinal ganglion cell subclasses and >50 visual projection neuron classes (VPNs), which transmit visual features from the retina or the optic lobe to the central brain in vertebrates and arthropods, respectively (Dhande and Huberman; Strausfeld, 1976; Wu et al., 2016). Circuits downstream of VPNs utilize this input to elicit appropriate behavioral outputs. One higher-order brain region of particular interest is the central complex (CX), which plays a pivotal role in innate and learned visually-guided behaviors. Importantly, definable neuronal subtypes in the CX are themselves visually-responsive, yet the VPNs that supply that input are unknown in *Drosophila* (el Jundi et al., 2014; Seelig and Jayaraman, 2013).

The anterior visual pathway (AVP) described in this work serves to define the architecture of a pathway that projects from peripheral circuits of the medulla to the EB neurons of the *Drosophila* CX sequentially via medullo-tubercular (MeTu) neurons, and parallel superior DALcl1 and inferior DALcl2 pathways ($TuBu_s$ and $TuBu_i$ neurons). Recent studies by Seelig and Jayaraman (2013, 2015) examined the physiological responses of neuronal subpopulations within the EB. They first observed that individual R neurons whose dendritic microglomeruli are localized in the superior bulb (R2 and R4d), respond to visual stimuli. Here, we identify the developmentally-related $TuBu_s$ neurons of DALcl1 as the direct pre-synaptic inputs to these superior bulb R neurons,

and demonstrate that many of their visual tuning properties can already be observed in the upstream $TuBu_s$ population (Fig 5). In addition, we identify DALcl2-derived $TuBu_i$ neurons, which exhibits distinct receptive field properties from $TuBu_s$ neurons (Fig 6), and likely supply the inferior bulb R neurons (presumably R3 neurons of the EBic domain) that have not been systematically characterized previously. We observed variable responses of $TuBu_i$ neurons (see Supplemental Experimental Procedures). One potential source of variability is our quiescent imaging paradigm, in which the animal's entire body is tethered and unable to move. We posit that, given the function of downstream circuits in the EB ("wedge neurons"; see below), the behavioral state of the animal and proprioceptive feedback, which cannot be assessed in our preparation, may influence the coherence of activity in this brain region.

R neurons, whose axons cover the entire perimeter of the ellipsoid body, provide input to the large number of columnar neurons [so called "wedge neurons"; (Wolff et al., 2015], the neurites of which subdivide the torus-shaped volume of the ellipsoid body into narrow radial partitions. The calcium dynamics recorded from the population of wedge neurons produces a localized "bump" of activity in the torus which, based on visual landmarks and proprioception, corresponds to an internal representation of the animal's orientation in space (Seelig and Jayaraman, 2015). Information likely reverberates between the EB and other CX neuropils, such as the protocerebral bridge, via different populations of columnar elements (wedge and tile neurons) which heavily interconnect them (Wolf et al., 2015). Similarly to the head direction system in mammalian brains, these dynamics produce stable neural activity consistent with an internal compass (Seelig and Jayaraman, 2015). The EB displays a common

organizational principle observed in complex nervous systems; in essence, it is a structure arranged into layers and columns by tangential (ring neurons) and columnar (wedge and tile neurons) elements, respectively. Although the EB has adopted a toroidal shape in dipterans, the homologous structure in many other insects (central body lower division) is not toroidal, but, similar to the fan-shaped body, forms a multilayered and multicolumnar neuropil domain straddling the midline (Pfeiffer and Homberg, 2014). A receptive field-specific response in a single R neuron would presumably influence activity in an entire layer, and thus multiple columns. One of the most insightful lines of inquiry will be to investigate how this tangential input is translated into (or is even compatible with) the observed localized activity (“bump”) within the wedge neurons of the EB. It is conceivable that R neurons, due to their peculiar bifurcated architecture, may influence EB wedges with a physiologically-relevant temporal offset, which could be utilized to modulate spatially-restricted activity patterns. Future work defining the circuit motifs present in this brain region may provide insight into the advantages of a layered and columnar organization for emergent neural properties, such as a cognitive-like internal representation and navigation.

With respect to neuronal location, shape, and connectivity, the *Drosophila* AVP strongly resembles the sky-compass pathway, known from detailed functional and anatomical studies in other insects (Held et al., 2016; Pfeiffer et al., 2005; El Jundi et al., 2014; Heinze and Reppert, 2011). Most notably recognized as the polarization (POL) vision pathway, neurons of the sky-compass network are tuned to the e-vectors of polarized light which reflect the location of the sun, thus providing compass information used by these insects to navigate during long range migrations or local path integration

in central place foraging (Heinze and Reppert, 2011; Homberg et al., 2011). Considering that *Drosophila* also exhibits physiological and behavioral correlates with POL sensitivity (Weir and Dickinson, 2012; Weir et al., 2016; Wernet et al., 2012), we posit that the fly AVP is the neural circuit for POL information transmission to the CX. However, a recent report demonstrated that when flies are presented with a rotating field of polarized UV light in conjunction with pan-neuronal calcium imaging, robust calcium signals in any CX neuropils, including the bulb, were not observed (Weir and Dickinson, 2015). In contrast, and in agreement with our findings, bright objects elicited strong responses in the bulb and other regions of the CX. Indeed, neurons of the sky-compass pathway can also encode the azimuthal position (both ipsi and contralaterally) of an unpolarized light source, depending on the insect and neuron type in question. The extent of encoding strength to a given stimulus (polarized versus unpolarized light) likely reflects the ethology and environment of the animal. For example, diurnal dung beetles utilize the position of a bright object (such as the sun or moon) to navigate regardless of ambient light intensity, whereas nocturnal beetles utilize polarized skylight specifically at low light intensities, rather than position of a celestial body such as the moon. This ethological distinction is reflected in the tuning properties of neurons within the sky-compass pathway, even between two closely-related insects. Therefore, although POL information is likely transmitted within this pathway, findings to date indicate that luminance cues from a bright source, such as a celestial body or an escape route from within foliage, would be represented more strongly in the *Drosophila* AVP than the skylight pattern of polarized light (Weir and Dickinson, 2015). This proposition is based on the following: 1) Contrast polarity and object size tuning:

Upstream TuBu as well as downstream R neurons and wedge neurons show strong excitation to bright objects (Seelig and Jayaraman, 2013; 2015), whereas dark object responses are weaker (Figs.5 and 6), suggesting specialization for detecting a bright object against a dark background. The ON-preference and indifference to object size by TuBu neurons (Figs.5 and 6) suggest that this pathway would poorly mediate stripe fixation behavior, which is activated more by dark bars or complex motion-defined edges (Maimon et al., 2008). Neither would the AVP be suitable for object aversion behavior in flies, which is activated only by small-sized objects (Maimon et al., 2008). However, the topographical organization of $TuBu_s$ neuron terminals (Fig.5) suggests that retinotopy is conserved and thus could serve spatial navigation, unlike other small-object VPNs where the retinotopy is apparently lost within the intermingled axon terminals of individual small-field columnar neurons (Wu et al., 2016). 2) Coarse receptive field properties: The preference for bright objects of varying size suggests that the CX receives rather primitive spatial information by comparison to the complex filtering properties exhibited by other VPN pathways. For example, the lobula and lobula plate contain cells that act as precise spatial filters for directional patterns of optic flow, the spatial dynamics of looming objects, and the omni-directional motion of small OFF-contrasting objects (Maisak et al., 2013; Wu et al., 2016). 3) Spatial interactions of excitation and inhibition: A single bright object presented ipsilaterally against a dark background would excite a spatially defined subset of ipsilateral $TuBu_s$ neurons while simultaneously exciting multiple (possibly all) canonical contralateral $TuBu_i$ neurons. By contrast, two bright spots appearing in the left and right visual fields would simultaneously stimulate $TuBu_s$ neurons on both right and left side while leading to

inhibition in all $TuBu_i$ neurons. Most intriguingly, $TuBu_i$ neurons show strong calcium currents as a bright object leaves the visual field suggesting that $TuBu_i$ neurons might be signaling to the R neurons some crucial information about 'losing' the visual bearing to a bright object. 4) Anatomical and ethological evidence: In comparison to other insects examined, in which an aspect of their behavioral repertoire is thought to depend on POL vision, the ethological lifestyle of *Drosophila* suggests that it may be less likely to use the pattern of polarized skylight to navigate. This fact is reflected in their relatively rudimentary dorsal rim area (DRA), a region of the eye with specialized, POL-sensitive photoreceptors, and correspondingly inconspicuous dorsal rim area of the medulla (MEDRA), which receives input from DRA photoreceptors. In addition, likely homologues of MeTu neurons in other insects (transmedulla neurons) often exhibit long, dorsally-projecting input neurites which ramify in the MEDRA, suggesting a high degree of POL input. In contrast, we did not observe this characteristic feature in MeTu neurons in *Drosophila*; dendritic arborizations ramified locally of the primary neurite, which were distributed relatively evenly throughout the dorsal half of, or the whole eye.

Here we provide ample evidence that DALc1 and DALcl2-derived neurons have unique functional properties, come from distinct lineages, and supply visual information to the central complex. To our knowledge, this is the first extensive characterization of the visual input to the central complex in *Drosophila*, and a definitive example of how developmentally distinct lineages give rise to functionally distinct circuits.

Figures

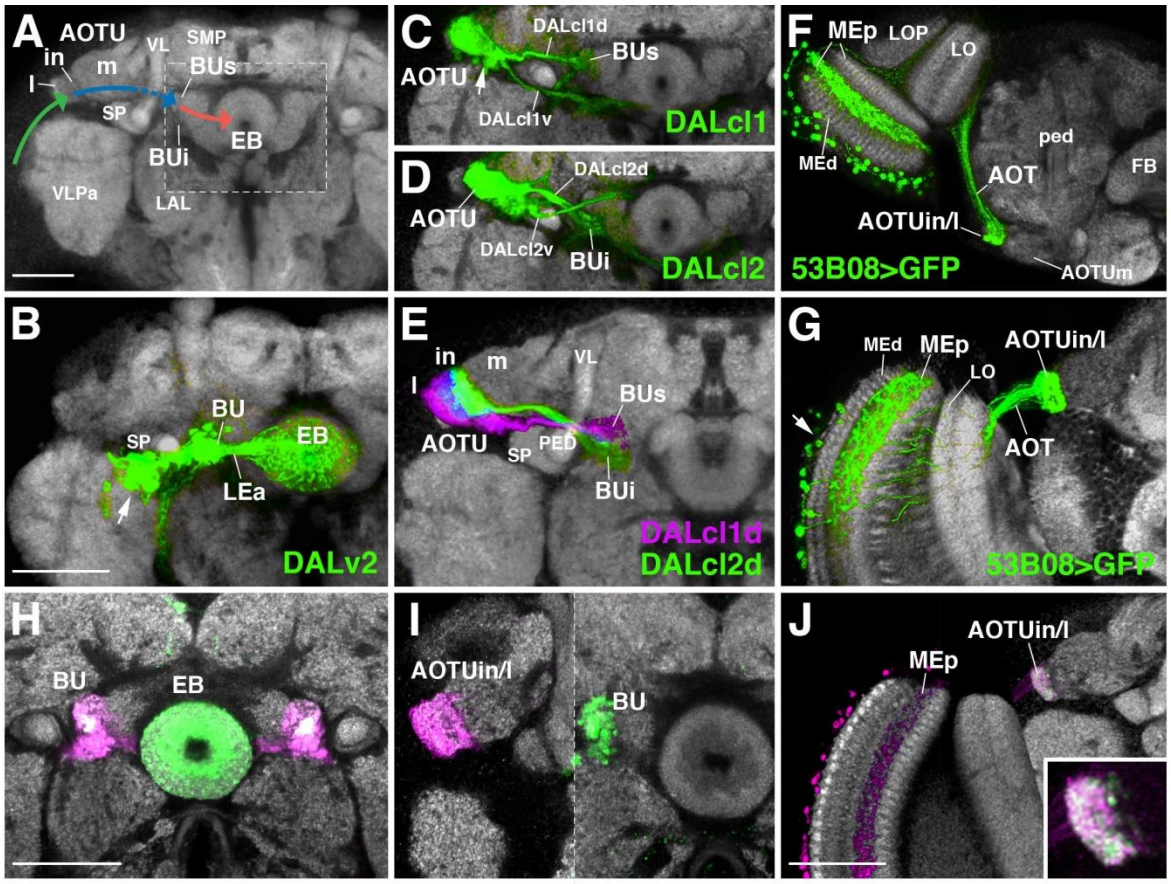

Figure 2-1: Discrete lineages constitute the central brain components of the anterior visual pathway.

(A-J) Confocal z-projections illustrating the anterior visual pathway (AVP) (frontal sections unless otherwise noted); adult brains labeled with anti-DN-cadherin (grey), cell body clusters depicted by arrows.

(A) Schematized overview of the three-legged AVP. First leg (green): from the optic lobe to the lateral (l) and intermediate (in) domains, but not the medial domain (m), of the anterior optic tubercle (AOTU). Second leg (blue): from the AOTU to bulb (BU), superior (BUs) and inferior (BUi) bulb depicted. Final leg (red): from the bulb (BU) to the ellipsoid body (EB) of the central complex (hatched lines).

(B-D) Mosaic analysis with a repressible cell marker (MARCM) clones of secondary lineages DALv2, DALcl1, and DALcl2 (green) (Nomenclature from [25,28]). (B) DALv2 forms all ring neurons of the EB (red leg in A), projecting from the BU to the EB *via* the anterior lateral ellipsoid body tract (LEa). (C and D) DALcl1 and DALcl2 form tuberculo-bulbar neurons (blue leg in A). Two tract components emanate from each neuroblast clone, a dorsal (DALcl1/2d) and a ventral (DALcl1/2v) component which we conclude are hemilineages. The dorsal, not ventral, hemilineages form the tuberculo-bulbar neurons.

(E) Isolation and registration of DALcl1/2 dorsal hemilineages (DALcl1d; magenta, DALcl2d; green). Neurites of DALcl1d projects from AOTUl to BUs, DALcl2d projects from AOTUin to BUi.

(F-G) Horizontal (F) and frontal (G) sections of *R53B05-Gal4* (green) labeling medullo-tubercular neurons, projecting from the medulla to the AOTUin/l *via* the anterior optic tract (AOT) (green leg in A).

(H-J) Expression of pre-synaptic marker *syt::GFP* (green) and dendritic marker DenMark (magenta) in distinct legs of the AVP. (H) *R20A02-Gal4* labels most ring neurons and shows enrichment of axonal output in the EB and dendrites in the BU. (I) *R48B06-Gal4* labels tuberculo-bulbar neurons and shows enrichment of output in the BU and dendrites in the AOTUin/l. (J) *R53B05-Gal4* demonstrates medullo-tubercular neurons are dendritic in the proximal medulla (MEp) but appears to have mixed dendritic and axonal specializations in the AOTUin/l (boxed inset).

Other abbreviations: LAL, lateral accessory lobe; LO, lobula; LOP, lobula plate; MEd, distal medulla; PED, peduncle of the mushroom body; SP, spur of the mushroom body;

SMP, superior medial protocerebrum; VL, vertical lobe; VLPa, anterior ventrolateral protocerebrum

Scale Bars: 50μm (A, C, D, F); 50μm (B, E, G, J); 50μm (H, I)

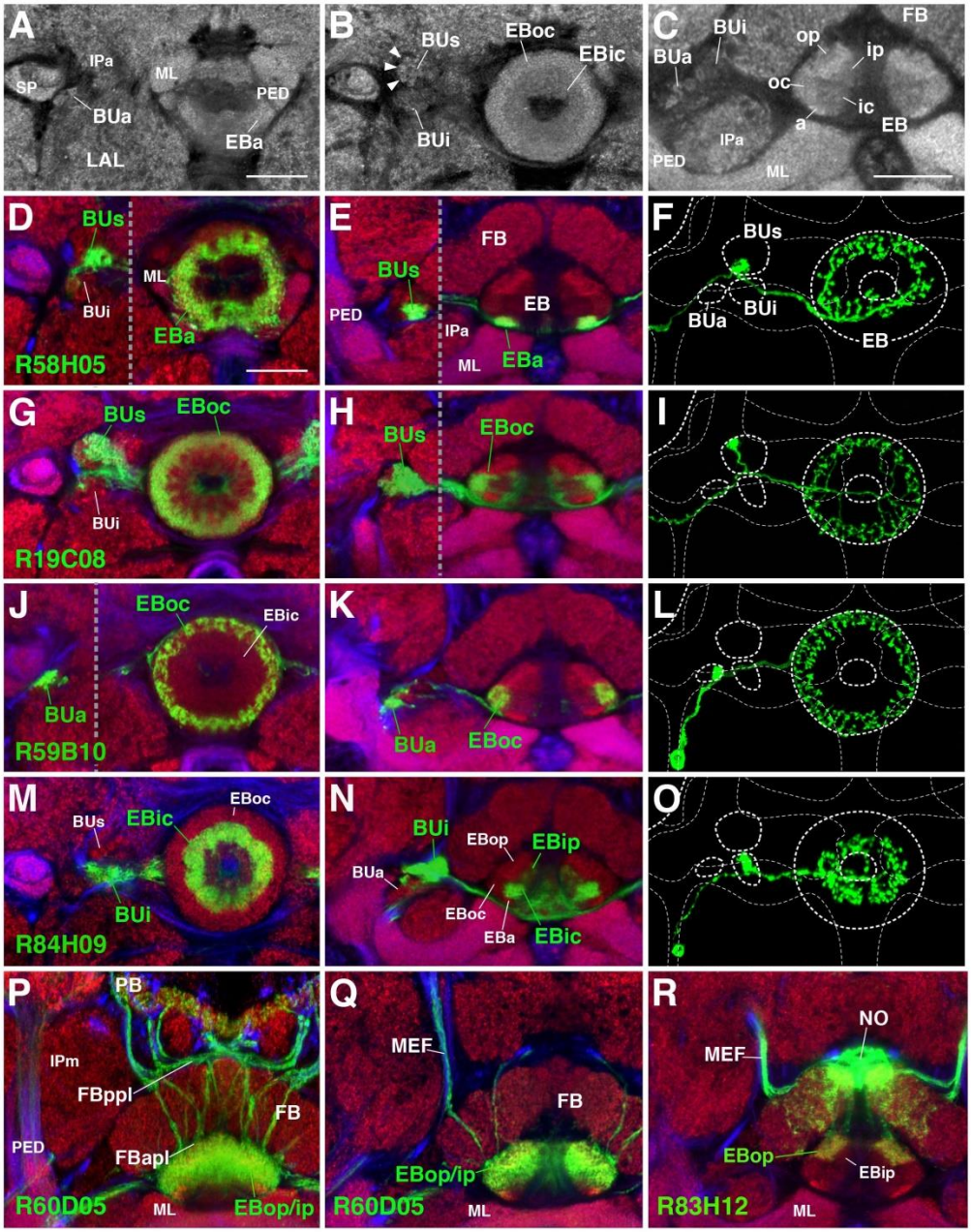

Figure 2-2: DN-Cadherin domains and single cell labeling define the topology and architecture of ellipsoid body neurons.

(A-C) High magnification frontal (A and B) and horizontal (C) z-projections of the bulb and ellipsoid body neuropil labeled by anti-DN-cadherin (grey) reveals three distinct

domains in the bulb and five distinct domains in the ellipsoid body. (A) Anterior frontal section reveals the anterior bulb (BUa) and the anterior domain of the EB (EBa). (B) Intermediate frontal section; reveals the superior (BUs) and inferior (BUi) domains of the bulb, and the outer central (EBoc) and inner central (EBic) domains of the EB. Arrowheads designate bulb microglomeruli. (C) Horizontal section through the EB canal reveals all five EB domains.

(D-O) Gal4 drivers which label distinct ring neuron subclasses defined by axon morphology, and topology within the BU and EB. Each row represents a distinct Gal4 driver; first and second columns are frontal and horizontal sections labeled with *10xUAS-mCD8::GFP*, respectively, grey hatched lines denote regions of interest that are not within the same plane. Neuropil labeled with anti-DN-cadherin (red) and axon tracts by anti-Neuroglian (blue). Third column is a single cell clone generated by MCFO using the same Gal4 (see Experimental Procedures); white hatched lines outline neuropil compartments from the same fly. (D-F) *R58H05-Gal4* (BUs to EBa). (G-I) *R19C08-Gal4* (BUs to EBoc). (J-L) *R59B10-Gal4* (BUa to EBoc). (M-P) *R84H09-Gal4* (BUi to EBic/ip).

(P-R) Horizontal confocal z-projections of Gal4 drivers labeling columnar elements. (P-Q) *R60D05-Gal4* labels PB-EB-gall (“wedge”) neurons. (P) Z-projection depicting the complete projection pattern of the population in the CX. (Q) Section through the EB canal; “wedge” neurons most densely occupy posterior EB domains, but diffusely project into intermediate and anterior domains as well. (R) *R83H12-Gal4* labels PB-EB-NO (“tile”) neurons, which fill the outer posterior domain of the EB (EBop).

Other abbreviations: FB, fan shaped body; FBapl and FBppl, anterior and posterior

plexus of the fan shaped body; IPa and IPm, anterior and medial inferior protocerebrum; LAL, lateral accessory lobe; MEF, medial equatorial fascicle; ML, medial lobe of the mushroom body; NO, noduli; PB; protocerebral bridge; PED, peduncle of the mushroom body; SMP, superior medial protocerebrum; SP, spur of the mushroom body; VL, vertical lobe

Scale Bars: 25μm (A, B); 25μm (C); 25μm (D-R)

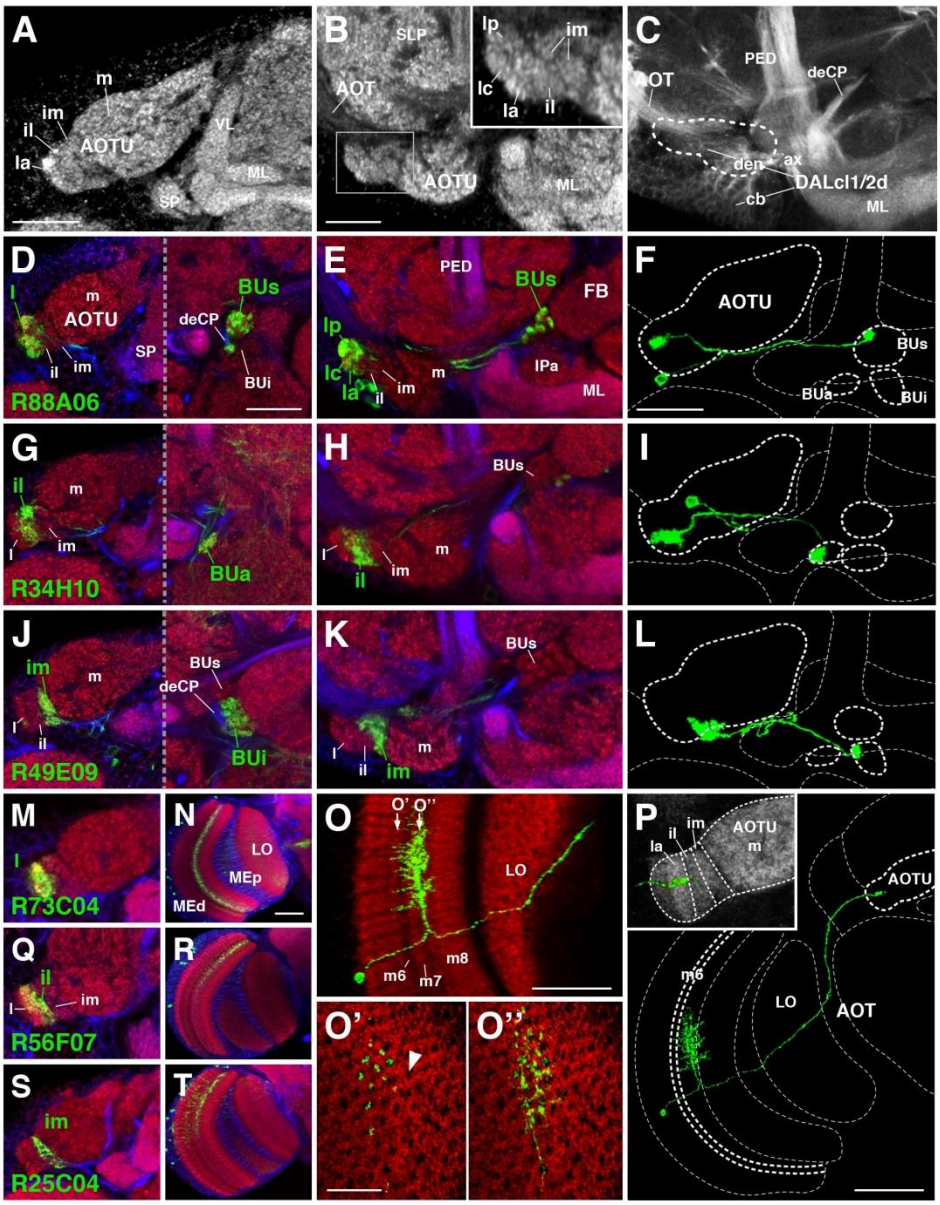

Figure 2-3: Topology and architecture of tuberculo-bulbar and medullo-tubercular neurons.

(A-C) High magnification frontal (A) and horizontal (B and C) z-projections of the anterior optic tubercle reveals six distinct domains in the AOTU (m, medial; im, intermediate medial; il, intermediate lateral; la/c/p, lateral anterior/central/posterior), highlighted by boxed inset in (B). Neuropil labeled by anti-DN-cadherin (grey; A and B),

axon tracts labeled by anti-Neuroglian (grey; C) with AOTU location denoted by white hatched line with locations of DALcl1/2d cell bodies (cb), dendrites (den), and axons (ax).

(D-L) Gal4 drivers which label distinct tuberculo-bulbar neuron subclasses defined by topology within the AOTU and BU. Each row represents a distinct Gal4 driver; first and second columns are frontal and horizontal sections labeled with *10xUAS-mCD8::GFP*, respectively. Neuropil labeled with anti-DN-cadherin (red) and axon tracts by anti-Neuroglian (blue). Third column is a single cell clone generated by MCFO using the same Gal4; white hatched lines outline neuropil compartments from the same fly. (D-F) *R88A06-Gal4* (AOTUla/c/p to BUs). (G-I) *R34H10-Gal4* (AOTUil to BUa). (J-L) *R49E09-Gal4* (AOTUim to BUi).

(M-T) Gal4 drivers which label distinct medullo-tubercular neuron subclasses defined by topology within the medulla and AOTU. (M-P) *R73C04-Gal4* labels a class of medullo-tubercular neurons projecting from m7 layer of the medulla to AOTUl. (M) High magnification image of the AOTU, (N) is the medulla from the same fly. Neuropil labeled with anti-DN-cadherin (red) and axon tracts by anti-Neuroglian (blue). (O-P) Single cell clone generated by MCFO with *R73C04-Gal4*, all panels are the same clone. Frontal section of the dendritic arborization (O) demonstrates that this cell type is not restricted to a single medulla layer. Successive tangential sections (O’ and O’’) reveal that the primary dendritic arborization (O’’) extends multiple distal processes which occupy individual medulla columns. Neuropil labeled with anti-Brp (O-O’’; red), white hatched lines outline neuropil compartments (P). (Q-R) *R56F07-Gal4* (dorsal half m7 layer to AOTUil). (J-L) *R25C04-Gal4* (dorsal half m7 layer to AOTUim).

Other abbreviations: AOT, anterior optic tract; deCP, central descending protocerebral fascicle; FB, fan shaped body; IPa, anterior inferior protocerebrum; IPm, medial inferior protocerebrum; LAL, lateral accessory lobe; LO, lobula; MEd, distal medulla; MEp, proximal medulla; ML, medial lobe of the mushroom body; PED, peduncle of the mushroom body; SLP, superior lateral protocerebrum; SP, spur of the mushroom body

Scale Bars: 25μm (A); 25μm (B-E, G, H, J, K, M, Q, S); 25μm (F, I, L); 50μm (N, R, T); 50μm (O); 20μm (O', O''); 50μm (P)

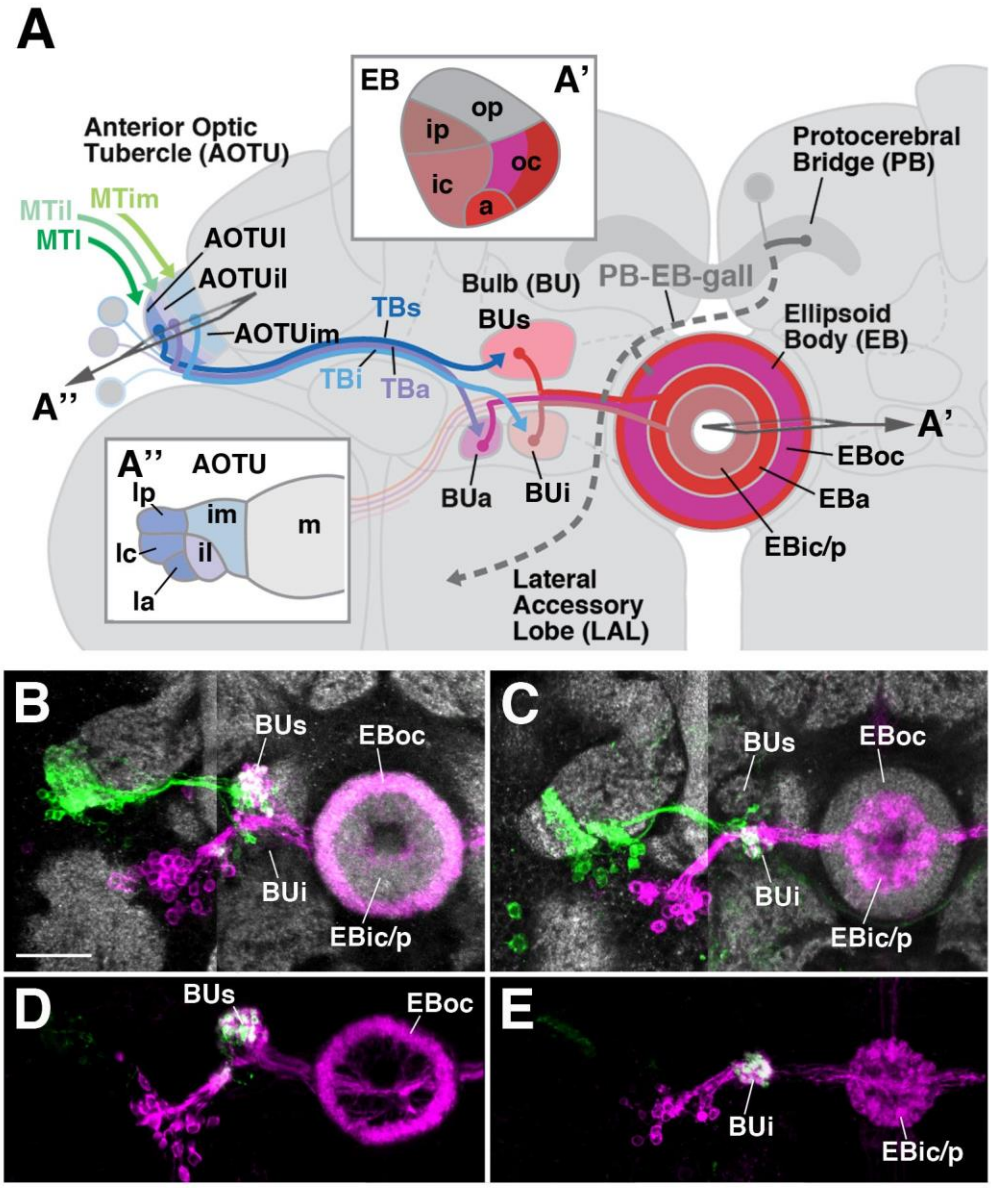

Figure 2-4: Framework of connectivity in the AVP - DALcl1 and DALcl2 provide direct, topographically-organized parallel input to ring neuron subclasses.

(A) Schematic overview of the anterior visual pathway. Insets depict horizontal sections of the EB (A') and AOTU (A'').

(B and C) Two-color labeling of superior bulb (B) and inferior bulb (C) components. Tuberculo-bulbar neurons labeled in green by Gal4, ring neurons labeled in magenta by

LexA. (B) *R88A06-Gal4* labels DALcl1d tuberculo-bulbar neurons, *R19C08-LexA* labels EBoc ring neurons; overlap observed in the superior bulb (BUs). (C) *R49E09-Gal4* labels DALcl2d tuberculo-bulbar neurons, *R54B05-LexA* labels EBic/ip ring neurons; overlap observed in the inferior bulb (BUi).

(D and E) GRASP analysis of tuberculo-bulbar neuron – ring neuron synapses using the same driver combinations as B and C; post-synaptic cells are expressing CD2-RFP and split-GFP11, presynaptic cells expressing split-GFP1-10. Strong GRASP signal observed in the expected bulb subdomain.

Scale Bars: 25μm (B-E)

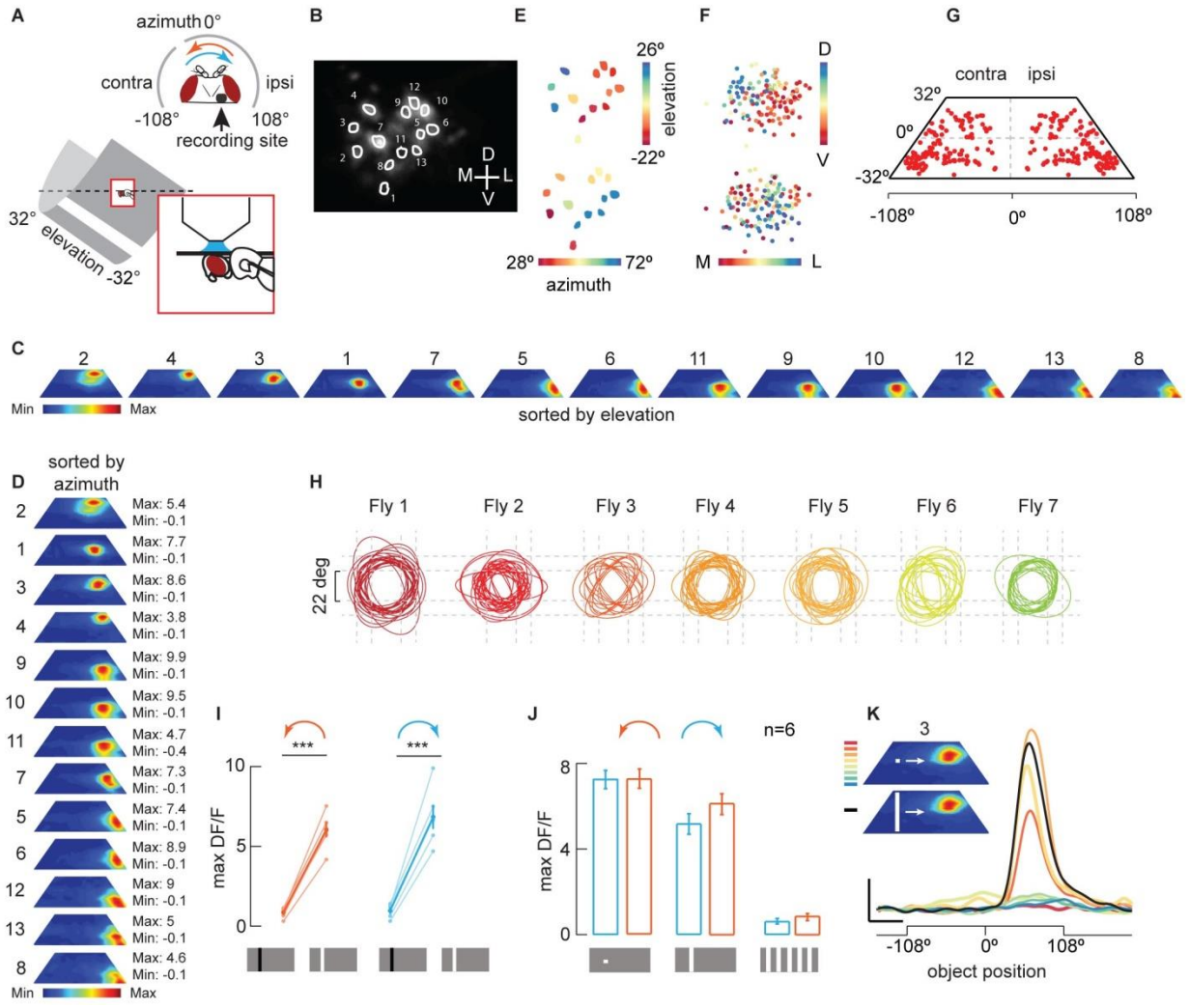

Figure 2-5: Physiological properties of tuberculo-bulbar neurons innervating the superior bulb

(A) Schematic of two-photon experimental setup. Quiescent female flies are spatially fixed in front of a curved array of LEDs. The upper corners of the LED display are obscured by the mounting stage and outside the field of view (dashed line), which is reflected in the parallelogram receptive field projections in C and D below.

(B) Two photon excitation image of a representative fly in which *R88A06-Gal4* is driving the expression of GCaMP6m in DALcl1-derived tubercular-bulbar neurons of the

superior bulb ($TuBu_s$). All recordings are from the microglomerular presynaptic terminals of the right bulb. Responsive microglomeruli are randomly indicated numerically as individual regions of interest (ROIs; white).

(C and D) For individual microglomeruli enumerated from representative fly in panel B, receptive field maps were generated using a small object passed at 8 different elevation trajectories in both directions. Maps from 13 microglomeruli are sorted from highest to lowest elevation center of the receptive field 'hotspot' (C) and sorted again from medial to lateral-most azimuth (D) to indicate the visual coverage by an ensemble of receptive fields. All receptive fields are mapped from ipsilateral microglomeruli.

(E) Spatial arrangement of traced microglomeruli in the brain recorded from a single fly (from panel B) color coded according to receptive field centers in azimuth (left) and elevation (right) to indicate retinotopic arrangment.

(F) Retinotopic organization demonstrated by superimposed population microglomeruli (represented as uniform size dots) from 7 flies totaling 136 microglomeruli.

(G) Overlaid receptive fields represented as red spheroids from representative fly in panel B, demonstrating wide coverage of the ipsilateral visual hemifield.

(H) Overlaid receptive fields represented as spheroids from 7 flies demonstrate spatially consistent receptive field sizes across microglomeruli and animals.

(I-J) Visual stimuli presented in both horizontal directions as shown in (A); ipsi-to-contra motion (orange) and contra-to-ipsi motion (blue). (H) Pairwise comparison between the mean of maximum $\Delta F/F$ responses from all ROIs from each preparation to both an OFF and ON bar; suggests ON selectivity. (I) Mean of pooled peak amplitude responses relative to stimulus onset from six flies to an ON object (left), an ON bar (middle), and

wide-field gratings (right).

(K) Individual calcium traces of 8 different elevation trajectories of an ON object (colors) compared to an ON bar (black) of a single representative ROI (microglomerulus 3 from fly in B). Scale bar is 200% $\Delta F/F$ and 2 seconds, y and x axis respectively.

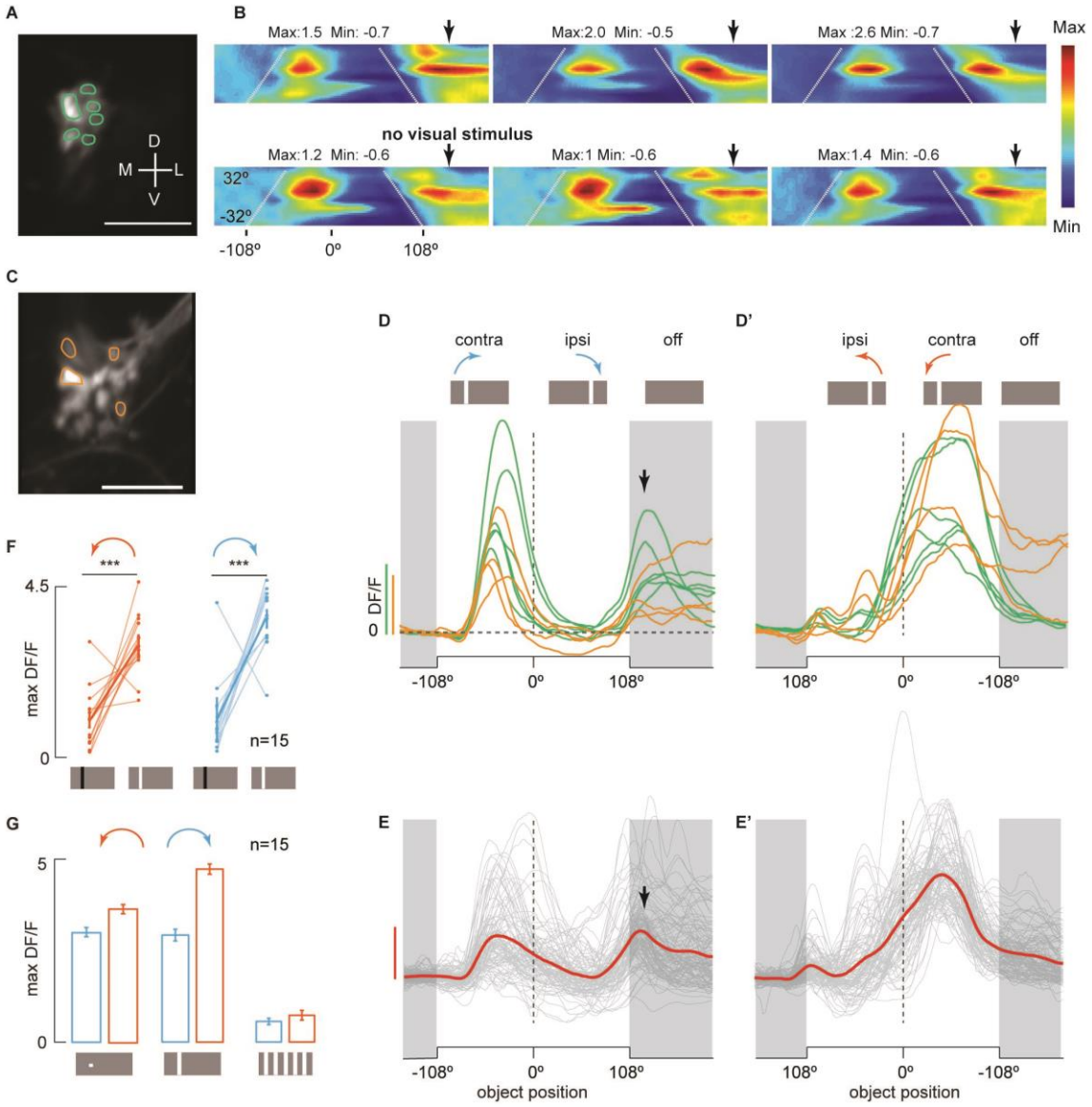

Figure 2-6: Physiological properties of tuberculo-bulbar neurons innervating the inferior bulb

(A-E') Canonical responses from a subset of inferior bulb microglomeruli.

(A) Two photon excitation image of a representative fly in which *R49E09-Gal4* is driving the expression of GCaMP6m in DALcl2 tubercular-bulbar neurons of the inferior bulb ($TuBu_i$). Imaging plane reflects the microglomeruli (ROIs; mint green) in the dorso-posterior most position in the inferior bulb.

(B) Receptive field maps of ROIs in (A) generated by contralateral to ipsilateral (contra-to-ipsi) motion of an ON object passed at 8 different elevation trajectories. Maps demonstrate homogeneity of a class of microglomeruli typically localized to this position in the inferior bulb; characterized by large spatial receptive fields in the contralateral visual hemifield, ipsilateral inhibitory receptive field, and additional excitation after the object has left the field of view (indicated with diagonal white lines).

(C) Second imaging plane from same preparation as (A) contains some microglomeruli which do (light orange), but many that do not (unlabeled microglomeruli), exhibit a canonical $TuBu_i$ response.

(D-D') ON bar responses from inferior bulb microglomeruli which exhibit the canonical response described in (B) from the representative fly shown in (A-C). Responses from ROIs from the first plane (mint green) and second plane (light orange) are shown as traces from contra-to-ipsi presentation (D) and ipsilateral to contralateral (ipsi-to-contra) presentation (D') of the ON bar. Scale bars are 400% $\Delta F/F$ for mint green and 100% $\Delta F/F$ for light orange. Shaded grey envelopes indicate portions of the experiment when the stimulus is out of the visual field. Black arrow indicates responses of microglomeruli when the ON bar leaves the visual field.

(E-E') Population data from all ROIs which exhibit a canonical $TuBu_i$ response for contra-to-ipsi (E) and ipsi-to-contra (E') presentation of the ON bar. Raw traces shown in grey, mean of all traces in red. Scale bar is 200% $\Delta F/F$. Shaded grey envelopes and black arrow as described in D-D'.

(F-G) Visual stimuli presented in both horizontal directions; ipsi-to-contra motion (blue) and contra-to-ipsi motion (orange). (F) Pairwise comparison between the mean of

maximum ΔF/F responses from all ROIs which exhibit a canonical $TuBu_i$ response from each preparation; suggests ON selectivity. (G) Mean of pooled peak amplitude responses relative to stimulus onset from fifteen flies to an ON object (left), an ON bar (middle), and wide-field gratings (right).

References

Dhande, O.S., and Huberman, A.D. (2014). Retinal ganglion cell maps in the brain: implications for visual processing. Curr. Opin. Neurobiol. 24, 133–142.

el Jundi, B., Pfeiffer, K., Heinze, S., and Homberg, U. (2014). Integration of polarization and chromatic cues in the insect sky compass. J. Comp. Physiol. A 200, 575–589.

Hanesch, U., Fischbach, K.-F., and Heisenberg, M. (1989). Neuronal architecture of the central complex in Drosophila melanogaster. Cell Tissue Res. 257, 343–366.

Hartenstein, V., Spindler, S., Pereanu, W., and Fung, S. (2008). The Development of the Drosophila Larval Brain. In Brain Development in Drosophila melanogaster (New York, NY: Springer New York), pp. 1–31.

Heinze, S., and Reppert, S.M. (2011). Sun Compass Integration of Skylight Cues in Migratory Monarch Butterflies. Neuron 69, 345–358.

Held, M., Berz, A., Hensgen, R., Muenz, T.S., Scholl, C., Rössler, W., Homberg, U., and Pfeiffer, K. (2016). Microglomerular Synaptic Complexes in the Sky-Compass Network of the Honeybee Connect Parallel Pathways from the Anterior Optic Tubercle to the Central Complex. Front. Behav. Neurosci. 10, 186.

Homberg, U., Heinze, S., Pfeiffer, K., Kinoshita, M., el Jundi, B. (2011). Central neural coding of sky polarization in insects. Philos Trans R Lond B Biol Sci. 336, 680-687.

Huber, F. (1960). Untersuchungen Über die Funktion des Zentralnervensystems und insbesondere des Gehirnes bei der Fortbewegung und der Lauterzeugung der Grillen. Zeitschrift für Vergleichende Physiol. 44, 60–132.

Ilius, M., Wolf, R., and Heisenberg, M. (1994). The central complex of Drosophila melanogaster is involved in flight control: studies on mutants and mosaics of the gene ellipsoid body open. J. Neurogenet. 9, 189–206.

Ito, M., Masuda, N., Shinomiya, K., Endo, K., and Ito, K. (2013). Systematic Analysis of Neural Projections Reveals Clonal Composition of the Drosophila Brain. Curr. Biol. 23, 644–655.

Ito, K., Shinomiya, K., Ito, M., Armstrong, J.D., Boyan, G., Hartenstein, V., Harzsch, S., Heisenberg, M., Homberg, U., Jenett, A., et al. (2014). A Systematic Nomenclature for the Insect Brain. Neuron 81, 755–765.

Jefferis, G.S.X.E., Vyas, R.M., Berdnik, D., Ramaekers, A., Stocker, R.F., Tanaka, N.K., Ito, K., and Luo, L. (2004). Developmental origin of wiring specificity in the olfactory system of Drosophila. Development 131, 117–130.

Jenett, A., Rubin, G.M., Ngo, T.T.B., Shepherd, D., Murphy, C., Dionne, H., Pfeiffer, B.D., Cavallaro, A., Hall, D., Jeter, J., et al. (2012). A GAL4-Driver Line Resource for Drosophila Neurobiology. Cell Rep. 2, 991–1001.

Lai, S.-L., Awasaki, T., Ito, K., and Lee, T. (2008). Clonal analysis of Drosophila antennal lobe neurons: diverse neuronal architectures in the lateral neuroblast lineage. Development 135, 2883-2893.

Lovick, J.K., Ngo, K.T., Omoto, J.J., Wong, D.C., Nguyen, J.D., and Hartenstein, V. (2013). Postembryonic lineages of the Drosophila brain: I. Development of the lineage-associated fiber tracts. Dev. Biol. 384, 228–257.

Maimon, G., Straw, A.D., and Dickinson, M.H. (2008). A Simple Vision-Based Algorithm for Decision Making in Flying Drosophila. Curr. Biol. 18, 464–470.

Maisak, M.S., Haag, J., Ammer, G., Serbe, E., Meier, M., Leonhardt, A., Schilling, T., Bahl, A., Rubin, G.M., Nern, A., et al. (2013). A directional tuning map of Drosophila elementary motion detectors. Nature 500, 212–6.

Marin, E.C., Jefferis, G.S.X.E., Komiyama, T., Zhu, H., and Luo, L. (2002). Representation of the glomerular olfactory map in the Drosophila brain. Cell 109, 243–55.

Namiki, S., and Kanzaki, R. (2016). Comparative Neuroanatomy of the Lateral Accessory Lobe in the Insect Brain. Front. Physiol. 7, 244.

Nern, A., Pfeiffer, B.D., and Rubin, G.M. (2015). Optimized tools for multicolor stochastic labeling reveal diverse stereotyped cell arrangements in the fly visual system. Proc. Natl. Acad. Sci. 112, 201506763.

Neuser, K., Triphan, T., Mronz, M., Poeck, B., and Strauss, R. (2008). Analysis of a spatial orientation memory in Drosophila. Nature 453, 1244–1247.

Ofstad, T.A., Zuker, C.S., and Reiser, M.B. (2011). Visual place learning in Drosophila melanogaster. Nature 474, 204–207.

Otsuna, H., and Ito, K. (2006). Systematic analysis of the visual projection neurons of Drosophila melanograster. I. Lobula-specific pathways. J. Comp. Neurol. 497, 928–958.

Otsuna, H., Shinomiya, K., and Ito, K. (2014). Parallel neural pathways in higher visual centers of the Drosophila brain that mediate wavelength-specific behavior. Front. Neural Circuits 8, 8.

Otto, D. (1971). Untersuchungen zur zentralnervösen Kontrolle der Lauterzeugung von Grillen. Zeitschrift für Vergleichende Physiol. 74, 227–271.

Panser, K., Tirian, L., Schulze, F., Villalba, S., Jefferis, G.S.X.E., Bühler, K., and Straw, A.D. (2016). Automatic Segmentation of Drosophila Neural Compartments Using GAL4 Expression Data Reveals Novel Visual Pathways. Curr. Biol. 26, 1943–1954.

Pereanu, W., Kumar, A., Jennett, A., Reichert, H., and Hartenstein, V. (2010). Development-based compartmentalization of the Drosophila central brain. J. Comp. Neurol. 518, 2996–3023.

Pfeiffer, K., and Homberg, U. (2014). Organization and Functional Roles of the Central Complex in the Insect Brain. Annu. Rev. Entomol. 59, 165–184.

Pfeiffer, K., Kinoshita, M., and Homberg, U. (2005). Polarization-Sensitive and Light-Sensitive Neurons in Two Parallel Pathways Passing Through the Anterior Optic Tubercle in the Locust Brain. J. Neurophysiol. 94, 3903-3915.

Poucet, B., Chaillan, F., Truchet, B., Save, E., Sargolini, F., and Hok, V. (2015). Is there a pilot in the brain? Contribution of the self-positioning system to spatial navigation. Front. Behav. Neurosci. 9, 292.

Renn, S.C., Armstrong, J.D., Yang, M., Wang, Z., An, X., Kaiser, K., and Taghert, P.H. (1999). Genetic analysis of the Drosophila ellipsoid body neuropil: organization and development of the central complex. J. Neurobiol. 41, 189–207.

Rowland, D.C., Roudi, Y., Moser, M.-B., and Moser, E.I. (2016). Ten Years of Grid Cells. Annu. Rev. Neurosci. 39, 19–40.

Seelig, J.D., and Jayaraman, V. (2013). Feature detection and orientation tuning in the Drosophila central complex. Nature 503, 262–6.

Seelig, J.D., and Jayaraman, V. (2015). Neural dynamics for landmark orientation and angular path integration. Nature 521, 186–191.

Strausfeld, N.J. (1976). Atlas of an Insect Brain. Springer 52, 1096–1109.

Strauss, R., and Heisenberg, M. (1993). A higher control center of locomotor behavior in the Drosophila brain. J. Neurosci. 13, 1852–61.

Strauss, R., Hanesch, U., Kinkelin, M., Wolf, R., and Heisenberg, M. (1992). No-bridge of Drosophila melanogaster: portrait of a structural brain mutant of the central complex. J. Neurogenet. 8, 125–55.

Weir, P.T., and Dickinson, M.H. (2012). Flying Drosophila Orient to Sky Polarization.

Weir, P.T., and Dickinson, M.H. (2015). Functional divisions for visual processing in the central brain of flying Drosophila. Proc. Natl. Acad. Sci. U. S. A. 112, E5523-32.

Weir, P.T., Henze, M.J., Bleul, C., Baumann-Klausener, F., Labhart, T., and Dickinson, M.H. (2016). Anatomical Reconstruction and Functional Imaging Reveal an Ordered Array of Skylight Polarization Detectors in Drosophila. J. Neurosci. 36, 5397-404.

Wernet, M.F., Velez, M.M., Clark, D.A., Baumann-Klausener, F., Brown, J.R., Klovstad, M., Labhart, T., and Clandinin, T.R. (2012). Genetic Dissection Reveals Two Separate Retinal Substrates for Polarization Vision in Drosophila. Curr. Biol. 22, 12–20.

Wolff, T., Iyer, N.A., and Rubin, G.M. (2015). Neuroarchitecture and neuroanatomy of the Drosophila central complex: A GAL4-based dissection of protocerebral bridge neurons and circuits. J. Comp. Neurol. 523, 997–1037.

Wong, A.M., Wang, J.W., and Axel, R. (2002). Spatial representation of the glomerular map in the Drosophila protocerebrum. Cell 109, 229–41.

Wong, D.C., Lovick, J.K., Ngo, K.T., Borisuthirattana, W., Omoto, J.J., and Hartenstein, V. (2013). Postembryonic lineages of the Drosophila brain: II. Identification of lineage projection patterns based on MARCM clones. Dev. Biol. 384, 258–89.

Wu, M., Nern, A., Williamson, W.R., Morimoto, M.M., Reiser, M.B., Card, G.M., and Rubin, G.M. (2016). Visual projection neurons in the Drosophila lobula link feature detection to distinct behavioral programs. Elife 5. doi: 10.7554/eLife.21022.

Yang, J.S., Awasaki, T., Yu, H.-H., He, Y., Ding, P., Kao, J.-C., and Lee, T. (2013). Diverse neuronal lineages make stereotyped contributions to the Drosophila locomotor control center, the central complex. J. Comp. Neurol. 521, 2645–2662.

Yu, H.-H., Awasaki, T., Schroeder, M.D., Long, F., Yang, J.S., He, Y., Ding, P., Kao, J.-C., Wu, G.Y.-Y., Peng, H., et al. (2013). Clonal Development and Organization of the Adult Drosophila Central Brain. Curr. Biol. 23, 633–643.

Chapter 3 - Development of the anterior visual input pathway to the Drosophila central complex

Abstract

The anterior visual pathway (AVP) conducts visual information from the medulla of the optic lobe via the anterior optic tubercle (AOTU) and bulb (BU) to the ellipsoid body (EB) of the central complex. The anatomically defined neuron classes connecting AOTU, BU, and EB represent discrete lineages, genetically and developmentally specified sets of cells derived from common progenitors (Omoto et al., 2017). In this paper, we have analyzed the formation of the AVP from early larval to adult stages. The fiber tracts of the AVP, formed by secondary neurons of lineages DALcl1/2 and DALv2, grow out during the larval period. Overlapping tufts of filopodia of these lineages assemble into structurally distinct primordia of the AOTU, BU, and EB which form prominent structures within the late larval brain. During the early pupal period (P6-P48) these primordia grow in size and differentiate into the definitive subcompartments of the AOTU, BU, and EB. The primordium of the EB has a complex composition. DALv2 neurons form the anterior EB primordium, which starts out as a bilateral structure, then crosses the midline between P6 and P12, and subsequently bends to adopt the ring shape of the mature EB. Columnar neurons of the central complex, generated by the type II lineages DM1-4, form the posterior EB primordium. Starting out as an integral part of the fan-shaped body (FB) primordium, the posterior EB primordium moves forward and merges with the anterior EB primordium. We document the extension of neuropil glia around the nascent EB and BU, and analyze the relationship of primary and secondary neurons of the AVP lineages.

Introduction

The central brain of *Drosophila* is formed by a relatively small number of fixed neural lineages that are produced by genetically unique, stem cell-like neuroblasts (Hartenstein et al., 2008; Ito and Awasaki, 2008). Neural lineages represent genetic modules, as well as structural modules. In the embryo, each neuroblast is defined by the dynamic expression of a specific set of transcription factors. The genetic address provided by these factors plays an essential role in shaping the morphology and function of the corresponding lineage (Pearson and Doe, 2004; Brody and Odenwald, 2005). Lineages also form structural modules, in that neurons of a lineage form compact clusters of cells and emit axons that bundle into one or two coherent fascicles, the primary and secondary lineage axon tracts. Furthermore, arborizations of a given lineage are spatially confined to one or a few individual neuropil compartment(s). Visualizing lineages by clonal analysis has provided a map of the “macrocircuitry” of the Drosophila brain (Ito et al., 2013; Wong et al., 2013; Yu et al., 2013).

In a recent study we had shown that the neural circuit providing visual input to the central complex, the anterior visual pathway (AVP), is formed by three lineages, DALv2, DALcl1, and DALcl2 (Omoto et al., 2017). Larvally-born (secondary) neurons of DALv2 are confined to the ellipsoid body and its input compartment, the bulb (BU; Fig.1). They form the so-called ring (R) neurons of the ellipsoid body (Larsen et al., 2009; Spindler and Hartenstein, 2011; Wong et al., 2013). Different neuron classes of the ellipsoid body are defined by their central-peripheral position in the ellipsoid body (Renn et al., 1999; Young and Armstrong, 2010), which in turn is correlated to dendritic location in the bulb. Most outer ring neurons with axons confined to the outer central

(Roc) and anterior domain (Ra) of the EB have dendritic endings in the superior bulb. Some outer ring neurons innervate the anterior bulb. The inner ring neurons that arborize in the inner central and inner posterior EB domain (Ric, Rip) possess dendrites in the inferior bulb (Omoto et al., 2017; Fig.1).

Input to the bulb (BU) originates in the anterior optic tubercle (AOTU), which in turn is a recipient of visual interneurons from the medulla. Two hemilineages (sets of neurons derived from the unequal division of the ganglion mother cells; Truman et al., 2010), DALcl1d and DALcl2d (Omoto et al., 2017), form a topographically ordered projection from AOTU to BU that respects the boundaries set by the subclasses of DALv2 ring neurons. One can distinguish two major parallel input channels. DALcl1d neurons connect the lateral domain of the AOTU (AOTUl) with the superior and anterior BU (TuBus; TUBua; Fig.1). DALcl2 neurons connect the intermediate domain of the AOTU (AOTUi) to the inferior BU (TuBui; Fig.1). The AOTUl and AOTUi receive input from the medulla of the optic lobe via different populations of multi-columnar medullary projection neurons (MeTu). Functional studies of DALcl1/2 input to the bulb demonstrated that the spatially and developmentally discrete subpopulations of neurons targeting the superior bulb have properties that fundamentally differ from the inferior bulb pathway: the former react to small ipsilateral stimuli and project in a precise retinotopic manner onto the bulb; the latter are inhibited by ipsilateral stimuli, and react to contralateral stimuli distributed widely over the visual field (Omoto et al., 2017).

Similar to the AVP itself, output pathways from the ellipsoid body are also structured around lineages. For example, PB-EB-gall neurons (Wolff et al., 2015) are sublineages of four large (type II) lineages (Yang et al., 2013). These include

DM1/DPMm1, DM2/DPMpm1, DM3/DPMpm2, DM4/CM4 (Ito et al.,2013; Wong et al., 2013; Yu et al., 2013), from here on onward called DM1-DM4. PB-EB-gall neurons form a topographically highly ordered pathway that interconnects small segments of the protocerebral bridge (PB; the posterior-most compartment of the central complex) with the ellipsoid body and the lateral accessory lobe, a known premotor area of the fly brain (Namiki and Kanzaki, 2016).

With the properties summarized above, the AVP exemplifies a circuit where structurally and functionally discrete classes of neurons represent developmental units, that is, components of a small number of lineages. In the present paper, we have investigated the development of the AVP. Using markers expressed throughout the development we were able to follow the first appearance of the different elements of the AVP in the larva, and map the larval primordia of this pathway. Like larval primordia of adult neuropil compartments in general, primordia of the AVP are formed by the undifferentiated axon tracts of lineages DALv2, DALcl1/2, and the posterior type II lineages, which represent dense bundles with filopodia, lacking the expression of synaptic markers that are characteristic for differentiated neuropil (Omoto et al., 2015). During the first 48 hours of metamorphosis, these primordia grow in size and differentiate into the definitive subcompartments of the AOTU, BU, and EB. Of particular interest was the formation of the EB, which consists of two very different populations of neurons: wide-field R neurons of lineage DALv2, located in the anterior brain, and small-field (columnar) neurons of the DM1-4 lineages, located in the posterior brain. We can show that these two groups initially form two separate primordia which later merge into the EB. Finally, we provide a first description of the projection of the primary

neurons of lineages DALv2 and DALcl1/2. Given that a central complex and AVP, in the anatomical sense, are not yet formed in the larval brain, we ask what compartments are innervated by the primary neurons of these lineages, and how they relate to the adult central complex. Our data provide a foundation for future studies addressing the genetic and developmental mechanisms by which complex, homotopically ordered pathways are controlled.

Materials and Methods

Fly Lines

insc-Gal4 (Mz1407; Betschinger et al, 2006; Bloomington Drosophila Stock Center (BDSC) #8751), poxn-Gal4 (Boll and Noll, 2002; kindly provided by Dr. H. Reichert), per¬-Gal4 (Kaneko and Hall, 2000; #7127, BDSC); NP6520-Gal4 (Awasaki et al., 2008) (Kyoto Department of Drosophila Genomics and Genetic Resources), Nrv2-Gal4 (Sun et al., 1999; kindly provided by Dr. P. Salvaterra); UAS-DenMark::mCherry, UAS-Syt::GFP (Nicolai et al., 2010; #33065); UAS-mCD8::GFP (Lee et al., 1999; #5137, BDSC); 442-Gal4 (Hitier et al., 2000; Chen and Hing, 2008; kindly provided by Dr.H.Hing); EB1-Gal4 (Renn et al., 1999; #44409); R19G02-Gal4, R40G10-Gal4, R48B06-Gal4, R52B11-Gal4, R53B08-Gal4, R83H08-Gal4, R82E10-Gal4 (Janelia Farm GAL4 Stock Collection, Jenett et al., 2012; #48860, #50101, #50349, #38821, #38865, #40372, #48625). Flies were grown at 25oC using standard fly media unless otherwise noted.

Immunohistochemistry

The following primary antibodies were used: mouse anti-Neurotactin (Nrt, BP106; RRID:AB_528404), mouse anti-Neuroglian (Nrg, BP104; RRID:AB_528402), rat anti-DNcadherin (DN-Ex #8; RRID:AB_2314331), mouse anti-Bruchpilot (Nc82; RRID:AB_2314868). All antibodies from Developmental Studies Hybridoma Bank (DSHB, University of Iowa, Iowa City, Iowa; each diluted 1:10). For fluorescent staining, the following secondary antibodies were used: Alexa Fluor 546 goat anti-Mouse IgG (H+L) (#A11030; Invitrogen, Carlsbad, CA; used at 1:500) and Cy5 goat anti-Rat IgG (H+L) (112-175-143; Jackson Immunoresearch, West Grove, PA; used at 1:400).

All larvae and adults were grown at 25oC on standard food media. Adults were aged 3 to 5 days post-eclosion before dissection. For antibody labeling, standard procedures were followed (Ashburner, 1989). Briefly, dissected brains were fixed with phosphate buffered saline (PBS), pH 7.4, containing 4% paraformaldehyde for 25 – 30 min. They were then washed with 1x PBS, pH 7.4, containing 0.1 % Triton X-100 for 3 X 10 min. Samples were then incubated in blocking buffer (2% bovine serum albumin (BSA) in 1X PBS, pH 7.4, containing 0.1 % Triton X-100) for 1 hour at room temperature. They were then incubated with primary antibody diluted in blocking buffer overnight at 4oC. They were subsequently washed 3 X 15 min in 1X PBS, pH 7.4, containing 0.1 % Triton X-100 at room temperature, followed by blocking buffer for 20 min. Samples were incubated with secondary antibody diluted in blocking buffer overnight at 4oC, followed by washes in 1X PBS, pH 7.4, containing 0.1 % Triton X-100 for 3 X 15 min, and mounting in Vectashield (Vector Laboratories).

Markers

The DN-cadherin antibody (DSHB DN-EX #8), a marker for neuropil, is a mouse monoclonal antibody raised against a peptide encoded by exon 8, amino acid residues 1210-1272 of the Drosophila CadN gene. The antibody detected two major bands, 300 kDa and 200 kDa molecular weights on Western blot of S2 cells only after transfection with a cDNA encoding the DN-cadherin protein (Iwai et al., 1997). In addition, the specificity of this antibody was tested with immunostaining of Drosophila embryos. Signal was hardly detectable in homozygous mutant, l(2)36DaM19 with nonsense mutation causes premature termination of protein translation. In contrast, this antibody gave a signal in mutant embryos with N-cadherin transgene.

The Neurotactin antibody (DSHB BP106) labels secondary neurons and their axons. It is a mouse monoclonal antibody raised against the first 280 aminoterminal amino acid residues (Hortsch et al., 1990) of the Drosophila Nrt gene. The monoclonal antibody detected the same Drosophila embryonic pattern to that of a polyclonal antisera raised against a fusion protein using part of the Neurotactin cDNA (Hortsch et al., 1990). In addition, another monoclonal antibody, MAb E1C, against Neurotactin gave a similar expression pattern in Drosophila embryos to that of BP106 (Piovant and Léna, 1988).

The Neuroglian antibody (DSHB BP104) labels secondary neurons and axons in the adult brain. It is a mouse monoclonal antibody from a library generated against isolated Drosophila embryonic nerve cords (Bieber et al., 1989). The Neuroglian antibody was used to purify protein from whole embryo extracts by immunoaffinity chromatography. Protein microsequencing of the purified protein was performed to determine that the 18 N-terminal amino acids that is identical to the sequence determined for the N-terminus of the protein based on a full-length cDNA clone (Bieber et al., 1989).

Monoclonal mouse anti-Bruchpilot antibody (DSHB Nc82) labels synapses. Antigen: Raised against adult Drosophila head homogenates. The specific immunogen was identified as Bruchpilot (Wagh et al., 2006). In Western blots of homogenized Drosophila heads, the antibody specifically recognized two proteins of 190 and 170 kDa apparent size which were later found to be part of the same transcription unit of the bruchpilot gene. In vivo, the antibody recognizes brain neuropil as well as synaptic active zones during most stages of Drosophila brain development.

Results

Axonal projections and neuropil primordia of the AVP form in the third instar larva

The central elements of the anterior visual pathway, formed by secondary neurons of lineages DALcl1, DALcl2, and DALv2 (Omoto et al., 2017), are born between 30 and ~100h after hatching and extend axons that coalesce in lineage-associated tracts (secondary axon tracts; SATs), but do not arborize and differentiate prior to metamorphosis (Lovick and Hartenstein, 2015; Lovick et al., 2016). In the late L3 larva, the anterior visual pathway appears as discrete axon bundles that interconnect the primordia of the medulla, optic tubercle, bulb, and ellipsoid body, respectively (Fig.2A). The primordia themselves can be recognized as tufts of filopodia branching off the axon bundles, expressing high levels of DN-cadherin. These filopodial tufts are negative for markers of differentiated synapses, such as Bruchpilot (Brp or Nc82; Wagh et al., 2006), which sets them apart from the surrounding differentiated, Brp-positive larval neuropil (Fig.2B-C'). We can recognize the primordia of the anterior optic tubercle (prAOTU), the anterior ellipsoid body (prEBa) that is merged with the primordium of the bulb (prBU), the posterior ellipsoid body (prEBp), the fan-shaped body (prFB), and noduli (prNO).

The larval primordium of the anterior optic tubercle (prAOTU; labeled by *R52B11-Gal4* in Fig.2D, D') forms a hemispherical domain at the anterior neuropil surface, laterally adjacent to the vertical lobe of the mushroom body. Filopodia foreshadowing the dendrites of tuberculo-bulbar (TeBu) neurons, formed by the dorsal hemi-lineages of DALcl1 and DALcl2, diffusely overlap in this domain with axonal filopodia of the

medullary MeTu neurons from the optic lobe, labeled by *R53B08-Gal4* (Fig.2E, E'). The TeBu tract projects medially across the peduncle of the mushroom body and terminates in two separate filopodial tufts which pioneer the superior and inferior bulb, respectively (prBUs, prBUi; Fig.2D). The bulb primordia are located in the anterior inferior proteocerebrum (IPa) compartment, posteriorly adjacent to the medial lobe of the mushroom body (Fig.2A).

Aside from the endings of DALcl1/2, the DALv2 lineage (labeled by *period-Gal4* or *poxn-Gal4*; Kaneko and Hall, 2000; Boll and Noll, 2002; Larsen et al., 2009) contributes to the primordium of the bulb and, in addition, pioneers the ellipsoid body. The DALv2 tract forms a straight, postero-medially directed bundle that passes underneath the medial lobe of the mushroom body before turning medially and terminating well short of the midline (Fig.2A, F, G). This bundle is called the anterior lateral ellipsoid fascicle (LEa; Strausfeld, 1976; Lovick et al., 2013; Wong et al., 2013 Fig.2F). Proximal filopodia branching off of DALv2 axons intermingle with the DALcl1/2 filopodia in the bulb primordium; more distal filopodia of DALv2 constitute the main, anterior part of the primordium of the ellipsoid body (prEBa; Fig.2A, F-H). An anatomical distinction between different classes of R neurons is not yet apparent within the prEBa, or the prBU. The tract of BAmv1 neurons, which also expresses *per-Gal4* (Larsen et al., 2009), converges onto the anterior prEBa from ventrally. It forms the posterior lateral ellipsoid fascicle (LEp; Lovick et al., 2013; Wong et al., 2013; Fig.2F).

In the adult EB, DALv2 ring neurons and columnar neurons produced by the type II lineages DM1-4, overlap widely (Omoto et al., 2017). By contrast, in the L3 larva, both populations of cells form discrete, spatially separate primordia, as shown by the marker

R19G02-Gal4 which labels specific subsets of columnar neurons, notably the ones connecting the protocerebral bridge, ellipsoid body, and LALgall (PB-EB-gall neurons; Wolff et al., 2015). Filopodial tufts of these neurons form the posterior component of the ellipsoid body primordium (prEBp) in the late larval brain (Fig.2A, I-L). Interestingly, this structure arises as a part of the previously defined fan-shaped body primordium (prFB; Pereanu et al., 2010; Riebli et al., 2013). Axon tracts DM1-4 project anteriorly and then turn medially to form a dense plexus of fibers at the posterior boundary of the prFB (Fig.2A, I, I'). This posterior plexus of the fan-shaped body (FBppl) remains visible into the adult stage as a distinctive anatomical landmark of the central complex. Further anteriorly, the combined fan-shaped body/posterior ellipsoid body primordium (prFB/EBp) is formed by dense, anteriorly directed filopodial tufts emerging from the plexus (Fig.2A, I, I'). The prFB/EBp directly abuts the anterior prEBa, formed by the DALv2 tract/filopodia (Fig.2A, K, L). As described in the following section, the prEBp separates from the prFB at the onset of metamorphosis, moving anteriorly and merging with the prEBa.

A subset of *R19G02-Gal4*-positive fibers continue anteriorly, then turn medially or laterally, forming a second plexus at the anterior boundary of the fan-shaped body primordium (Fig.2A, J, J'). This anterior plexus of the fan-shaped body (FBapl) also develops into a prominent fiber system of the adult brain, capping the fan-shaped body anteriorly, and the ellipsoid body dorsally (Omoto et al., 2017). The *R19G02-Gal4*-positive elements of the FBapl terminate in a small focus at the dorso-lateral surface of the lateral accessory lobe (Fig.2A, J-K), pioneering the gall of the lateral accessory lobe (prLALg), which receives axonal terminals of the PB-EB-gall neurons of the adult brain.

Morphogenesis of the anterior ellipsoid body and bulb

During the early pupal period (P6-P48), the primordia of the anterior visual pathway grow in size, and the ellipsoid body takes on its definitive, layered shape. During the first 12h after onset of metamorphosis, axons of the DALv2 derived R-neurons have crossed the brain midline, and sorted out into a dorsal component, the future outer ring (Roc) and a ventral component, which foreshadows the inner ring (Ric; Fig.3A, C, C', D, D'). These two layers, which form the anterior primordium of the ellipsoid body (prEBa), are recognizable on the basis of differential labeling with Gal4 driver lines specific for R-neuron subsets, as well as DNcadherin (Fig.3C-D'). Between P12 and P48, R axons bend, with the result that the initially straight Roc and Ric domains adopt their characteristic ring shape. Roc fibers bend ventrally, around the inner mass of Ric fibers, whereas the Ric fibers grow dorsally (Fig.3B, E-F'), eventually completing an inner ring surrounded by the outer ring at P48 (Fig.3G-J').

The primordium of the bulb (prBU) is recognizable as a DNcad-rich domain separable from the ellipsoid body primordium from stage P6 onward. Flanking the prEB laterally, the superior part of the prBU is located at the level of the presumptive outer ring, the inferior part next to the presumptive inner ring neurons (Fig.3A-C, K). Labeling of DALcl1/2d neurons at this stage with *R83H08-Gal4* shows a clear separation of dorsal and ventral axon terminals (Fig.3K), demarcating the primordia of the BUs and BUi, respectively. However, based on neuropil markers (anti-DNcadherin), a boundary between presumptive BUs and BUi is not apparent yet (arrowhead in Fig.3K'). This boundary appears at around P24, when the bending of DALv2 axons into a ring-shape is well under way and, as a result, the primordium of the ellipsoid body has become

narrower and spatially separated from the bulb primordium (Fig.3L, L'). A lateral indentation demarcates the boundary between BUs and BUi (arrow in Fig.3L'). At this stage, dendritic branches of inner and outer DALv2 R-neurons have also separated; as shown in Fig.3H, dendrites of outer ring neurons, labeled by *EB1-Gal4*, are restricted to the dorsal bulb. Morphogenesis of the bulb is complete by P48, when neuropil markers delineate discrete BUs, BUi, and BUa (Fig.3M-N').

Differentiation of the anterior optic tubercle

The AOTU of the adult brain is comprised of a medial division (AOTUm), which receives input from the lobula, and an intermediate and lateral subdivision (AOTUi, AOTUl) targeted by medullary MeTu neurons, and connected to the bulb by DALcl1/2d neurons. The AOTUl is further subdivided into three smaller domains, the anterior, intermediate, and posterior AOTUl (Omoto et al., 2017). The gradual differentiation of the AOTU from its larval primordium can be followed by labeling DALcl1/2d neurons with *R83H08-Gal4*, which is expressed throughout larval and pupal development (Fig.4). As described above, the larval prAOTU is represented by a small, homogenous domain in which the distal filopodia of afferent optic lobe interneurons and proximal filopodia of DALcl1/2d neurons overlap completely. During the first 12h of metamorphosis the prAOTU grows significantly, and differentiates into a ventro-lateral, DNcadherin-rich domain which is innervated by the bulk of *R83H08-Gal4*-positive fibers, and a dorso-medial, DNcadherin-poor region (Fig.4A-B'). The former domain represents the primordium of the intermediate and lateral tubercle (prAOTUi/l), and the latter one the primordium of the medial tubercle (prAOTUm), which does not receive DALcl1/2d dendrites. By P24, the axis of the prAOTU has tilted more towards the horizontal,

bringing the prAOTUi/l to a position laterally adjacent to the prAOTUm, at which it remains until the adult stage (Fig.4C-D'). However, the subdivision of the lateral part of the tubercle into AOTUim, AOTUil, and AOTUla-p is not yet evident at this stage. This subdivision starts to be visible at around P48, when the lateral tubercle clearly shows two separate domains, set apart by a sharp boundary (Fig.4E-F'). The lateral domain (AOTUl) is already characterized by a higher intensity of DNcad expression than the intermediate domain (AOTUi; Fig.4E', F'). The further distinction of the three subdomains of the AOTUl, arranged along the anterior-posterior (AOTUla, AOTUi, AOTUp) becomes morphologically visible around the time of eclosion (Fig.4G, H).

Formation of the ellipsoid body from an anterior and posterior primordium

This process can be followed in frontal and horizontal sections of pupal brains labeled with BP104, in conjunction with more specific markers such as *R19G02-Gal4*, which is expressed in columnar neurons interconnecting the protocerebral bridge (PB) with the fan-shaped body, ellipsoid body, and gall of the lateral accessory lobe (Omoto et al., 2017). As described above, in the late larva, these axon bundles of the four clusters of *R19G02-Gal4*-positive neurons project from posteriorly into the primordium of the central complex. Tufts of filopodia form the primordium of the fan-shaped body, which at this early stage also includes the primordium of the posterior ellipsoid body (see Fig.2). Around 12h APF, these two primordia have separated and form two layers (Fig.5A-D), a thick dorso-posterior layer (prFB) which will develop into the fan-shaped body (light blue arrow in Fig.5C, C', D), and a thinner ventro-anterior layer (prEBp; dark blue arrow in Fig.5C, C', D), which will become incorporated into the ellipsoid body. The prEBp is directly juxtaposed to the anteriorly adjacent prEBa, formed by the distal fibers

of DALv2 (red arrow in Fig.5C, C', D). Between P12 and P24, the prEBp moves anteriorly and becomes further separated from the prFB (Fig.5E-H, I). At that stage it appears as a curved, DNcadherin-rich bar that is filled with filopodial endings of *R19G02-Gal4*-positive PB-EB-gall neurons (Fig.5F). At P24, the prEBp and prEBa are still largely non-overlapping: *R19G02-Gal4* label is restricted to the DNcadherin-rich prEBp, and DALv2 markers (e.g., *poxn-Gal4*) to the DNcadherin-poor prEBa (Fig.5H). By P48, as the anterior and posterior primordia of the ellipsoid body merge into one compartment (thick purple arrow in Fig.5I, L, M); this separation has all but disappeared. *R19G02-Gal4*-positive fibers have expanded through most of the prEB, with the exception of the anterior domain (Fig.5L). R-neurons also fill most of the volume of the prEB at P48, leaving only a narrow posterior shell empty (Fig.5M). The subdivision of the EB neuropil into its five distinct domains with different DNcadherin expression levels (EBa, EBoc, EBic, EBop, EBip; Omoto et al., 2017) becomes apparent only around the time of eclosion.

Development of the LALgall

The spreading and elongation of the forward directed PB-EB-gall fibers that terminate in the gall of the LAL can also be followed in pupal brains expressing *R19G02-Gal4*. At P6 and P12 these fibers penetrate through a central, DNcadherin-poor layer of the prFB (arrow in Fig.5A, N). Extending forward they converge in the anterior plexus of the fan-shaped body (FBapl), from which the primordia of the LAL gall (prLALg) protrude as two lateral processes (Fig.5B, C, D). These primordia are directly adjacent to the anterior lateral ellipsoid body tract formed by the DALv2 (R-neuron) lineage (Fig.5D). From P24 onward, accompanying the pronounced dorso-ventral

growth of the prFB (Fig.5E), the fiber bundles spread out, forming two tiers of eight tracts each (arrows in Fig.5E). The primordium of the LALgall adopts its characteristic oval shape and position in the crevice formed by the dorsal surface of the LAL and anterior surface of the bulb (Fig.5F, I, K).

Differentiation of neuropil glia during the formation of the AVP and central complex

As shown in the previous sections, the primordia of the ellipsoid body and fan-shaped body evolve from a system of closely apposed transverse fiber bundles, formed by several discrete neural lineages. Crossing the midline, these bundles are enveloped by a layer of ensheathing glia (Fig.6A), and are surrounded on all sides by other commissural tracts, each wrapped into its own coat of ensheathing glia (Fig.6A-D). The ensheathing glia located at the brain midline represents a small, genetically distinct class of glia that was originally described as the “interhemispheric ring” (Simon et al., 1998). It is labeled by *Nrv2-Gal4*, a global marker for glia (Younossi-Hartenstein et al., 2003), *NP6520-Gal4*, a marker for ensheathing glia, (Awasaki et al., 2008), as well as *442-Gal4* (Hitier et al., 2000), whose expression, during pupal stages, is restricted to the interhemispheric ring glia. Using these glial markers in conjunction with BP104 and anti-Fasciclin II we followed the development of glial sheaths as formation of the central complex takes place.

During the first 12h of metamorphosis, the primordium of the central complex grows in volume, but remains enclosed in an undivided glial cavity. As described in the previous section, the primordium of the anterior ellipsoid body (prEBa) crosses the midline, and the primordia of the posterior ellipsoid body and fan-shaped body become

spatially separated and grow in volume during this time interval, but both remain in direct contact, with no intervening glial layer (Fig.6E-H). Between 24h and 36h APF, the primordia of the ellipsoid body merge together and adopt their elliptical shape, while still growing in volume. Still, the entire prEB and prFB, and at this stage even the medial lobe of the mushroom body, are enclosed in a shared glial covering (Fig.6I-P). Around 48h APF, glial processes, formed by secondary ensheathing glia born in the larva (Omoto et al., 2015), start to grow in between the prFB and prEB, as well as between the prEB and the medial lobe (Fig.6P, T, X; orange arrowhead/arrow). By 72h APF, a thick, largely uninterrupted layer of ensheathing glia surrounds each individual compartment of the central complex and the mushroom body (Fig.6U-X).

Projection of primary neurons generated by AVP lineages

Secondary neurons forming the central complex and AVP are born and extend their axons during the larval period. In general, secondary axon tracts fasciculate with the existing tracts extended (during embryogenesis) by the corresponding primary neurons (Larsen et al., 2009; Hartenstein et al., 2015). In this manner, primary axons of the type II lineages DM1-4 pioneer the primordium of the fan-shaped body (Riebli et al., 2013; Hartenstein et al., 2015). Primary tracts also precede the formation of the AVP. As shown in Fig.7A/A' and 7C/C' for the late second instar larva (L2), primary axons of lineages DALcl1 and DALcl2 (labeled by anti-Neuroglian; green in Fig.7A/A', B/B') approach the mushroom body spur from laterally and split into a dorsal bundle and ventral bundle. Secondary axon tracts of these lineages (labeled by *insc-Gal4*; magenta in Fig.7A/A', B'/C) adopt the same pattern. The dorsal tract is formed by the two dorsal hemilineages, DALcl1d and DALcl2d (Lovick et al., 2013), which represent the TuBu

neurons of the anterior visual pathway described in this paper. We speculate that the primary DALcl1/2 neurons contributing to the dorsal tract may similarly represent hemilineages. The same applies for the neurons projecting ventrally. Here, secondary axons of the DALcl1/2v hemilineages form a ventro-medially directed tract that splits into two branches. DALcl1v continues medially and eventually crosses the midline in the SuEC commissure (Lovick et al., 2013; Fig.7C); DALcl2v turns postero-dorsally, passes underneath the medial lobe of the mushroom body, and approaches the midline at the level of the fan-shaped body primordium (Fig.7C/C'). Secondary DALcl2v neurons form a major subset of large-field fan-shaped body neurons (Wong et al., 2013). As shown in Fig.7A, the secondary DALcl1/2v tract is well established 48h after hatching and extends along its primary counterpart. The secondary DALcl1/2d hemilineages differentiate slightly later; they are present 64h after hatching and extend their axons along the primary DALcl1/2d tract (Fig.7B-B'').

In contrast to DALcl1/2 and all other brain lineages analyzed to date, the secondary tract of DALv2, which configures the primordium of the ellipsoid body and bulb in the late larva, does not fasciculate with the primary DALv2 axons (Lovick et al., 2016). Primary DALv2 axons enter the LAL compartment at its anterior-ventral surface. The majority of DALv2 primary neurons appear to arborize within the LAL (see below); a subset of primary DALv2 axons continues dorsally along the LAL surface and approaches the medial lobe of the mushroom body (arrow in Fig.7C'-C'''). The secondary DALv2 tract extends along the lateral surface of the LAL (small arrowhead in Fig.7C', C''). At the position where it enters the neuropil it joins the DALcl2v tract (large

arrowhead in Fig.7C'), passing underneath the medial lobe, and turning medially right posterior to the lobe.

Given that the AVP develops during metamorphosis, where do primary neurons of DALcl1/2d and DALv2 project in the larval brain? The markers *R48B06-Gal4* (DALcl1/2d), *R82E10-Gal4* (DALcl1d/v), and *Poxn-Gal4* (DALv2) are already expressed in the early larva and allowed us to address this question. *R48B06-Gal4* labels a cluster of approximately eight neurons which project along the DALcl1/2d tract, crossing the peduncle at its dorsal surface (Fig.7D, see above). Axons arborize in the LAL, as well as the anterior inferior protocerebrum (IPa) that surrounds the medial lobe of the mushroom body (Fig.7D/D'). Expression of *R82E10-Gal4* (DALcl1d/v) confirms this projection pattern (not shown). Primary DALv2 neurons project to the same compartments (Fig.7E), filling the lateral half of the LAL, and a dense, cuff-shaped domain surrounding the middle of the medial lobe. Expressing DenMark and Synaptotagmin in these neurons shows that pre- and postsynaptic sites of primary DALv2 neurons are present in both the LAL and IPa (Fig.7F). Postsynaptic sites in the latter are most likely contacted by Kenyon cell axons, which would indicate that primary DALv2 neurons form a pathway interconnecting the mushroom body with the surrounding IPa and LAL.

Discussion

Morphogenesis of the central complex neuropil

The central complex, defined as a set of compartments with terminal neurites and synapses spanning the brain midline, is an adult-specific structure of the *Drosophila* brain that differentiates during metamorphosis. Similarly, the anterior optic tubercle and bulb, which provide visual input to the central complex, develop during metamorphosis. The only contribution of embryonically-born, primary neurons that we currently know about are the “fan-shaped body pioneer neurons” that form a thin bundle of undifferentiated, commissural axons visible already in the early larva (Hartenstein et al., 2015), and that will later differentiate into a subtype of columnar neurons of the central complex (Riebli et al., 2013).

At late larval stages, secondary lineages that will give rise to the bulk of columnar and tangential neurons of the central complex make their appearance. These lineages form tracts that associate themselves with the fan-shaped body pioneers. The tracts, and tufts of filopodia emerging from them, form discrete primordia that are recognizable by a high expression level of DN-cadherin and the absence of markers for mature synapses, like Bruchpilot or Synaptotagmin. The combination of high levels of DN-cadherin and missing expression of synaptic markers is a robust criterion to morphologically recognize immature, non-functional primordia of adult neuropil compartments in the larval brain.

The emergence of the central complex architecture that takes place during the first half of pupal development involves several sequential following steps. First, the bilateral primordia of fan-shaped body and ellipsoid body advance towards the midline,

resulting in the formation of a bar-shaped neuropil that straddles the midline. This process is accompanied by a widening of the glial sheath surrounding these primordia. Initially, this sheath forms a tight cuff, enclosing only the commissural tract formed by the fan-shaped body pioneers. During the first 12 hours APF the cuff widens, to accommodate both the fan-shaped body primordium and anteriorly adjacent ellipsoid body primordium (see Fig.6). The cuff enveloping the developing central complex is formed by the interhemispheric ring glia, a subset of the ensheathing glia surrounding the neuropil (Omoto et al., 2015; see Fig.6). An important (presumably permissive) role of the interhemispheric ring glia can be gleaned from the results of genetic studies where factors expressed in the interhemispheric ring glia are mutated. Examples of such genetic factors are the receptor tyrosine kinase Linotte/Derailed, whose disruption results in structural defects of the central complex, in particular the appearance of clefts in the midline that divide the fan-shaped body and/or ellipsoid body into a paired neuropil (Simon et al., 1998).

The second major event that shapes the central complex consists in the separation of different layers and columns which, at least in part, represent different channels of input and different functionalities. Columns can be recognized in the prFB and prPB as soon as these primordia make their appearance in the larva (Riebli et al., 2013). By contrast, the hemilineages and sublineages of DALcl1/2 and DALv2, forming the anterior optic tubercle, bulb, and ellipsoid body, appear to overlap widely in the respective primordia of these compartments. A sorting out that begins during the first day of metamorphosis results in the appearance of morphologically distinct subdivisions, including the four different subdomains of the tubercle (AOTUi, AOTUla,

AOTUli, AOTUlp), the three domains of the bulb (BUs, BUi, BUa), and the five ring domains of the ellipsoid body (EBa, EBoc, EBic, EBop, EBip).

We speculate that repulsive and adhesive membrane components, expressed by DALcl1/2 and DALv2 neurons themselves, as well as by surrounding glial cells, control the growth and spatial sorting that takes place in the EB, BU, and AOTU. In other parts of the developing larval and adult brain, roles of the repulsive Slit/Robo, Semaphorin/Plexin, and Ephrin/Ephrin receptor pathways have been analyzed. The Slit/Robo system is best known for its repulsive action that directs the growth of axons of larval VNC interneurons relative to the midline (Ypsilanti et al., 2010). However, Robo receptors are also expressed and required for the formation of the adult central complex (Nicolas and Preat, 2005). Similarly, Semaphorins/Plexins play a role during early as well as late stages of brain development. In the embryo, they control the layering of VNC interneuronal projections along the dorso-ventral axis (Zlatic et al., 2009). At later stages, in the primordium of the adult antennal lobe, Semaphorin 1a is expressed in a gradient and specifies the location and volume of arborization of olfactory afferents, as well as antennal projection neurons (Komiyama et al., 2007). The same system of repellant cues also played a role in restricting the axonal arborizations of antennal projection neurons in the calyx. Furthermore, Semaphorin 1a acts a receptor for repulsive interactions in the emerging layers of the optic lobe medulla. The molecule is expressed on afferent lamina neurons, which initially form filopodia spreading out over superficial and deep layers of the medulla primordium. At a mid-pupal stage, neuronal processes that express Plexin A (acting as a ligand in this system) grow towards the deep layers of the medulla primordium and repel lamina afferents from these layers

(Pecot et al., 2013). In a similar manner, neurites of sublineages of DALv2 might be sorted out by reacting to repulsive cues acting throughout the primordia of the ellipsoid body and bulb. A recent study (Xie et al., in press) confirms that Semaphorin/Plexin mediated repulsive interactions between inner and outer R-neurons, play an important role in the proper layering of the ellipsoid body.

Ontogeny and phylogeny of the central complex

The central complex and its related neuropils are highly conserved among insects (Loesel et al., 2002). However, developmental studies addressing these brain compartments are rare (for a recent review, see Koniszewski et al., 2016; Boyan and Reichert, 2011). In hemimetabolan taxa all compartments of the central complex seem to be generated during the embryonic period. The formation of the locust fan-shaped body, which has been studied in detail by Boyan and collaborators (Boyan and Liu, 2014; 2016), shows numerous features which are amazingly similar to the corresponding process in *Drosophila*, in particular when considering the relationship between lineages and columnar architecture (see below). However, in the locust, FB columnar neurons appear at around 50% of embryonic development, whereas they are born during the larval period in *Drosophila*. We assume the same applies to the lineages forming the anterior visual pathway, but no detailed information exists on the development of these lineages in the locust.

In most holometabolous taxa, larvae hatch without a fully formed central complex. However, a rudimentary, but differentiated fan-shaped body crossing the midline is typically present. In the coleopteran *Tenebrio molitor* (mealworm), the fan-shaped body, clearly recognizable by its eight vertical modules already existed in freshly

hatched larvae (Wegerhoff and Breidbach, 1992). Interestingly, the columnar units are initially formed by regularly spaced branches of large tangential neurons, rather than the large number of small-field columnar neurons that (in *Tenebrio* as in other insects) innervate the vertical modules of the fan-shaped body. These columnar neurons, along with the ellipsoid body, make their appearance in the late larva, similar to what has been described in *Drosophila* (Hartenstein et al., 2015; Lovick and Hartenstein, 2015). We speculate that the early differentiating tangential neurons forming the rudimentary fan-shaped body primordium in *Tenebrio* may be homologous to the primary neurons whose axons assemble into the simple commissural bundle that constitutes the fly fan-shaped body primordium of the early larva (Riebli et al., 2013). However, whereas these early wide-field neurons differentiate and produce regularly spaced side branches that prefigure the columns of the mature fan-shaped body in *Tenebrio*, such behavior is not displayed by their *Drosophila* counterparts, which do not start to differentiate prior to metamorphosis (Riebli et al., 2013).

The ellipsoid body (called “lower unit of the central body” in other insects) generally appears later in development than the fan-shaped body (“upper unit of the central body”). In insect species other than higher diptera, the ellipsoid body forms a bar-shaped neuropil layer across the midline anterior-ventrally to the fan-shaped body (Loesel et al., 2002). In flies, the ellipsoid body resembles the bar-shaped lower division of other insects at early stages (P6-P12), but subsequently detaches fully from the fan-shaped body and bends full circle into an ellipse, as described in the present paper. We speculate that a number of *Drosophila* mutant phenotypes affecting the central complex represent cases of developmental arrest. For example, the ellipsoid body of flies

carrying mutations in *ellipsoid body open* (*ebo*; Ilius et al., 2007) show a ventral cleft, suggesting that the primordium of this compartment may have started out normally, but was subsequently prevented from completing the curvature.

Columnar and tangential neuronal elements of the central complex in different taxa are probably formed by homologous lineages. Since the bold paper putting forward this hypothesis (Thomas et al., 1984), it is generally assumed that the pattern of neuroblasts and the lineages they form is highly conserved across all insect groups. During the past three decades, not many lineage comparisons were made; the four lineages forming the columnar neurons of the central complex form a notable exception. In the holometabolous locust (*Schistocerca gregaria)*, the central complex contains four prominent lineages (W, X, Y, Z) that generate the columnar neurons of the fan-shaped body and protocerebral bridge (Boyan and Williams, 1997). They bear many of the hallmarks of the four lineages DM1-4 which have the same projections in *Drosophila*. In both species, the four lineages are produced by type II neuroblasts, which first divide to give rise to a type of cell called “intermediate progenitor” (Bello et al., 2008; Boyan et al., 2010). Intermediate progenitors in turn generate ganglion mother cells, followed by neurons. It is also noteworthy that the axonal scaffold built by the neurons of the four lineages bears an extraordinary resemblance between *Schistocerca* and *Drosophila*.

We speculate that the lineages generating the AVP in *Drosophila* will also have counterparts in the locust and other insects. For *Schistocerca*, so called LT neurons with morphologies very much like that of DALv2 neurons have been described (Müller et al., 1997). Like Drosophila DALv2 neurons, cell bodies of these neurons in *Schistocerca* are located in the anterior cortex, and extend a cohesive axon bundle towards the

lateral triangle (the neuropil corresponding to the bulb in *Drosophila*; Homberg et al., 2003; Pfeiffer and Homberg, 2014; Omoto et al., 2017). Similarly, two coherent clusters of neurons, TuLAL1a and TuLAL1b, were described that have cell bodies forming groups lateral of the LT neurons. These neurons interconnect the anterior optic tubercle with the lateral triangle/bulb, and are likely to correspond to the *Drosophila* TuBu neurons, generated by the lineages DALcl1 and DALcl2.

Forerunners of the central complex in the *Drosophila* larva

Lineages of the *Drosophila* brain are comprised of a set of primary neurons that are born and differentiate in the embryo ("primary neurons"), and a larger set of "secondary neurons" that are born in the larva and differentiate during metamorphosis. In general, primary neurons show characteristics that are fundamentally similar to their secondary siblings. For example, most primary neurons of the four mushroom body lineages, or the antennal lobe projection lineages, have dendritic and axonal arborizations that project in a similar manner as the corresponding secondary neurons (Lee et al., 1999; Das et al., 2013). By contrast, primary neurons forming the characteristic, highly ordered orthogonal lattice of midline-spanning tangential and columnar elements seen in the protocerebral bridge, fan-shaped body, and ellipsoid body do not exist in the larva. This raises the question of where the primary neurons of lineages that form the adult central complex project in the embryo. Furthermore, can one consider this larval neuropil domain innervated by primary neurons of central complex-associated lineages as a precursor of the adult central complex?

We propose that the lateral accessory lobe (LAL), which is an easily recognized part of both larval and adult brain, plays an important role in the context of

understanding the emergence of the adult central complex. The LAL has been long recognized as a major output region of the protocerebrum that projects towards motor centers in the subesophageal and thoracic ganglia (Namiki and Kanzaki, 2016). Long projection neurons with arborizations in the LAL can be backfilled when applying tracer molecules to the VNC (Cardona et al., 2009). In the adult brain, neurons of lineage DALd possess the exact same structure (Wong et al., 2013), and we speculate that primary neurons of the DALd lineage have a similar projection (Fig.8A, B). The adult LAL (specifically: the gall of the LAL) is the only compartment known to receive bundled efferent projections from the columnar neurons of the central complex (Hanesch et al., 1989; Wolff et al., 2015). Thus, when considering the pathway by which the electric patterns generated in the central complex, such as recorded during the control of sleep (Pimentel et al., 2016), aggression (Alekseyenko et al., 2013), body orientation (Strauss, 2002; Seelig and Jayaraman, 2015) and many other activities reach the motor centers, the LAL is likely to represent a key node (Namiki and Kanzaki, 2016).

The LAL also forms dense afferent connections with the central complex. Neurons of lineage BAmv1 have widespread proximal arbors in the LAL, and distal, axonal projections that constitute a type of large-field neuron of the fan-shaped body (Wong et al., 2013; Fig.8B). The locust lateral triangle, counterpart of the bulb in *Drosophila* and provider of the visual input to the central complex, is anatomically considered part of the LAL (Homberg et al., 2003). In *Drosophila*, as shown in this paper, the small neuropil constituting the bulb arises outside, but in direct spatial contact with, the LAL (Fig.8B)

Interestingly, lineages whose neurons form the AVP of the adult brain also innervate the LAL. Both (secondary) DALcl1 and DALcl2 have dense arborizations in the LAL. DALcl1v neurons form a major source of commissural connections between the LALs of either side (Wong et al., 2013), and the same is true for the primary DALcl1v neurons (Hartenstein et al., 2015). Secondary DALcl2v neurons have sparser projections to the LAL, but interconnect the IPa compartments, located dorsally adjacent to the LAL, and form a class of fan-shaped body tangential neurons (Wong et al., 2013). We speculate that primary DALcl2v and DALcl1v neurons also have properties similar to their secondary siblings, interconnecting the LAL and IPa compartments of either side (Fig.8A). As to the DALv2 lineage, whose secondary neurons represent the ring neurons of the ellipsoid body: most of its primary neurons also widely arborize in the ipsilateral LAL; a second subset of primary DALv2 neurons forms arborizations in the IPa, in close contact with the mushroom body lobes (Fig.8A; see also Fig.7B'). These projections remain intact in the adult brain as well (J.L. and V.H., unpublished observation). Finally, sublineages of some of the type II lineages, notably CM4/DM1, which generate the posterior, columnar neurons of the central complex, also densely innervate the LAL, both in the adult brain (Wong et al., 2013) and the larva (J.L. and V.H., unpublished).

We speculate that the LAL and adjacent IPa may fulfill fundamental functions in locomotor control, informing the organism about its location and orientation in space, and adjusting motor output accordingly. A defined set of lineages, including DALcl1/2, DALd, DALv2, CM4, and a few others not mentioned here, scaffold the circuitry of the larval LAL/IPa. For the worm-shaped architecture of the larval body this circuitry is

sufficient. To process much more complex tasks, related to the possession of jointed legs and wings for locomotion, and complex sensory arrays like compound eyes and antennae for perceiving the environment, a much larger number of neurons with precisely specified connections would be required. These neurons, constituting the columnar and tangential neurons of the central complex, are added to the existing LAL circuitry by the same lineages that formed the LAL in the first place (Fig.8B). The central complex could be viewed as an “extension” of the LAL in terms of input and output relationships: the LAL proper still provides much of the input to the central complex via tangential neurons of the fan-shaped body (e.g., lineage BAmv1); in addition, the DALcl1/2d neurons bring in massive visual input via the lateral triangle/bulb, which we would consider a developmentally late add-on to the LAL proper. Output from the central complex reaches another late-forming component of the LAL, the gall.

In conclusion, the central components of the anterior visual pathway (bulb and ellipsoid body), formed by secondary neurons of the lineages DALcl1/2 and DALv2, develop within the territory innervated by primary neurons of these lineages. Bulb and anterior ellipsoid body condense within the IPa, posteriorly adjacent to the medial lobe of the mushroom body. Furthermore, the LALgall, a major output site for the central complex, develops at the dorso-lateral surface of the LAL. One might speculate that primary neurons of the lineages forming the adult central complex build a larval circuit that has a function already resembling that of the adult central complex.

Figures

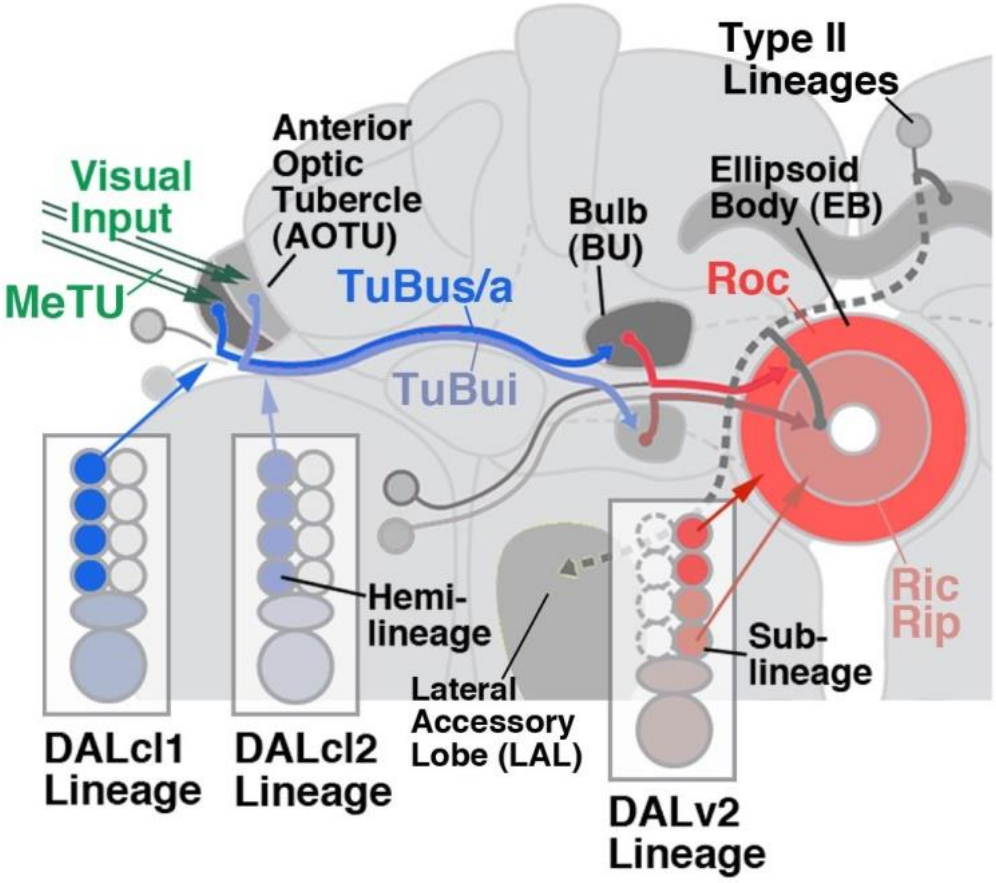

Figure 3-1: Anterior visual pathway of the *Drosophila* brain.

(A) Schematic frontal view of brain hemisphere depicting the neuronal elements forming the anterior visual pathway, as described in Omoto et al. (2017). Medullo-tubercular (MeTu) neurons project via the anterior optic tract to the lateral and intermediate domain of the anterior optic tubercle; AOTU). Two hemilineages, DALcl1d and DALcl2d, form the tuberculo-bulbar (TuBu) neurons that connect the tubercle to the bulb (BU). Lineage DALv2 forms multiple classes of ring (R) neurons with dendrites in the bulb, and axons in the ellipsoid body (EB).

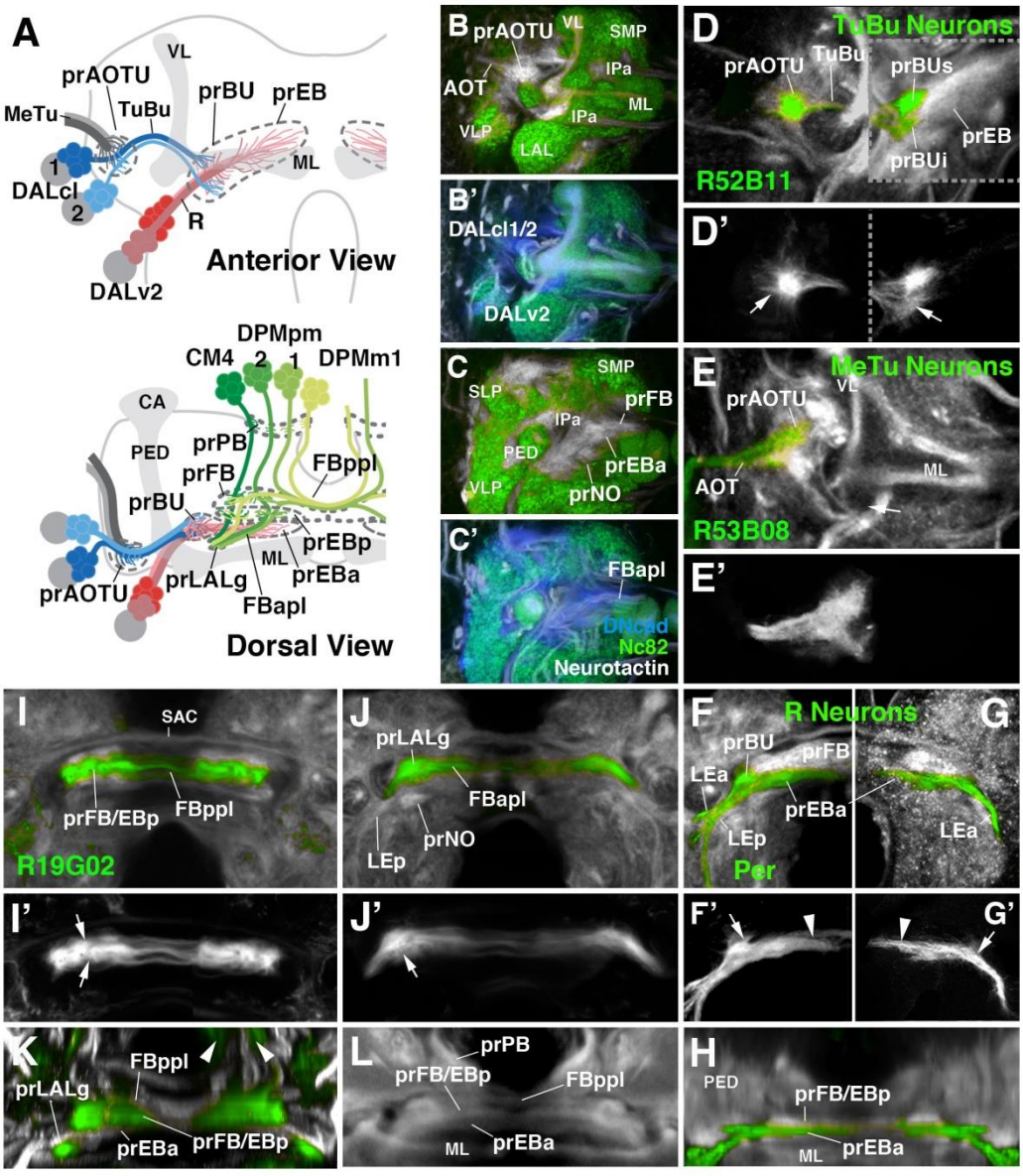

Figure 3-2: Larval primordia of the central complex and anterior visual pathway.

(A) Schematic view of larval brain hemisphere (top: anterior view, dorsal up; bottom: dorsal view, posterior up). Secondary lineages contributing to the primordia of anterior visual pathway and central complex are rendered in different colors; mushroom body (gray) is shown as reference. (B, B', C, C') Z-projections of frontal confocal sections of

late larval brain hemisphere labeled with anti-Bruchpilot (Nc82; green), anti-DNcadherin (DNcad; white in B, C; blue in B', C') and anti-Neurotactin (BP106; white in B', C'). Note domains which are negative for Nc82, indicating absence of synapses; these domains are positive for DNcad and BP106, showing presence of (undifferentiated) secondary fibers and filopodia which make up primordia of adult-specific compartments. Labeled are primordia of anterior optic tubercle (prAOTU), anterior ellipsoid body (prEBa), bulb (prBU), fan-shaped body (prFB), noduli (prNO. (D-K): Z-projections of confocal sections of late larval brain hemispheres in which individual cell classes forming part of anterior visual pathway and central complex are labeled by specific Gal4 drivers (green). In (D-L), DNcad antibody labels neuropil (white); (D'-G') show only GFP expression. (D-G') and (I, J) show frontal sections, (H) and (K, L) are digitally tilted dorsal views. (D, D') Tuberculo-bulbar (TuBu) neurons of DALcl1/2 lineages, labeled by R52B11-Gal4. Shown to the left of hatched line is a more anterior plane, containing tufts of proximal filopodia (marked by arrow in D') that constitute the primordium of the anterior optic tubercle. To the right of the hatched line is a slightly more posterior plane, featuring endings and distal filopodia of TuBu neurons, which form the primordia of the superior and inferior bulb (prBUs, prBUi), respectively. (E, E') Axonal endings of medullo-tubercular (MeTu) neurons in the primordium of the anterior optic tubercle, labeled by R53B08-Gal4. (F-H) Ring (R) neurons of DALv2 lineage, labeled by Period (Per)-Gal4 (F, F', H) or as MARCM clone (G, G'). DALv2 neurons form a straight, medially-directed bundle, the anterior lateral ellipsoid body tract (LEa), which extends posterior to the medial lobe of mushroom body (ML in panel A) to end close to the midline. Filopodial tufts of these axons form the primordia of the anterior ellipsoid body (prEBa;

arrowheads in F', G') and, further laterally, the bulb (prBU; arrows in F', G'). (I-L) Subset of columnar neurons of the central complex, labeled by R19G02-Gal4. These neurons form part of four type II lineages, DM1/DPMm1, DM2/DPMpm1, DM3/DPMpm2, DM4/CM4, as shown in panel (A). Axons project forward and proximal filopodia form the primordium of the protocerebral bridge (arrowheads in K; prPB in A). Axons then branch and turn medially, forming the posterior plexus of the fan-shaped body (FBppl in A, I, K). Filopodial tufts branch in the primordium of the fan-shaped body (A, I, K) and the posterior ellipsoid body (prFB/EBp in I, K). Axons continue forward, branching towards medially and laterally, forming the anterior plexus of the fan-shaped body (FBapl; A, J). Distal tips of this projection defines the primordium of the gall of the LAL (prLALg; A, J, K). For other abbreviations, see Table 1. Bar: 25μm

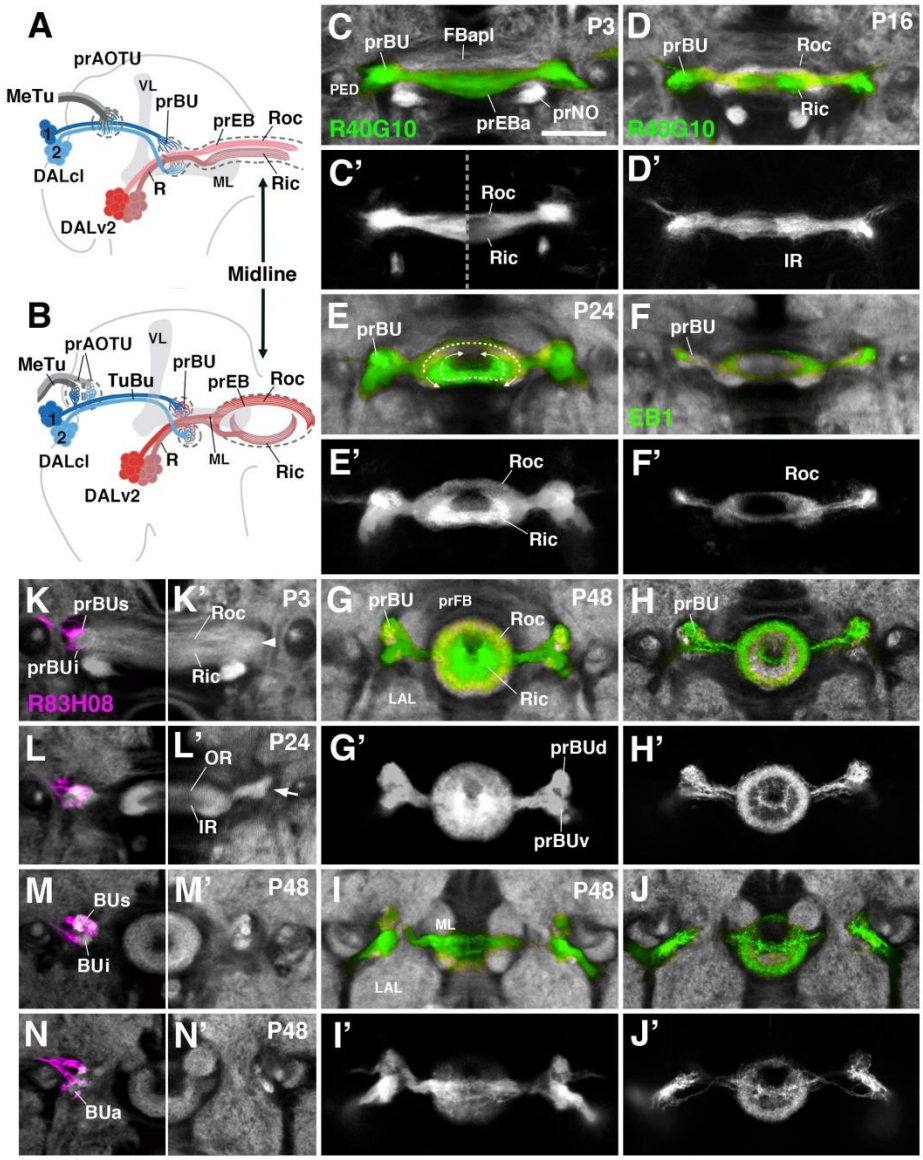

Figure 3-3: Morphogenesis of the ellipsoid body and bulb.

(A, B) Schematic anterior view of pupal brain hemisphere at 6hrs (A) and 24hrs (B) after puparium formation (APF). Secondary lineages contributing to the primordia of the anterior visual pathway are rendered in different colors; mushroom body (gray) is shown as reference. (C-N') Z-projections of frontal confocal sections of pupal brain hemispheres at different stages, indicated in upper left corner of panels (P3 3hrs after puparium formation (APF); P16 16hrs APF; P24 24hrs APF; P48 48hrs APF). In

panels of the middle column (C/C', E/E', G/G', I/I') and in D/D', R40G10-Gal4 labels preferentially inner ring (Ric) neurons; in the right column (F/F', H/H', J/J'), outer ring neurons (Roc) are labeled by EB1-Gal4. In panels (C-J), antibody against DNcadherin marks neuropil (white). For the P48 stage, panels (G-H') show a section through center of the ellipsoid body, panels (I-J') illustrate a level near the anterior surface of the ellipsoid body. (K-N): Z-projections of frontal confocal sections at stages P3-P48, showing axonal endings of tuberculo-bulbar neurons labeled by R83H08-Gal4 (magenta) in the developing bulb primordium (prBUs, prBUi, prBUa) of left brain hemisphere. Panels (K'-N') show opposite hemisphere, labeled only with anti-DNcadherin (white). For other abbreviations, see Table 1. Bar: 25μm

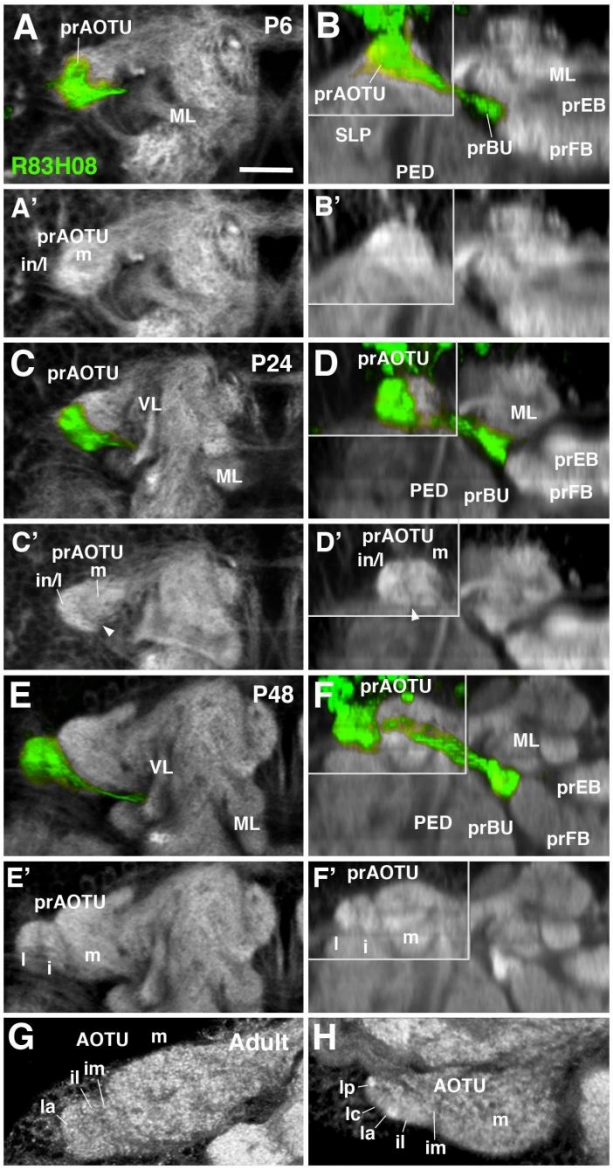

Figure 3-4: Morphogenesis of the anterior optic tubercle. Panels show Z-projections of frontal confocal sections (left column; A, C, E, G) and corresponding, digitally-tilted horizontal sections (right column; B, D, F, H) of brain hemisphere at different stages of development, from 6hrs APF (P6) to Adult (stages indicated in upper right corner of panels). In panels of right column, the area in upper left boxed by gray line represents a dorsal level, including the prAOTU; remainder of the panels show horizontal sections at

a more ventral level, including the prBU. Proximal arborizations of TuBu neurons, labeled by R83H08-Gal4 (green), mark the developing primordium of the anterior optic tubercle (prAOTU); distal arborizations outline the primordium of the bulb (prBU). Neuropil is labeled by anti-DNcadherin (white). In early pupa (P6; A-B') the prAOTU forms an undifferentiated, ovoid, DNcadherin-rich domain at the anterior-lateral surface of the superior lateral protocerebrum (SLP). GFP-positive fibers of TuBu neurons are largely restricted to the lateral half of the prAOTU (A), which will give rise to the intermediate and lateral subdomains of this compartment (in/l in A'). The medial part of the prAOTU (m in A') does not receive GFP-positive fibers. At P24 (C-D'), a sharp boundary separates the medial from the intermediate/lateral subdomain (arrowhead in C', D'). At P48 (E-F'), the GFP-positive domain has differentiated into a lateral (l) and intermediate (i) subdomain. During late pupal development, these become further subdivided into smaller subdomains, including the intermediate medial (im), intermediate lateral (il), lateral anterior (la), lateral central (lc), and lateral posterior (lp; G, H). For other abbreviations: see Table 1. Bar: 25μm.

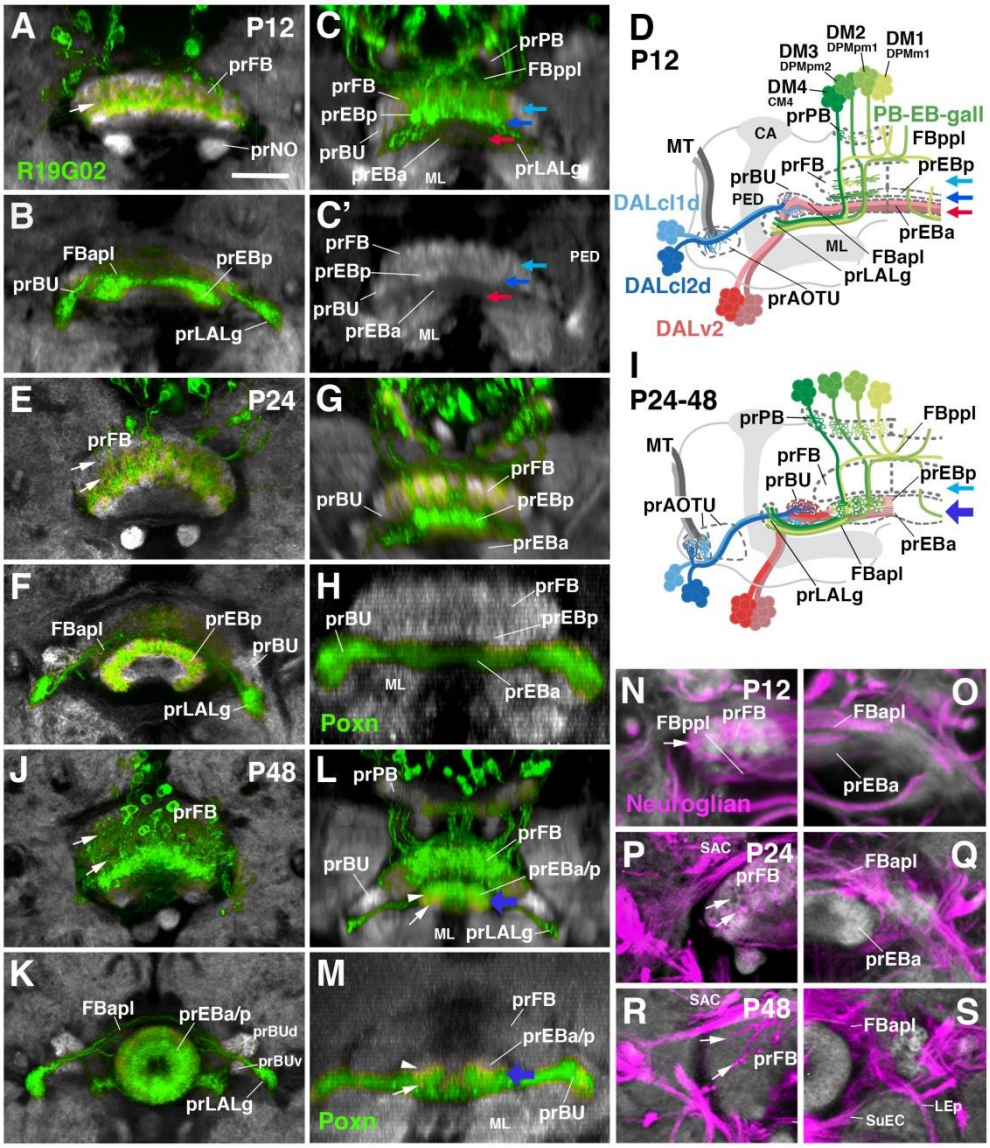

Figure 3-5: Formation of the ellipsoid body from an anterior and posterior primordium. Panels of the left column (A, B, E, F, J, K) show Z-projections of frontal confocal sections of pupal brains in which a subset of columnar neurons of the central complex are labeled by R19G02-Gal4 (green); neuropil is labeled by anti-DNcadherin (white). Middle column (C, C', G, H, L, M) presents digitally-tilted horizontal sections of brains labeled with R19G02-Gal4 (C, G, L) or Poxn-Gal4 (H, M). Upper two rows (A-C') show 12h pupa (P12), middle two rows (E-H) 24h pupa (P24), and bottom two rows 48h pupa

(P48). Frontal sections of left column alternatingly show a more posterior plane, containing the primordium of the fan-shaped body (prFB; A, E, J) and an anterior plane with primordium of the ellipsoid body (prEB) and lateral accessory lobe (prLALg; B, F, K). Panels (D, I) are schematic representations of pupal brain hemisphere viewed from dorsally, illustrating architecture of central complex primordia at an early pupal stage (P12, shown in D) and early-mid pupal stage (P24-48, shown in I). In these schematics, neurons of the DALv2 lineage, forming R-neurons of the ellipsoid body, are rendered in red; DALcl1/2d neurons, connecting anterior optic tubercle with bulb, are in blue; columnar neurons of the posterior type II lineages, are in green. Light blue arrows in (C, C', D, I) point at prFB; dark blue arrows in (C, C', D) indicate prEBp, which at this early stage forms part of the prFB; red arrows in (C, C', D) indicate prEBa; purple arrow in (I, L, M) indicates prEB after the anterior and posterior domains (prEBa, prEBp) have merged. Panels (N-S) are Z-projections of frontal confocal sections of pupal brains (N, O: P12; P, Q: P24; R, S: P48) labeled with anti-Neuroglian (secondary axon tracts; magenta) and anti-DNcadherin (neuropil; white). Left column (N, P, R) represent posterior plane, containing left half of fan-shaped body primordium (prFB); Right panels (O, Q, S) show anterior planes with right halves of ellipsoid body primordium (prEB). Arrows in (N, P, R) point at longitudinal bundles of PB-EB-LALg axons penetrating the prFB.

For other abbreviations see Table 1. Bar: 25μm.

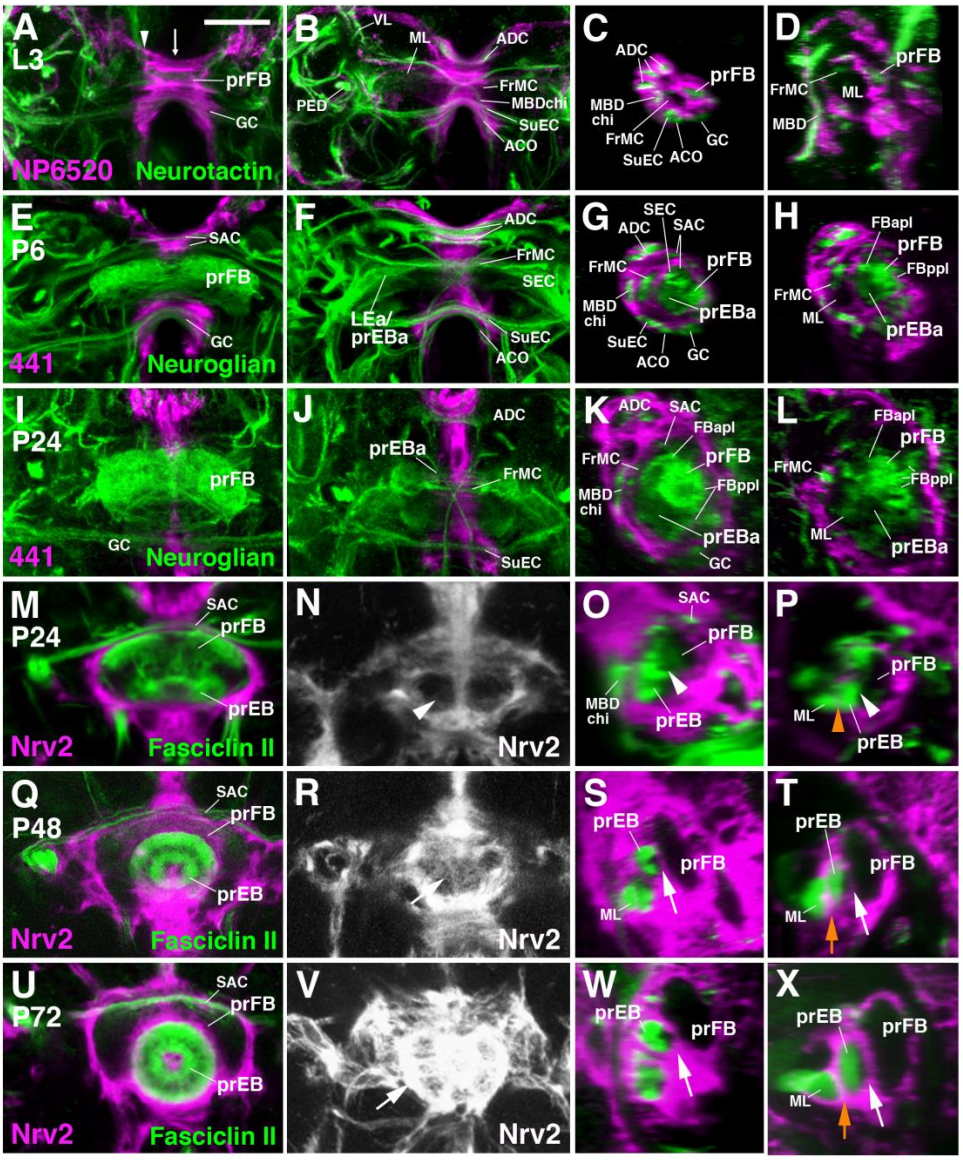

Figure 3-6: Development of the glial layer of the central complex.

Panels of the first and second column show Z-projections of frontal confocal sections of late larval (A, B) and pupal brains at stages indicated in upper left corner. The third and fourth columns present sagittal sections at the corresponding stages. Panels of the first column (A, E, I, M, Q, U) represent a posterior plane, showing the primordium of the fan-shaped body (prFB); second column panels (B, F, J, N, R, V) are taken at a more anterior plane representing the primordium of the ellipsoid body. Panels of the third

column (C, G, K, O, S, W) show sagittal plane right at midline [indicated by arrow in panel (A)], panels of the fourth column (D, H, L, P, T, X) represent a parasagittal plane at approximately 5-10μm lateral of midline [indicated by arrowhead in (A)]. Neuropil glia is labeled by NP6520-Gal4 (A-D), 442-Gal4 (E-L), or Nrv2-Gal4 (M-X; magenta). In all panels except (N, R, V), secondary axon tracts (green) are labeled by anti-Neurotactin (A-D), anti-Neuroglian (E-L) or anti-Fasciclin II (M-X). Processes of neuropil glia forming stable sheaths around individual commissural tracts, or combinations of neighboring tracts, can be recognized in sagittal sections (panels of third column) from larval stages to the late pupa and adult. In the larva and early pupa (C, D, G, H), a common sheath surrounds a system of tracts that includes the primordia of the fan-shaped body (prFB, including posterior primordium of ellipsoid body), anterior ellipsoid body (prEBa), several commissures (supraesophageal commissure, SEC; part of superior arch commissure, SAC) and the tip of the medial lobe of the mushroom body (ML). After P24, a layer of glial processes starts to separate the medial lobe from the ellipsoid body primordium (orange arrow in T, X; orange arrowhead in P, representing 24h pupa, points at position where glial septum will appear at later stages). Concomitantly, glial processes grow in between the primordia of the ellipsoid body and fan-shaped body (white arrows S, T, W, X). Panels (N, R, V) represent the frontal plane that contains the emerging glial sheath (arrowhead in N: no glia present yet; arrows in R, V: glial septum has formed) between ellipsoid body and fan-shaped body primordium; note increasing intensity of the Nrv2 signal, attesting to the growth in thickness of the glial layer.

Other abbreviations: see Table 1. Bar: 25μm.

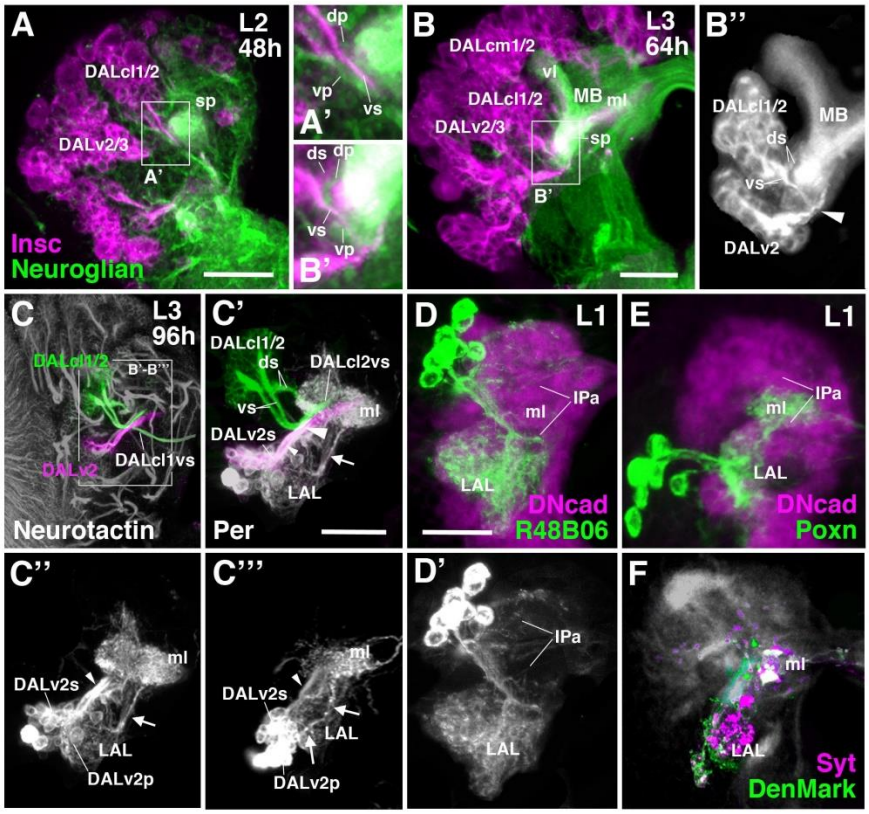

Figure 3-7: Elements of the AVP in the early larva.

(A-B'') Z-projections of frontal confocal section of larval brain hemisphere labeled with Insc-Gal4>UAS-mcd8GFP (magenta; secondary neurons) and anti-Neuroglian (green; primary neurons) at the L2 stage (48h post hatching; A, A') and early L3 stage (64h post hatching; B-B''). Note close association of primary and secondary fiber bundles of DALcl1 and DALcl2 (DALcl1/2dp and DALcl1/2ds; DALcl1/2vp and DALcl1/2vs) in (A') and (B'), respectively. (B'') shows enlarged view of early secondary tracts of DALcl1/2 and DALv2, labeled by Insc-Gal4>UAS-mcd8GFP (white; all other labeled lineages were digitally erased; mushroom body (MB) shown as reference). (C-C''') Frontal confocal sections of late third instar larval brain hemisphere labeled with anti-Neurotactin (secondary neurons) and Per-Gal4>UAS-mcd8GFP (labels secondary and

primary neurons of the DALv2 lineage). In (C), only the Neurotactin labeling is shown; secondary tracts of lineages DALcl1/2 and DALv2 were digitally rendered green and magenta, respectively. (C'-C''') show Per-Gal4 labeling of both primary neurons (DALv2p) and secondary neurons (DALv2s) of the DALv2 lineage. In (C'), Neurotactin labeling of secondary DALcl1/2 tract and DALv2 tract (digitally rendered green and magenta, respectively) is left; Neurotactin signal of all other secondary neurons was digitally erased. (C'') and (C''') show Per-Gal4> mcd8GFP in DALv2 in brain of two different L3 specimens. Small arrowhead in (C'-C''') indicates secondary DALv2 tract (DALv2s); large arrowhead in (C') and (B'') points at convergence of secondary tracts of DALv2 and DALcl2v. Arrow in (C'-C''') indicates primary DALv2 tract (DALv2p). (D-E) Z-projections of frontal confocal section of first instar larval brain hemisphere, showing labeling of primary neurons of DALcl1/2d [R48B06-Gal4>UAS-mcd8GFP in (D)] and DALv2 [Poxn-Gal4>UAS-mcd8GFP in (E)]. Antibody against DNcadherin labels neuropil (magenta). (F) Z-projection of frontal confocal section of late third instar larval brain hemisphere. Constructs labeling postsynaptic sites (DenMark; green) and presynaptic sites (Syntaxin; Syt; magenta) were driven by DALv2 driver Poxn-Gal4. Bars: 20μm (A, B, D-E); 50μm (C-C''')

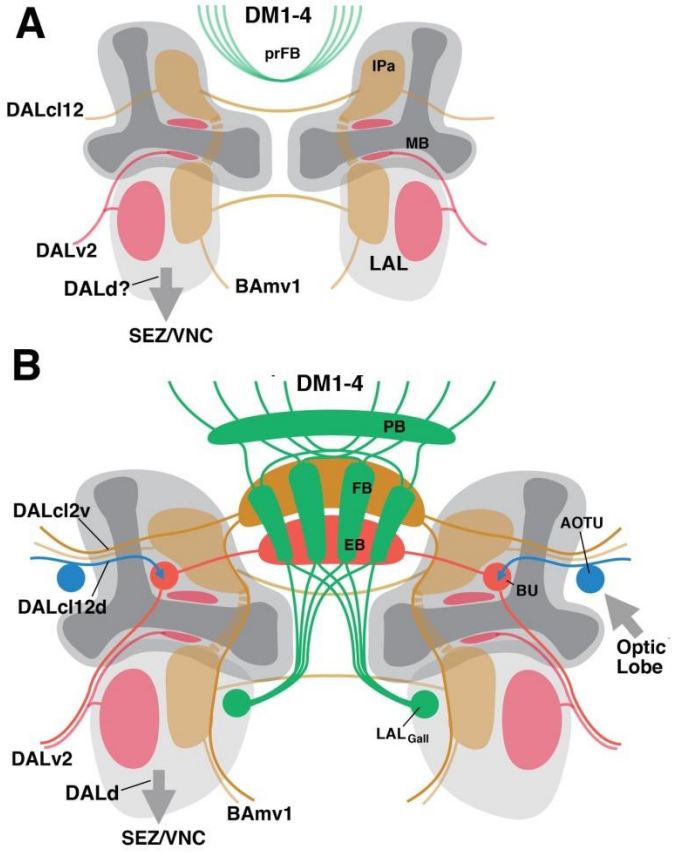

Figure 3-8: Schematic representation of projection patterns of lineages building the central complex at the larval stage (A) and adult stage (B).

Abbreviations used in figures:

ACO antennal lobe commissure; ADC anterior dorsal commissure; AOT anterior optic tract; CA calyx; FBapl anterior plexus of fan-shaped body; FBppl posterior plexus of fan-shaped body; FrMC fronto-medial commissure; GC great commissure; IPa anterior domain of inferior protocerebrum; LAL lateral accessory lobe; LEa anterior lateral ellipsoid body fascicle; LEp posterior lateral ellipsoid body fascicle; MB mushroom body; MDBchi chiasm of median bundle; ML medial lobe; MeTu axon

bundle formed by medullo-tubercular neurons; PED peduncle; prAOTU primordium of anterior optic tubercle (il intermediate lateral subdivision of prAOTU; im intermediate-medial subdivision of prAOTU; in intermediate subdivision of prAOTU; l lateral subdivision of prAOTU; la anterior lateral subdivision of prAOTU; lc central lateral subdivision of prAOTU; lp posterior lateral subdivision of prAOTU; m medial subdivision of prAOTU; prBU primordium of bulb; prBUs primordium of superior bulb; prBUi primordium inferior bulb; prEBa primordium of anterior ellipsoid body; prEBp primordium of posterior ellipsoid body; prFB primordium of fan-shaped body; prLALg primordium of gall of lateral accessory complex; prNO primordium of noduli; prPB priordium of protocerebral bridge; R axon bundle formed by ring neurons (lineage DALv2); Ric inner central domain of ellipsoid body; Rip inner posterior domain of ellipsoid body; Roc outer central domain of ellipsoid body; SAC superior arch commissure; SEC supraellipsoid body commissure; SLP superior lateral protocerebrum; SMP superior medial protocerebrum; SuEC subellipsoid body commissure; TuBu axon bundle formed by tuberculo-bulbar neurons (lineages DALcl1/2); TuBua tuberculo-bulbar neurons projecting to anterior bulb; TuBui tuberculo-bulbar neurons projecting to inferior bulb; TuBus tuberculo-bulbar neurons projecting to superior bulb; VL vertical lobe; VLP ventrolateral protocerebrum

References

Alekseyenko OV, Chan YB, Li R, Kravitz EA. 2013. Single dopaminergic neurons that modulate aggression in Drosophila. Proc Natl Acad Sci U S A 110:6151-6156.

Ashburner M. 1989. Drosophila. A laboratory manual. Cold Spring Harbor, NY: Cold Spring Harbor laboratory Press. Pp 214-217.

Awasaki T, Lai SL, Ito K, Lee T. 2008. Organization and postembryonic development of glial cells in the adult central brain of Drosophila. J Neurosci. 28:13742-13753.

Bello BC, Izergina N, Caussinus E, Reichert H. 2008. Amplification of neural stem cell proliferation by intermediate progenitor cells in Drosophila brain development. Neural Dev 3:5.

Betschinger J, Mechtler K, Knoblich JA. 2006. Asymmetric segregation of the tumor suppressor brat regulates self-renewal in Drosophila neural stem cells. Cell 124:1241-1253.

Bieber AJ, Snow PM, Hortsch M, Patel NH, Jacobs JR, Traquina ZR, Schilling J, Goodman CS. 1989. Drosophila neuroglian: a member of the immunoglobulin superfamily with extensive homology to the vertebrate neural adhesion molecule L1. Cell 59:447-460.

Boll W, Noll M. 2002. The Drosophila Pox neuro gene: control of male courtship behavior and fertility as revealed by a complete dissection of all enhancers. Development 129:5667-5681.

Boyan GS, Williams JL. 1997. Embryonic development of the pars intercerebralis/central complex of the grasshopper. Dev Genes Evol 207:317-329.

Boyan G, Williams L, Legl A, Herbert Z. 2010. Proliferative cell types in embryonic lineages of the central complex of the grasshopper Schistocerca gregaria. Cell Tissue Res 341:259-277.

Boyan GS, Reichert H. 2011. Mechanisms for complexity in the brain: generating the insect central complex. Trends Neurosci 34:247-257.

Boyan G, Liu Y. 2014. Timelines in the insect brain: fates of identified neural stem cells generating the central complex in the grasshopper Schistocerca gregaria. Dev Genes Evol 224:37-51.

Boyan GS, Liu Y. 2016. Development of the Neurochemical Architecture of the Central Complex. Front Behav Neurosci 10:167.

Brody T, Odenwald WF. 2005. Regulation of temporal identities during Drosophila neuroblast lineage development. Curr Opin Cell Biol 17:672-675.

Cardona A, Larsen C, Hartenstein V. 2009. Neuronal fiber tracts connecting the brain and ventral nerve cord of the early Drosophila larva. J Comp Neurol 515: 427-440.

Chen W, Hing H. 2008. The L1-CAM, Neuroglian, functions in glial cells for Drosophila antennal lobe development. Dev Neurobiol:1029-45.

Das A, Gupta T, Davla S, Prieto-Godino LL, Diegelmann S, Reddy OV, Raghavan KV, Reichert H, Lovick J, Hartenstein V. 2013. Neuroblast lineage-specific origin of the neurons of the Drosophila larval olfactory system. Dev Biol 373: 322-337.

Hanesch U, Fischbach KF, Heisenberg M. 1989. Neuronal architecture of the central complex in Drosophila melanogaster. Cell Tissue Res 257:343–366.

Hartenstein V, Spindler S, Pereanu W, Fung S. 2008. The development of the Drosophila larval brain. Adv Exp Med Biol 628:1-31.

Hartenstein V, Younossi-Hartenstein A, Lovick JK, Kong A, Omoto JJ, Ngo KT, Viktorin G. 2015. Lineage-associated tracts defining the anatomy of the Drosophila first instar larval brain. Dev Biol 406:14-39.

Hitier R, Simon AF, Savarit F, Préat T. 2000. no-bridge and linotte act jointly at the interhemispheric junction to build up the adult central brain of Drosophila melanogaster. Mech Dev 99:93-100.

Homberg U, Hofer S, Pfeiffer K, Gebhardt S. 2003. Organization and neural connections of the anterior optic tubercle in the brain of the locust, Schistocerca gregaria. J Comp Neurol 462:415-430.

Hortsch M, Patel NH, Bieber AJ, Traguina ZR, Goodman CS. 1990. Drosophila neurotactin, a surface glycoprotein with homology to serine esterases, is dynamically expressed during embryogenesis. Development 110:1327-1340.

Ilius M, Wolf R, Heisenberg M. 2007. The central complex of Drosophila melanogaster is involved in flight control: studies on mutants and mosaics of the gene ellipsoid body open. J Neurogenet 21:321-338.

Ito K, Awasaki T. 2008. Clonal unit architecture of the adult fly brain. Adv Exp Med Biol 628:137-158.

Ito M, Masuda N, Shinomiya K, Endo K, Ito K. 2013. Systematic analysis of neural projections reveals clonal composition of the Drosophila brain. Curr Biol 23: 644-655.

Iwai Y, Usui T, Hirano S, Steward R, Takeichi M, Uemura T. 1997. Axon patterning requires DN-cadherin, a novel neuronal adhesion receptor, in the Drosophila embryonic CNS. Neuron 19:77-89.

Jenett A, Rubin GM, Ngo TT, Shepherd D, Murphy C, Dionne H, Pfeiffer BD, Cavallaro A, Hall D, Jeter J, Iyer N, Fetter D, Hausenfluck JH, Peng H, Trautman ET, Svirskas RR, Myers EW, Iwinski ZR, Aso Y, DePasquale GM, Enos A, Hulamm P, Lam SC, Li HH, Laverty TR, Long F, Qu L, Murphy SD, Rokicki K, Safford T, Shaw K, Simpson JH, Sowell A, Tae S, Yu Y, Zugates CT. 2012. A GAL4-driver line resource for Drosophila neurobiology. Cell Rep 2: 991-1001.

Kaneko M, Hall JC. 2000. Neuroanatomy of cells expressing clock genes in Drosophila: transgenic manipulation of the period and timeless genes to mark the perikarya of circadian pacemaker neurons and their projections. J Comp Neurol 422:66-94.

Komiyama T, Sweeney LB, Schuldiner O, Garcia KC, Luo L. 2007. Graded expression of semaphorin-1a cell-autonomously directs dendritic targeting of olfactory projection neurons. Cell 128:399-410.

Koniszewski ND, Kollmann M, Bigham M, Farnworth M, He B, Büscher M, Hütteroth W, Binzer M, Schachtner J, Bucher G. 2016. The insect central complex as model for heterochronic brain development-background, concepts, and tools. Dev Genes Evol 226:209-219.

Larsen C, Shy D, Spindler S, Fung S, Younossi-Hartenstein A, Hartenstein V. 2009. Patterns of growth, axonal extension and axonal arborization of neuronal lineages in the developing Drosophila brain. Dev Biol 335:289-304.

Lee T, Lee A, Luo L. 1999. Development of the Drosophila mushroom bodies: sequential generation of three distinct types of neurons from a neuroblast. Development 126:4065-4076.

Lovick JK, Ngo KT, Omoto JJ, Wong DC, Nguyen JD, Hartenstein V. 2013. Postembryonic lineages of the Drosophila brain: I. Development of the lineage-associated fiber tracts. Dev Biol 384: 228-257.

Lovick JK, Hartenstein V. 2015. Hydroxyurea-mediated neuroblast ablation establishes birth dates of secondary lineages and addresses neuronal interactions in the developing Drosophila brain. Dev Biol 402:32-47.

Lovick JK, Kong A, Omoto JJ, Ngo KT, Younossi-Hartenstein A, Hartenstein V. 2016. Patterns of growth and tract formation during the early development of secondary lineages in the Drosophila larval brain. Dev Neurobiol 76:434-451.

Müller M, Homberg U, Kühn A. 1997. Neuroarchitecture of the lower division of the central body in the brain of the locust (Schistocerca gregaria). Cell Tissue Res 288:159-176.

Namiki S, Kanzaki R. 2016. Comparative Neuroanatomy of the Lateral Accessory Lobe in the Insect Brain. Front Physiol 7:244.

Nicolaï LJ1, Ramaekers A, Raemaekers T, Drozdzecki A, Mauss AS, Yan J, Landgraf M, Annaert W, Hassan BA. 2010. Genetically encoded dendritic marker sheds light on neuronal connectivity in Drosophila. Proc Natl Acad Sci U S A 107:20553-20558.

Nicolas E, Preat T. 2005. Drosophila central brain formation requires Robo proteins. Dev Genes Evol 215:530-536.

Omoto JJ, Yogi P, Hartenstein V. 2015. Origin and development of neuropil glia of the Drosophila larval and adult brain: Two distinct glial populations derived from separate progenitors. Dev Biol 404:2-20.

Omoto JJ, Keleş MF, Nguyen B, Bolanos C, Lovick JK, Frye MA, Hartenstein V. 2017. Visual input to the Drosophila central complex by developmentally and functionally distinct neuronal populations. Curr Biol (in press)

Pearson BJ, Doe CQ. 2004. Specification of temporal identity in the developing nervous system. Annu Rev Cell Dev Biol 20: 619-647.

Pecot MY, Tadros W, Nern A, Bader M, Chen Y, Zipursky SL. 2013. Multiple interactions control synaptic layer specificity in the Drosophila visual system. Neuron 77:299-310.

Pereanu W, Kumar A, Jenett A, Reichert H, Hartenstein V. 2010. Development-based compartmentalization of the Drosophila central brain. J Comp Neur 518:2996-3023.

Pfeiffer K, Homberg U. 2014. Organization and functional roles of the central complex in the insect brain. Annu Rev Entomol 59:165-184.

Pimentel D, Donlea JM, Talbot CB, Song SM, Thurston AJ, Miesenböck G. 2016. Operation of a homeostatic sleep switch. Nature 536:333-337.

Piovant M, Léna P. 1988. Membrane glycoproteins immunologically related to the human insulin receptor are associated with presumptive neuronal territories and developing neurones in Drosophila melanogaster. Development 103:145-156.

Renn SC, Armstrong JD, Yang M, Wang Z, An X, Kaiser K, Taghert PH. 1999. Genetic analysis of the Drosophila ellipsoid body neuropil: organization and development of the central complex. J Neurobiol 41:189-207.

Riebli N, Viktorin G, Reichert H. 2013. Early-born neurons in type II neuroblast lineages establish a larval primordium and integrate into adult circuitry during central complex development in Drosophila. Neural Dev 8:6.

Seelig JD, Jayaraman V. 2015. Neural dynamics for landmark orientation and angular path integration. Nature 521:186-191.

Simon AF, Boquet I, Synguélakis M, Préat T. 1998. The Drosophila putative kinase linotte (derailed) prevents central brain axons from converging on a newly described interhemispheric ring. Mech Dev 76:45-55.

Spindler SR, Hartenstein V. 2011. Bazooka mediates secondary axon morphology in Drosophila brain lineages. Neural Dev 6:16.

Strausfeld NJ.1976. Atlas of an Insect Brain. Springer-Verlag, Berlin, pp.1–214.

Strauss R. 2002. The central complex and the genetic dissection of locomotor behaviour. Curr Opin Neurobiol 12:633-638.

Sun B, Xu P, Salvaterra PM. 1999. Dynamic visualization of nervous system in live Drosophila. Proc Natl Acad Sci U S A 96:10438-10443.

Thomas JB, Bastiani MJ, Bate M, Goodman CS. 1984. From grasshopper to Drosophila: a common plan for neuronal development. Nature 310:203-207.

Truman JW, Moats W, Altman J, Marin EC, Williams DW. 2010 Role of Notch signaling in establishing the hemilineages of secondary neurons in Drosophila melanogaster. Development 137:53-61.

Wagh DA, Rasse TM, Asan E, Hofbauer A, Schwenkert I, Dürrbeck H, Buchner S, Dabauvalle MC, Schmidt M, Qin G, Wichmann C, Kittel R, Sigrist SJ, Buchner E. 2006. Bruchpilot, a protein with homology to ELKS/CAST, is required for structural integrity and function of synaptic active zones in Drosophila. Neuron 49:833-844.

Wegerhoff R, Breidbach O. 1992. Structure and development of the larval central complex in a homometbolous insect, the beetle Tenebrio molitor. Cell Tissue Res 268:341–358.

Wolff T, Iyer NA, Rubin GM. 2015. Neuroarchitecture and neuroanatomy of the Drosophila central complex: A GAL4-based dissection of protocerebral bridge neurons and circuits. J Comp Neurol 523:997-1037.

Wong DC, Lovick JK, Ngo KT, Borisuthirattana W, Omoto JJ, Hartenstein V. 2013. Postembryonic lineages of the Drosophila brain: II. Identification of lineage projection patterns based on MARCM clones. Dev Biol 384:258-289.

Yang JS, Awasaki T, Yu HH, He Y, Ding P, Kao JC, Lee T. 2013. Diverse neuronal lineages make stereotyped contributions to the Drosophila locomotor control center, the central complex. J Comp Neurol 521:2645-2662.

Ypsilanti AR, Zagar Y, Chédotal A. 2010. Moving away from the midline: new developments for Slit and Robo. Development 137:1939-1952.

Young JM, Armstrong JD. 2010. Structure of the adult central complex in Drosophila: organization of distinct neuronal subsets. J Comp Neurol 518:1500-1524.

Younossi-Hartenstein A, Salvaterra P, Hartenstein, V. 2003. Early development of the Drosophila brain IV. Larval neuropile compartments defined by glial septa. J Comp Neurol 455:435-450.

Yu HH, Awasaki T, Schroeder MD, Long F, Yang JS, He Y, Ding P, Kao JC, Wu GY, Peng H, Myers G, Lee T. 2013. Clonal development and organization of the adult Drosophila central brain. Curr Biol 23:633-643.

Zlatic M, Li F, Strigini M, Grueber W, Bate M. 2009. Positional cues in the Drosophila nerve cord: semaphorins pattern the dorso-ventral axis. PLoS Biol 7(6):e1000135.